People's Democratic Republic of Algeria

Ministry of Higher Education and Scientific Research

University of El Oued

Faculty of Nature and Life Sciences

Department of Cellular and Molecular Biology

MASTER THESIS

In partial fulfilment of the requirements for the degree of Master

Major: Biological Sciences

Speciality: Applied Biochemistry

THEME

Targeting Acetylcholinesterase: Design, Synthesis and Multimodal Evaluation of Ferrocenyl Acetylaniline Derivatives as Potential Anti-Alzheimer Agents

Presented by:

- KHELEF Hanane
- KHEEF Nour Elhouda
- TABAI Aicha

Jury Members:

• Dr.	Imane CHELLALBA	MCA	President
• Dr.	Housseyn CHAOUA	MCA	Examiner
• Dr.	Elhafnaoui LANEZ	MCA	Supervisor

Academic Year: 2025 – 2026

شكر وعرفان

الحمد لله أولاً وآخراً على نعمه وتوفيقه لنا لإتمام هذا العمل.

نتقدم بجزيل الشكر وعظيم الامتنان إلى الأستاذ المشرف الدكتور العانز الحفناوي، على إشرافه القيّم وتوجيهاته السديدة ونصائحه العلمية التي كانت خير عون لنا طوال فترة إعداد هذه المذكرة، وعلى ما أبداه من صبر واهتمام ومتابعة مستمرة، فله منا خالص الشكر والتقدير والاحترام

ولا يفوتنا أن نتقدم بالشكر إلى كل من ساعدنا وساندنا من قريب أو بعيد وساهم في إنجاز هذه المذكرة.

والحمد لله رب العالمين

إهـــــــداء

المتواضع العمل هذا لإتمام وفقني الذي لله الحمد

ونجاحي وجودي سبب كانا من إلى وتخرجي جهدي ثمرة أهدي

العزيز أبي إلى

الجد قيم نفسي في وغرس له، حدود لا الطموح أن علمني الذي الحياة، هذه في وسندي والعطاء، القوة رمز مستقبلي أجل من تضحيات من قدمته ما لكل شكراً .والصبر والاجتهاد

الغالية أمي إلى

منحتني والتي خطوة، كل في ترافقني دعواتها كانت التي الكبير، القلب وصاحبة والرحمة، الحنان ينبوع والعرفان الامتنان كل لكِ .مقابل دون والدعم الحب

العزيز زوجي إلى

والضغط، التعب أوقات في وساندني دائم، ودعم تشجيع مصدر كان الذي دربي، ورفيق حياتي شريك العمل هذا إتمام على معين خير فكان

وأخواتي إخوتي إلى

الطيبة بالكلمة جانبي إلى دائماً وكانوا والمساندة، المحبة منحوني الذين الذكريات، وأجمل الطفولة رفقاء الصادق والتشجيع

العمل، هذا إعداد خلال معاً بذلناها التي التعاون روح على لكما شكراً المذكرة هذه إنجاز في زميلتيَّ إلى النجاح من بمزيد لكما الأمنيات أطيب مع

بعيد أو قريب من ومساندتي دعمي في ساهم من كل إلى

حنان خلف

الإهـــــــداء

﴿وَآخِرُ دَعْوَاهُمْ أَنِ الْحَمْدُ لِلَّهِ رَبِّ الْعَالَمِينَ﴾

لم تكن الرحلة قصيرة، ولا الطريق ممهَّدة بالتسهيلات، لكنني وصلت بفضل الله

فالحمد لله الذي يسَّر البدايات، وأتمَّ النهايات، وبلَّغنا الغايات، وبكل حب أهدي ثمرة نجاحي وتخرجي

إلى من غرسا في قلبي حب العلم، وسقيا حلمي بالصبر والدعاء

إلى من كانت دعواتهما الصادقة تمهِّد لي الطرقات وتضيء لي العثرات

إلى الذي زيَّن اسمي بأجمل الألقاب، إلى من دعمني بلا حدود وأعطاني بلا مقابل، إلى من علمني أن الدنيا كفاح وسلاحها العلم والمعرفة، إلى داعمي الأول في مسيرتي، وسندي وقوتي فخري واعتزازي

" أبي الغالي "

إلى التي جعل الله الجنة تحت قدميها، إلى التي كان حضنها وطنًا وصوتها سكينة، إلى من كان دعاؤها سر نجاحي وحنانها بلسم جراحي، قدوتي ومعلمتي الأولى

" أمي الحنونة "

شكرًا لكما بعدد الليالي التي سهرتماها قلقًا من أجلي، وبعدد الدعوات التي رفعتماها إلى السماء من أجل نجاحي

إلى الذين شددت عضدي بهم، فكانوا خير سند وعون في مختلف مراحل حياتي

" أخوتي الأعزاء "

إلى خيرة أيامي وصفوتها، إلى من غمرنني بالدعم والتوجيه، وكان لهن الأثر الجميل في مسيرتي

" أخواتي الغاليات "

إلى سبب سعادتي وبهجة أيامي، ونبض الروح وزينة الحياة

" أبناء إخوتي و أخواتي"

إلى من اختاره قلبي شريكًا لدربي، شكرًا لأنك كنت القوة حين ضعفت، والثقة حين ترددت، والسند الذي لم يتخلَّ عني في أصعب اللحظات

وإلى كل من ساهم في إنجاز هذا العمل، أهدي هذه اللحظة التي خُطَّت بالتعب وتُوِّجت بالفخر والنجاح

نور الهدى

Dedicate

« IF I HAVE SEEN FURTHER IT IS BY STANDING ON THE SHOULDERS OF GIANTS »

ISAAC NEWTON

To express my gratitude to all those who contributed in many ways to the success of this modest work and made it an unforgettable experience for me.

To my **beloved parents**, for their unconditional support, trust and encouragements throughout my whole life.

My dear father **BRAHIM** and my dear mother **OUM EL KHEIR BENNACEUR**, for their sacrifices and devotion to care for me.

To my **grandmother**, for her love, support and endless Duaas.

To my late **grandfather**, the one who's missing but present in our hearts.

To my siblings **MOHAMMED, MERIEM, OUMAYMA**, for their everlasting love and care, utmost support and encouragements.

To the late souls of my uncle and his wife that we lost this year.

To my partners **HANANE** and **NOUR ELHOUDA**, for their support and hard work with love and patience.

To my supervisor **Dr Elhafnaoui LANEZ**, for their assistance, guidance, valuable presence, patience and priceless advice.

To all my friends and loved ones, **SANA, HANANE**, **ASMA**, for the support, comfort and kindness they provided along the journey.

AICHA

Abstract

This thesis presents the design, synthesis, physicochemical characterisation, and comprehensive in silico evaluation of a series of ferrocenyl acetylaniline derivatives (FcMe2Ac, FcMe3Ac, and FcMe4Ac), with particular emphasis on elucidating the relationships between molecular structure, electronic properties, and interaction behaviour toward acetylcholinesterase (AChE), a key enzymatic target in Alzheimer's disease.

The target compounds were synthesised via a nucleophilic substitution strategy, yielding the desired regioisomers in moderate to high yields (48–80%) with good reproducibility. Structural confirmation was achieved through complementary spectroscopic techniques, including FT-IR, UV–Visible spectroscopy, and one- and two-dimensional NMR analyses. FT-IR spectra displayed characteristic bands corresponding to N–H stretching (~3290–3445 cm^{-1}) and carbonyl functionalities (~1647–1651 cm^{-1}), while UV–Visible spectra revealed absorption maxima in the range of 259–432 nm, attributed to $\pi \rightarrow \pi^*$ transitions within the aromatic system and metal-centred d–d transitions. NMR data confirmed the expected molecular architecture, with distinctive signals corresponding to the ferrocenyl unit (~4.1–4.3 ppm) and aromatic protons (~6.6–7.8 ppm).

Electrochemical characterisation by cyclic voltammetry demonstrated a quasi-reversible Fe(II)/Fe(III) redox process for all derivatives, with formal potentials ranging from 43.9 to 57.5 mV. The observed peak separations (ΔEp = 87.8–115 mV) and near-unity current ratios confirmed quasi-reversible behaviour. Diffusion coefficients (1.11×10^{-7}–5.74×10^{-7} $cm^2 \cdot s^{-1}$) and heterogeneous electron-transfer rate constants (0.14×10^{-3}–0.62×10^{-3} $cm \cdot s^{-1}$) indicated that both transport and kinetic properties are strongly influenced by substitution pattern.

Density functional theory calculations provided detailed insight into the electronic structure, revealing HOMO energies between −5.83 and −5.68 eV and HOMO–LUMO gaps of 3.99–4.29 eV, indicative of moderate chemical stability and controlled reactivity. Global reactivity descriptors confirmed this behaviour, with hardness values ranging from 1.995 to 2.143 eV and electrophilicity indices up to 3.519 eV. The progressive increase in dipole moment (3.82–5.12 D) reflects enhanced molecular polarity across the series.

Molecular docking studies targeting acetylcholinesterase demonstrated favourable binding affinities (−7.34 to −8.58 $kcal \cdot mol^{-1}$), with FcMe4Ac exhibiting the strongest interaction. Binding mode analysis revealed stabilisation within the catalytic gorge through hydrophobic contacts, π–π stacking, and hydrogen bonding interactions involving key residues. Molecular dynamics simulations over 100 ns confirmed the stability of the ligand–enzyme

complexes, with RMSD values stabilising within ~0.10–0.25 nm and reduced residue fluctuations, indicating a stable and persistent binding mode.

In silico ADMET predictions revealed favourable pharmacokinetic and safety profiles, including high gastrointestinal absorption, balanced lipophilicity (LogP = 3.12–3.45), and absence of predicted mutagenic or hepatotoxic effects. However, the limited predicted blood–brain barrier permeability suggests that further optimisation may be required to enhance central nervous system availability.

Overall, the results demonstrate that structural modulation of ferrocenyl derivatives through acetylaniline substitution significantly influences their electronic properties, electrochemical behaviour, and interaction profiles with acetylcholinesterase. Among the investigated compounds, FcMe4Ac emerges as the most promising candidate, combining optimal redox characteristics, strong binding affinity, high dynamic stability, and favourable pharmacokinetic properties, thereby representing a valuable scaffold for the development of novel anti-Alzheimer agents.

Key words: Ferrocenyl acetylaniline derivatives, AChE, Density functional theory, Molecular docking, ADMET.

Résumé

Ce travail présente la conception, la synthèse, la caractérisation physico-chimique et l'évaluation in silico approfondie d'une série de dérivés de l'acétylaniline ferrocénylique (FcMe2Ac, FcMe3Ac et FcMe4Ac), en mettant particulièrement l'accent sur l'élucidation des relations entre la structure moléculaire, les propriétés électroniques et le comportement d'interaction avec l'acétylcholinestérase (AChE), une cible enzymatique clé dans la maladie d'Alzheimer.

Les composés cibles ont été synthétisés par une stratégie de substitution nucléophile, donnant les régioisomères souhaités avec des rendements modérés à élevés (48–80 %) et une bonne reproductibilité. La confirmation de la structure a été obtenue grâce à des techniques spectroscopiques complémentaires, notamment la spectroscopie FT-IR, la spectroscopie UV-visible et des analyses RMN unidimensionnelles et bidimensionnelles. Les spectres FT-IR ont montré des bandes caractéristiques correspondant à l'étirement N–H (~3290–3445 cm^{-1}) et aux fonctionnalités carbonyles (~1647–1651 cm^{-1}), tandis que les spectres UV-visible ont révélé des maxima d'absorption dans la gamme de 259 à 432 nm, attribués à des transitions $\pi \rightarrow \pi^*$ au sein du système aromatique et à des transitions d–d centrées sur le métal. Les données RMN ont confirmé l'architecture moléculaire attendue, avec des signaux distinctifs correspondant à l'unité ferrocényle (~4,1–4,3 ppm) et aux protons aromatiques (~6,6–7,8 ppm).

La caractérisation électrochimique par voltamétrie cyclique a mis en évidence un processus redox Fe(II)/Fe(III) quasi-réversible pour tous les dérivés, avec des potentiels formels compris entre 43,9 et 57,5 mV. Les écarts entre les pics observés (ΔEp = 87,8–115 mV) et les rapports de courant proches de l'unité ont confirmé ce comportement quasi-réversible. Les coefficients de diffusion ($1{,}11 \times 10^{-7}$–$5{,}74 \times 10^{-7}$ $cm^2 \cdot s^{-1}$) et les constantes de vitesse de transfert d'électrons hétérogène ($0{,}14 \times 10^{-3}$–$0{,}62 \times 10^{-3}$ $cm \cdot s^{-1}$) ont indiqué que les propriétés de transport et cinétiques sont fortement influencées par le schéma de substitution.

Les calculs de la théorie fonctionnelle de la densité ont fourni des informations détaillées sur la structure électronique, révélant des énergies HOMO comprises entre −5,83 et −5,68 eV et des écarts HOMO–LUMO de 3,99–4,29 eV, indiquant une stabilité chimique modérée et une réactivité contrôlée. Les descripteurs de réactivité globaux ont confirmé ce comportement, avec des valeurs de dureté comprises entre 1,995 et 2,143 eV et des indices d'électrophilicité allant jusqu'à 3,519 eV. L'augmentation progressive du moment dipolaire (3,82–5,12 D) reflète une polarité moléculaire accrue dans toute la série.

Des études de docking moléculaire ciblant l'acétylcholinestérase ont démontré des affinités de liaison favorables (−7,34 à −8,58 $kcal \cdot mol^{-1}$), le FcMe4Ac présentant l'interaction

la plus forte. L'analyse du mode de liaison a révélé une stabilisation au sein de la gorge catalytique par le biais de contacts hydrophobes, d'empilements π–π et d'interactions par liaisons hydrogène impliquant des résidus clés.

Des simulations de dynamique moléculaire sur 100 ns ont confirmé la stabilité des complexes ligand-enzyme, avec des valeurs de RMSD se stabilisant entre environ 0,10 et 0,25 nm et une réduction des fluctuations des résidus, ce qui indique un mode de liaison stable et persistant.

Les prédictions ADMET in silico ont révélé des profils pharmacocinétiques et de sécurité favorables, notamment une absorption gastro-intestinale élevée, une lipophilie équilibrée (LogP = 3,12–3,45) et l'absence d'effets mutagènes ou hépatotoxiques prédits. Cependant, la perméabilité prédite limitée de la barrière hémato-encéphalique suggère qu'une optimisation supplémentaire pourrait être nécessaire pour améliorer la disponibilité dans le système nerveux central.

Dans l'ensemble, les résultats démontrent que la modulation structurelle des dérivés de ferrocényle par substitution d'acétylaniline influence significativement leurs propriétés électroniques, leur comportement électrochimique et leurs profils d'interaction avec l'acétylcholinestérase. Parmi les composés étudiés, le FcMe4Ac apparaît comme le candidat le plus prometteur, combinant des caractéristiques redox optimales, une forte affinité de liaison, une grande stabilité dynamique et des propriétés pharmacocinétiques favorables, représentant ainsi un squelette précieux pour le développement de nouveaux agents anti-Alzheimer.

Mots clés : Dérivés de l'acétylaniline ferrocénylique, AChE, Théorie fonctionnelle de la densité, Docking moléculaire, ADMET.

ملخص:

تقدم هذه الأطروحة تصميم وتركيب وتحليل الخصائص الفيزيائية والكيميائية وتقييمًا شاملاً عبر الحاسوب لسلسلة من مشتقات فيروسينيل أسيتيل أنيلي(FcMe2Ac، FcMe3Ac وFcMe4Ac) مع التركيز بشكل خاص على توضيح العلاقات بين البنية الجزيئية والخصائص الإلكترونية والسلوك التفاعلي تجاه إنزيم أستيل كولينستراز (AChE)، وهو الإنزيم المستهدف الرئيسي في مرض الزهايمر.

تم تصنيع المركبات المستهدفة عبر استراتيجية الاستبدال النووي، مما أدى إلى إنتاج الأيزومرات المكانية المطلوبة بنسب إنتاجية متوسطة إلى عالية (48–80٪) مع قابلية تكرار جيدة. تم تأكيد البنية من خلال تقنيات طيفية تكميلية، بما في ذلك التحليل الطيفي بالأشعة تحت الحمراء (FT-IR)، والتحليل الطيفي بالأشعة فوق البنفسجية والمرئية (UV–Visible)، وتحليلات الرنين المغناطيسي النووي (NMR) أحادية وثنائية الأبعاد. أظهرت أطياف FT-IR نطاقات مُميزة تتوافق مع تمدد N–H (~3290–3445 سم⁻¹) ووظائف الكربونيل (~1647–1651 سم⁻¹)، بينما كشفت أطياف الأشعة فوق البنفسجية والمرئية عن قيم امتصاص قصوى في النطاق 259–432 نانومتر، ترجع إلى انتقالات $\pi \rightarrow \pi^*$ داخل النظام العطري وانتقالات d–d حول المركز المعدني. أكدت بيانات الرنين المغناطيسي النووي (NMR) البنية الجزيئية المتوقعة، مع إشارات مميزة تتوافق مع وحدة الفيروسينيل (~4.1–4.3 ppm) والبروتونات العطرية (~6.6–7.8 ppm).

أظهرت الخصائص الكهروكيميائية التي تم تحديدها بواسطة القياس الدوري للجهد وجود عملية أكسدة واختزال شبه قابل للعكس لـــ Fe(II)/Fe(III) لجميع المشتقات، مع جهد رسمي يتراوح بين 43.9 و57.5 مللي فولت. وقد أكدت الفواصل بين القمم الملحوظة (ΔEp = 87.8–115 مللي فولت) ونسب التيار القريبة من الوحدة السلوك شبه قابل للعكس. وأشارت معاملات الانتشار (1.11×10^{-7}–5.74×10^{-7} سم²·ثانية⁻¹) وثوابت معدل نقل الإلكترونات غير المتجانسة (0.14×10^{-3}–0.62×10^{-3} سم·ثانية⁻¹) إلى أن خصائص النقل والحركية تتأثر بشدة بنمط الاستبدال.

قدمت حسابات نظرية وظيفية الكثافة نظرة ثاقبة مفصلة للبنية الإلكترونية، وكشفت عن طاقات HOMO تتراوح بين −5.83 و−5.68 eV وفجوات HOMO–LUMO تتراوح بين 3.99 و4.29 eV، مما يشير إلى استقرار كيميائي معتدل وتفاعلية خاضعة للسيطرة. أكدت واصفات التفاعلية الشاملة هذا السلوك، حيث تراوحت قيم الصلابة بين 1.995 و2.143 إلكترون فولت ووصلت مؤشرات الكهربية إلى 3.519 إلكترون فولت. يعكس الارتفاع التدريجي في عزم ثنائي القطب (3.82–5.12 D) زيادة في القطبية الجزيئية عبر السلسلة.

أظهرت الخصائص الكهروكيميائية التي تم تحديدها بواسطة القياس الدوري للجهد وجود عملية أكسدة واختزال شبه عكسية لـــ Fe(II)/Fe(III) لجميع المشتقات، حيث أظهرت دراسات الارتباط الجزيئي التي استهدفت إنزيم الأسيتيل كولينستراز وجود تفاعلات ارتباط مواتية (−7.34 إلى −8.58 كيلو كالوري/مول)، مع إظهار FcMe4Ac لأقوى تفاعل. كشف تحليل نمط الارتباط عن استقرار داخل الممر التحفيزي من خلال التلامس الكاره للماء، والتراص π–π، وتفاعلات الروابط الهيدروجينية التي تشمل بقايا رئيسية. أكدت محاكاة الديناميكا الجزيئية على مدى 100 نانو ثانية استقرار مجمعات الرابط-الإنزيم، حيث استقرت قيم RMSD في نطاق ~0.10–0.25 نانومتر وانخفضت تقلبات البقايا، مما يشير إلى نمط ارتباط مستقر ومستمر.

كشفت تنبؤات ADMET الحاسوبية عن ملامح دوائية وسلامة إيجابية، بما في ذلك امتصاص معدي معوي مرتفع، وجاذبية دهنية متوازنة (LogP = 3.12–3.45)، وغياب الآثار المتوقعة المسببة للطفرات أو التسمم الكبدي. ومع ذلك،

تشـــير النفاذية المتوقعة المحدودة لحاجز الدم-الدماغ إلى أنه قد تكون هناك حاجة إلى مزيد من التحســـين لتعزيز توافره في الجهاز العصبي المركزي.

في المجمل، تُظهر النتائج أن التعديل الهيكلي لمشـتقات الفيروسـينيل من خلال اسـتبدال الأسـيتيل أنيلين يؤثر بشـكل كبير على خصـائصـها الإلكترونية وسـلوكها الكهروكيميائي وخصـائص تفاعلها مع إنزيم الأسـيتيل كولينسـتراز. ومن بين المركبات التي خضـعت للدراسـة، برز مركب FcMe4Ac باعتباره المرشـح الواعد، حيث يجمع بين خصـائص الأكسـدة والاختزال المثلى، وقوة الارتباط العالية، والاســتقرار الديناميكي الكبير، والخصـــائص الدوائية الإيجابية، مما يجعله هيكلاً أساسياً قيماً لتطوير وسائل جديدة لمكافحة مرض الزهايمر.

الكلمات المفتاحية: مشتقات فيروسينيل أسيتيل أنيلي، أستيل كولينستراز (AChE)، نظرية وظيفية الكثافة، الارتباط الجزيئي، ADMET.

Abbreviations list

Abbreviation	Meaning
AChE	Acetylcholinesterase
AD	Alzheimer's disease
ADMET	Absorption, Distribution, Metabolism, Excretion, and Toxicity
ADT	AutoDock Tools
Å	Ångström
BBB	Blood–brain barrier
BChE	Butyrylcholinesterase
CADD	Computer-Aided Drug Design
CAS	Catalytic active site
CI	Configuration Interaction
Cm	Centimeter
Cp	Cyclopentadienyl
CQ	Chloroquine
D	Diffusion coefficient
DFT	Density Functional Theory
DNA	Deoxyribonucleic Acid
DMSO	Dimethyl sulfoxide
ELF	Electron localisation function
Fc	Ferrocene
FcOHTAM	Hydroxyferrocifene
FcTAM	Ferrocifene
FMO	Frontier Molecular Orbitals
FQ	Ferroquine
FT-IR	Fourier Transform Infrared Spectroscopy

GROMACS	GROningen MAchine for Chemical Simulations
HF	Hartree–Fock
HIV	Human Immunodeficiency Virus
HOMO	Highest Occupied Molecular Orbital
IC50	Half Maximal Inhibitory Concentration
Ipa	Anodic peak current
Ipc	Cathodic peak current
LMCT	Ligand-to-metal charge transfer
LOL	Localised orbital locator
LUMO	Lowest Unoccupied Molecular Orbital
Λmax	Absorption maximum
M	Molar
MD	Molecular Dynamics
MEP	Molecular electrostatic potential
MM-PBSA	Molecular Mechanics Poisson–Boltzmann Surface Area
MolSA	Molecular surface area
MPn	Møller–Plesset perturbation theory
Mm	Millimole per liter
NCI	Non-covalent interaction
Nm	Nanometer
NMR	Nuclear Magnetic Resonance
PAS	Peripheral anionic site
PDB	Protein Data Bank

Figures list

Tables list

Table of contents

GENERAL INTRODUCTION

GENERAL INTRODUCTION

The primary cause of dementia is Alzheimer's disease (AD), for which there is now no clinically proven therapy or way to halt its progression. Significant research has been done over the past two decades to comprehend the pathophysiology of AD, which has created a foundation for the development of successful pharmaceutical treatments.[1]

Following its discovery in the early 1950s, ferrocene (Fc), the first known and prototype metallocene, sparked a lot of interest. However, despite the fact that it was first discovered more than 50 years ago study effort did not completely stop once the intense period of pioneering studies focused mostly on comprehending its fundamental characteristics and reactivity had faded. Rather, it expanded into numerous areas of chemistry as well as affiliated neighbouring disciplines, where it is still growing in terms of publishing activity. These studies range from primarily academic research focused on investigating its use in the preparation of various organometallic compounds to practically focused applications in catalysis, material science, and, more recently, biomedicinal chemistry. Ferrocene has since been seen as a broadly applicable organometallic scaffold for the synthesis of functional derivatives that are being used in a wide range of applications rather than as a chemical curiosity. [2]

The synthesis of this sandwich system in all of its flavours, its adaptable reaction chemistry, its structural characteristics, the accompanying mechanistic and theoretical investigations, its application in homogeneous catalysis, particularly in stereoselective and asymmetric transformations, in electrochemistry, particularly in electron-transfer processes, as new materials including polymer chemistry, as fuel additives, as anticancer reagents, in bioorganometallic chemistry, etc., have all contributed to the fast growth and consequently rapidly expanding frontiers of this family of compounds .[3]

The use of Fc derivatives as agents for the treatment of neurodegenerative diseases, including the dementia caused by Alzheimer (AD), has received less research attention despite these advancements in many therapeutic fields. Fc's reversible oxidation capability, which can change the electron-donating Fc group into an electron-deficient ferrocenium cation (Fc+), is an appealing feature given the crucial role oxidative stress plays in AD development. Furthermore, there are instances of Fc derivatives that inhibit cholinesterases, exhibiting selective BChE inhibition as well as moderate to high inhibitory activity against acetylcholinesterase (AChE) and butyrylcholinesterase (BChE). Additionally, Fc moieties are often thought of as effective carriers that can improve targeted drug delivery to the brain by passing through the blood–brain barrier (BBB).[4]

Based on the ferrocene applications mentioned above, we proposed a research topic titled: Targeting Acetylcholinesterase: Design, Synthesis and Multimodal Evaluation of Ferrocenyl Acetylaniline Derivatives as Potential Anti-Alzheimer Agents. Therefore, the objective of this work was to synthesize several ferrocene derivatives in the laboratory, to study the interaction of the synthesized ferrocene derivatives with Acetylcholinesterase and the in silico ADMET predictions using methods adopted in our study: FT-IR, UV–Visible spectroscopy, one- and two-dimensional NMR analyses, cyclic voltammetry, Density functional theory calculations and molecular docking (The calculations were performed using the Gaussian9 and AutoDock Tools software).

This study is divided into two main parts:

❖ The first part consists of a bibliographic overview, which is itself divided into two chapters (Ferrocene Derivatives: Structure, Reactivity and Applications and Computational Approaches in Molecular Modelling and Drug Design).

❖ The second part covers materials and methods, while by the end it presents the results and discussion, including a presentation of the various results obtained and their interpretations.

Part I:
Bibliographic Study

Chapter 1: Ferrocene Derivatives: Structure, Reactivity and Applications

1. Introduction

In 1951, the first report on ferrocene synthesis was released. Kealy and Pauson unintentionally discovered it while attempting to synthesize fulvene by reacting (cyclopentadienyl) magnesium bromide with FeCl2. Instead, they discovered an orange-coloured solid that proved to be highly resistant to acids and bases [5].

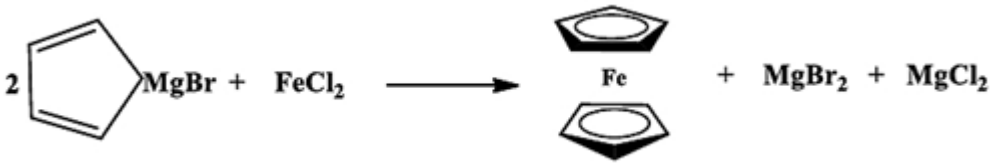

Figure I.1: The first synthesis of ferrocene.[6]

The first publications represented the compound with a linear structure of two monohapto cyclopentadienyl ligands as [Fe(η1C5H5)].2 in which a sigma bond connects the iron to the cyclopentadiene. It wasn't until Wilkinson and Fischer independently proposed the actual sandwich structure [Fe(η5-C5H5)]2 shortly afterwards that it was revealed. Wilkinson employed chemical, physical, and spectroscopic techniques to determine the precise structure of dicyclopentadienyl iron, while Fischer utilized X-ray crystallography to characterize the compound [7] [8] [9] [10].

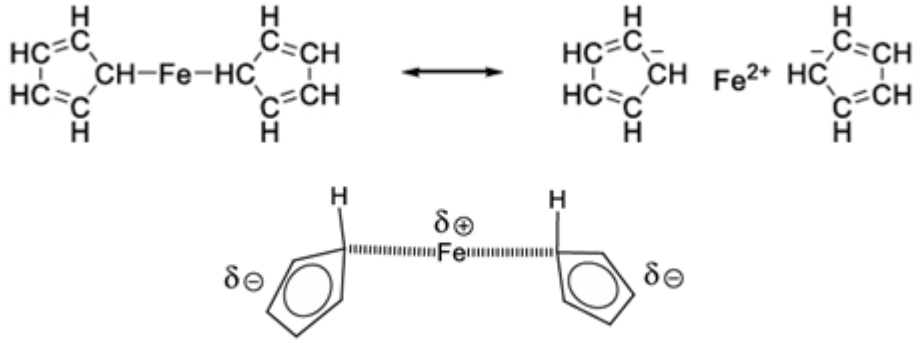

Figure I.2: First proposed structure for ferrocene.[8] [10]

This chapter is dedicated to a bibliographic review of ferrocene and its derivatives, covering its main physical, chemical, and electronic properties along with its reactivity and biological and pharmacological applications.

2. Structural and Electronic Properties of Ferrocene

Ferrocene is an organometallic compound built of two Cp (cyclopentadienyl) rings [11], each of which has a negative charge and is attached to a Fe2+ central atom[4]. A solid crystallized at room temperature, orange in colour and with a camphor-like odor, highly stable

in air, with the formula Fe(C5H5)2 (FigureI.3). Its solubility in most organic solvents but not in water can be explained by its zero dipole moment. The carbon atoms are equidistant from one another and from the metal. The weak barrier of rotation along the metal-cycle axis (4 kJ.mol 1) is predominantly caused by Van der Waals forces between the two cyclopentadienyl groups [12].

Bonds	**Distance**
Fe−C	2,05 Å
C−C	1,43 Å
Cp	3.3 Å

Figure I.3: Ferrocene in the form of an orange powder.[13]

The short distance between two cyclopentadiene indicates the close proximity of the substituents in both rings and syn-conformations may be favoured by supramolecular interactions such as H-bonding or π-π interactions. In contrast, interactions due to electrostatic repulsions may favour anti-conformations over syn-conformations. Ferrocene may therefore be tapped as a switch between syn- and anti-conformations.

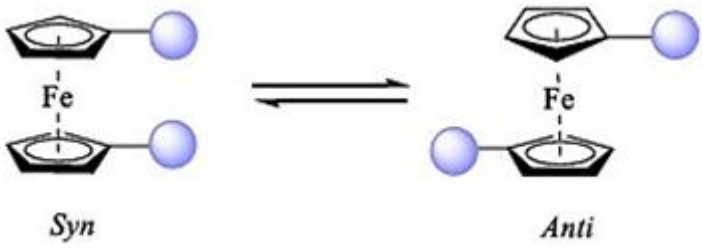

Figure I.4: Substituted ferrocene with syn and anti-conformations.[14]

Ferrocene has a pentagonal anti-prismatic structure; It exhibits D5h and D5d symmetries in eclipsed and staggered conformations, respectively[14].

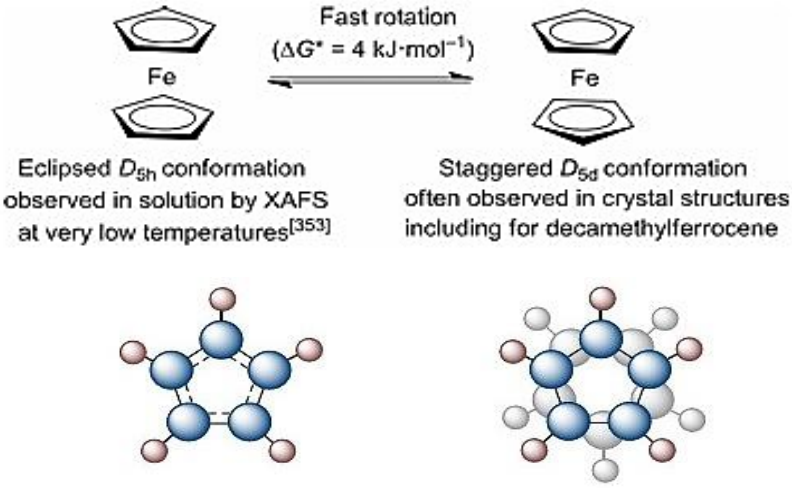

Figure I.5: The two conformations of ferrocene. [9][14]

Differentiation of ferrocene arrangements is a result of a mere energy barrier value between the highest occupied molecular orbitals HOMOs and the lowest unoccupied molecular orbitals LUMOs of the eclipsed and staggered conformer. The schematic representation of the general molecular orbital diagram for generic metallocenes, Cp2M, is presented below, taking ferrocene as an example.

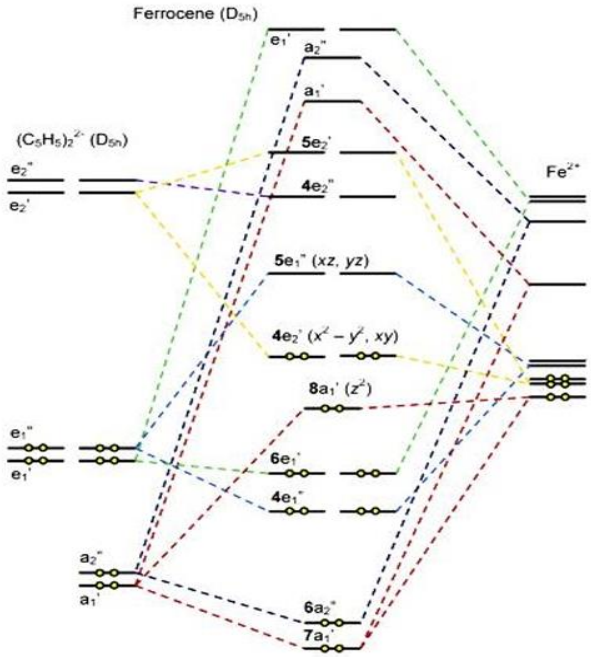

Figure I.6: Molecular orbital diagram of ferrocene molecule.[6]

Ferrocene being the most stable member of the metallocene family simply because it obeys the 18-valence electron rule. The hydrogen atoms on the Cp rings in ferrocene are also proven to be slightly tilted towards the iron center by neutron diffraction studies. This shift is presumably owing to the fact that it permits the Fe orbitals to have a better overlap with the Cp rings' π-orbitals [15].

Infrared spectroscopy of ferrocene shows an absorption band at 3075 cm^{-1} equivalents to the stretching of the aromatic C-H bond. There are four other apparent bands: two at 811 and 1002 cm^{-1} associated with the flexion vibration of C-H, and one at 1108 cm^{-1} associated with antisymmetric ring deformation. The absorption band at 1411 cm^{-1} corresponds to the asymmetric C–C stretching vibration of the unsubstituted cyclopentadienyl group[10].

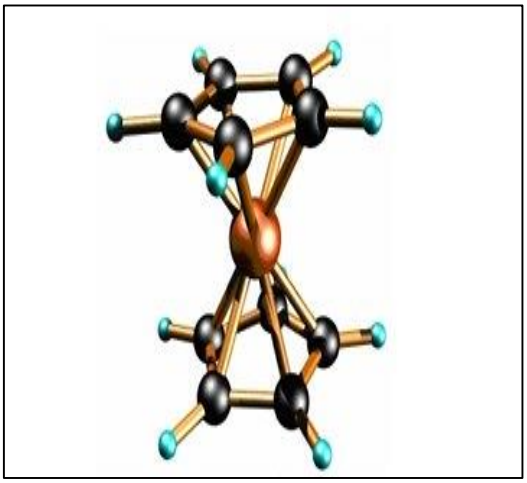

General properties of ferrocene [10]

Molecular weight: 186.04 $g.mol^{-1}$

Boiling point: 249 °C

Melting point: 173-174 °C

Decomposition above 400 °C

Solubility in water is about 0.1 mg/ml at 21 °C, 100 mg/ml in DMSO at 19.5°C.).

Figure I.7: Structure model of ferrocene.[16]

The angle between two consecutive substituents on ferrocene averages 72°, which is greater than the corresponding angle in benzene, which is 60°. The angle between two substituents of ferrocene at positions 1 and 3 is 144°, intermediate between the 1,3 (120°) and 1,4 (180°) substitutions of benzene; this wider angle suggests potential applications in the design of molecules capable of binding to cell-level active sites.

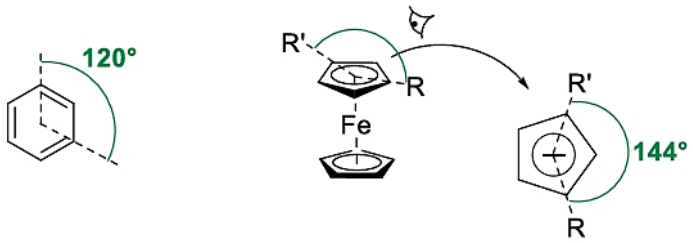

Figure I.8: Difference in angles between benzene and ferrocene.[8]

3. Synthesis and Functionalisation of Ferrocenyl Derivatives

The synthesis of ligands is a broad field within ferrocene chemistry that is worthy of further study. Due to the ease with which electrophilic aromatic substitution can occur on cyclopentadienyl rings, a wide range of ferrocene derivatives has been reported in the literature since its discovery. The well-defined electrochemical and spectroscopic behaviour, chemical stability, and low toxicity of ferrocene[12], make this organometallic compound the foremost choice as starting material in the synthesis of various ferrocenyl derivatives[15].

Substituted ferrocenes can be prepared directly or indirectly. In the direct synthesis, the substituted ferrocene is created by reacting a suitably substituted cyclopentadiene derivative compound with iron using procedures that are comparable to those used to prepare ferrocene itself. In the indirect preparation, the ferrocene molecule serves as a starting point for the synthesis of other ferrocene derivatives [17].

A total of three concepts has been raised to explain ferrocene's electrophilic substitution (E'+'). In the first mechanism, electrophilic substituents interact with the iron atom's weakly bonding electrons. The electrophilic substituent then transfers to the Cp ring in the endo position, where it forms substituted ferrocene following proton elimination (Route I). According to the second mechanism, the product is formed after proton loss, and electrophilic attack takes place on the less hindered exo face of the ligand's ring without involving direct engagement of the metal (Route II). In the third mechanism, the electrophile is added to the ligand's endo face without any metal interaction (Route III).

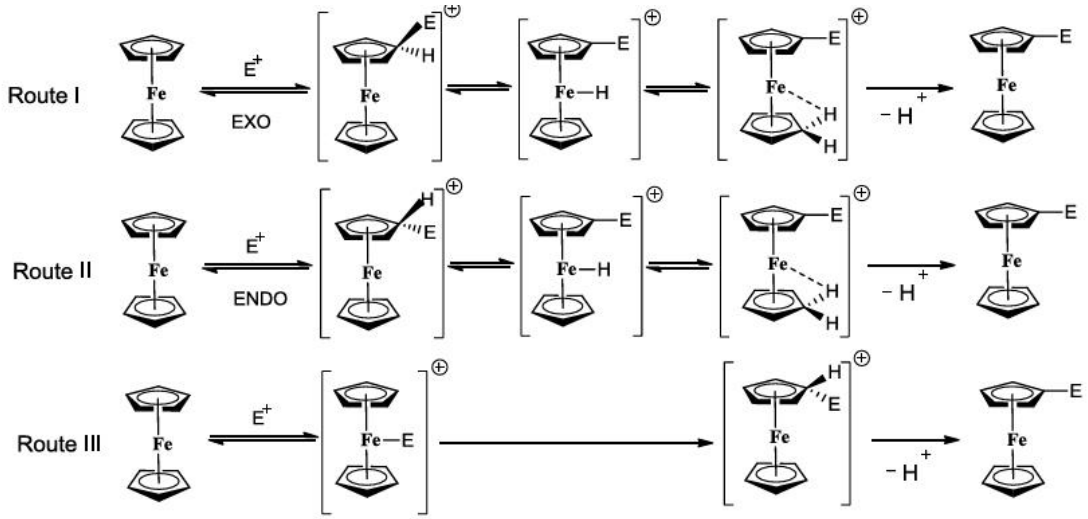

Figure I.9: Proposed mechanisms for electrophilic substitution of ferrocene.[7]

Ferrocene undergoes several electrophilic reactions more easily and quickly than benzene, except with highly oxidizing electrophiles such as H_2SO_4 or HNO_3. Formylation and

carboxylation reactions generally result in a single substitution on the ring because the introduced group is highly disabling toward the sandwich. Metallation or acylation may be followed by a second identical reaction on the second ring, leading to a derivative known as 1,1'-disubstituted. The ferrocene derivatives most used for functionalization are acetylferrocene, carboxaldehyde ferrocenes, lithium ferrocenes, and chloromercury ferrocenes. Lithiation and dilithiation reactions are used to introduce many other functional groups. Various electrophiles can react with lithium ferrocenyl derivatives[10].

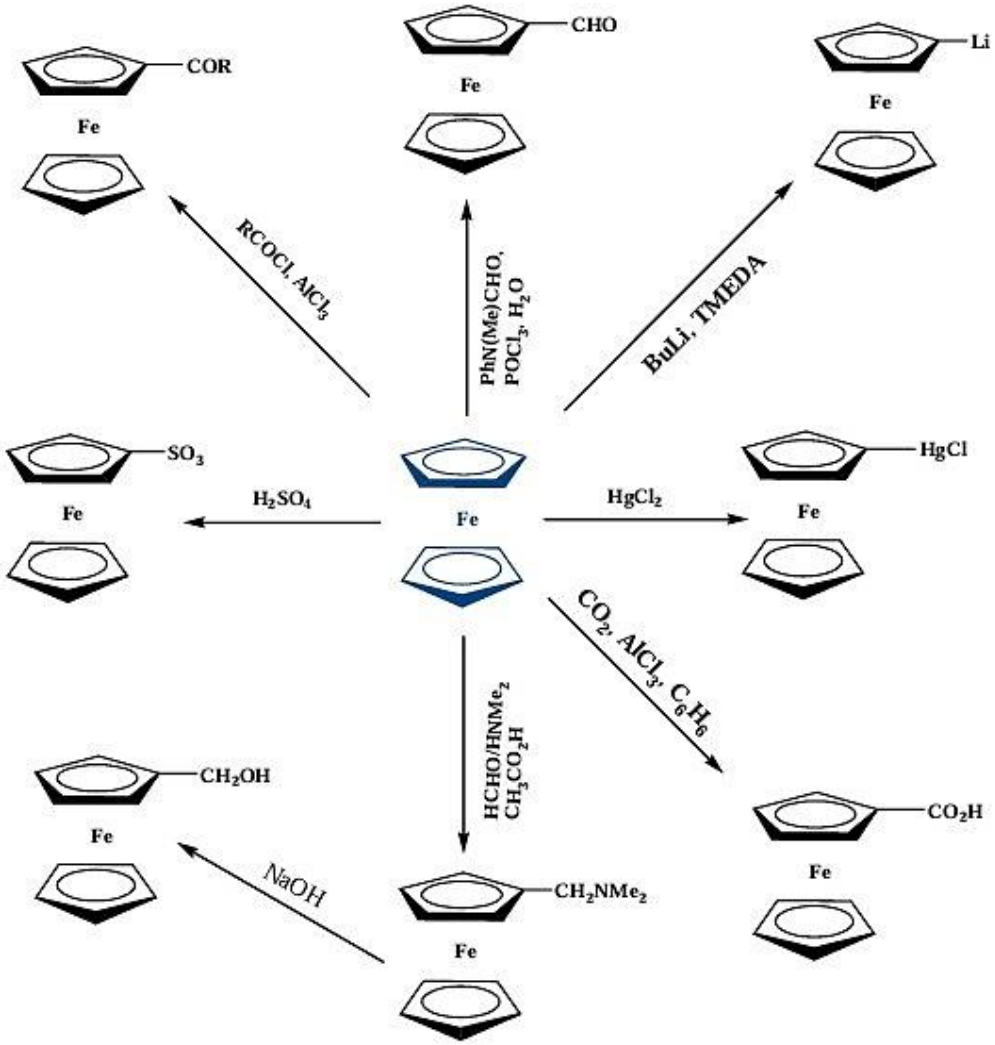

Figure I.10: The important substitution reactions of ferrocene.[18]

One of the most widely utilised intermediates for the synthesis of substituted ferrocenes is N,N-dialkylaminomethylferrocene derivatives, such as N,N-dimethylaminomethylferrocene. A great deal of monosubstituted ferrocene derivatives are prepared employing ferrocenylmethyltrimethylammonium iodide as a starting material.

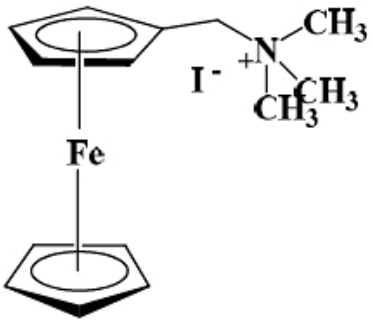

Figure I.11: The structure of ferrocenylmethyltrimethylammonium iodide.[19]

The main structure of the majority of derivatives based on substitution processes is the quaternary salt of ferrocinylmethyltrimethylammonium iodide, which facilitate the nucleophilic substitution including alkoside ions, cyanide, Grignard reagents, carbon reagents, amines.

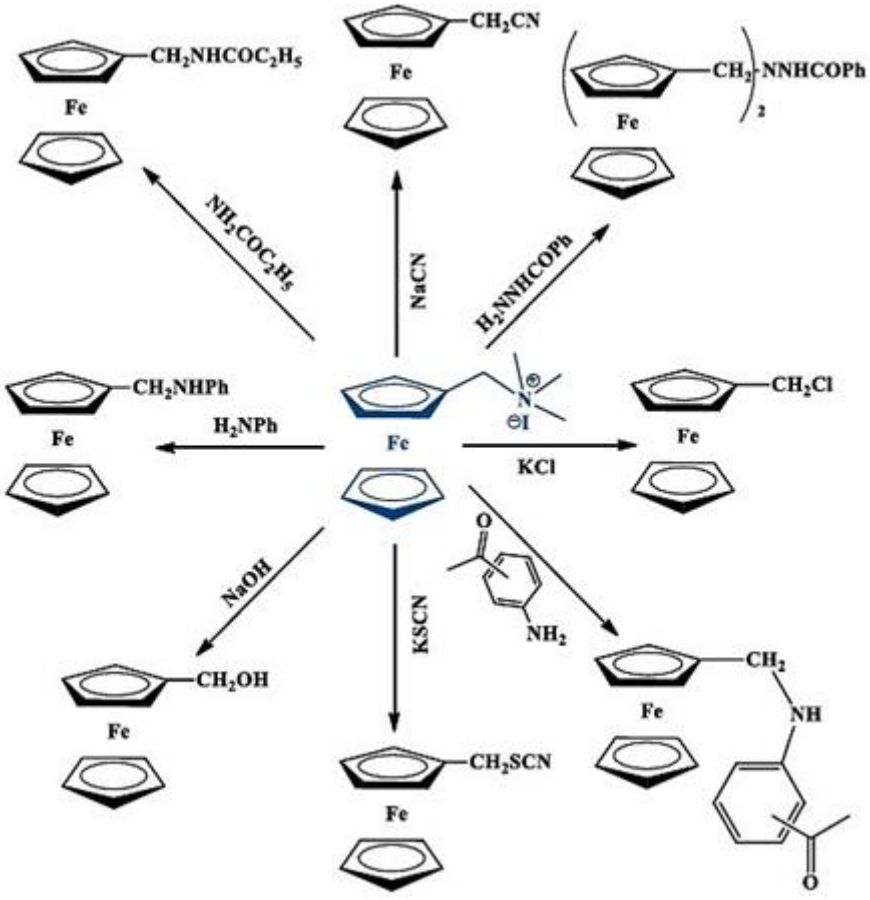

Figure I.12: The important substitution reactions of the quaternary salt.[18]

4. Electrochemical Behaviour of Ferrocene Compounds

From an electrochemical perspective, a calomel electrode can oxidise ferrocene in the +2 oxidation state (where Cp is a monoanionic ligand) once at a minimal potential of 0.5 V. [20],

The redox process is a very visual reaction that manifests in a colour shift from orange, which is characteristic of ferrocene, to dark blue, corresponding to the ferrocenium ion Fe(III) [8]. The ferrocene/ferrocenium pair can be used as a reference in electrochemistry due to the reversibility of the redox reaction. Additionally, the oxidation can be done with silver nitrate or in the presence of FeCl3 to produce the [Fe(C6H5)2]+ ion. The redox properties of ferrocene provide various applications in medicinal chemistry[20].

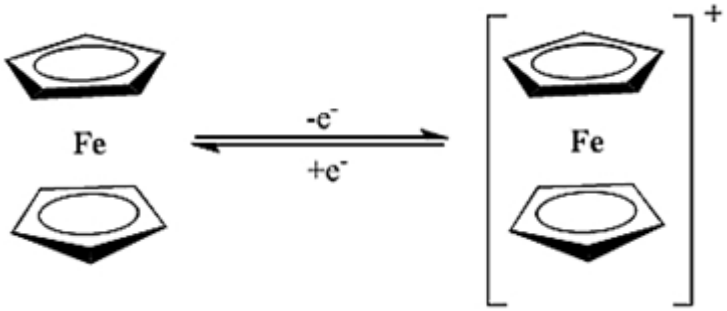

Figure I.13: Reversible mono electronic oxidation of ferrocene.[21]

The reversibility of the redox reaction was evidenced by cyclic voltammetry; the electrochemical parameters extracted from the ferrocene voltammogram indicate that the redox process is quick, reversible, and monoelectronic.

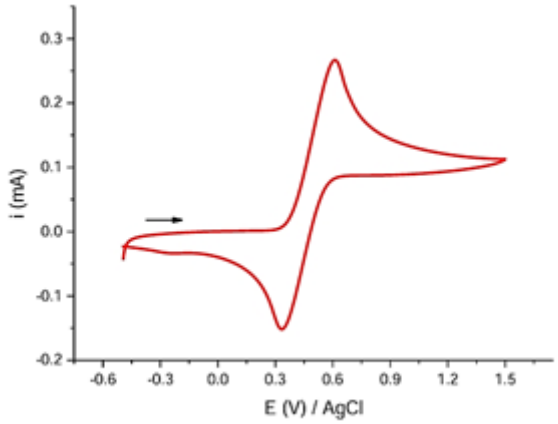

Figure I.14: Ferrocene voltammogram recorded on a platinum electrode in acetonitrile 10-3 M in the presence of Tetrabutylammoniumpairchlorate 10-1 M at υ = 100 mv/s.[17]

Ferrocene's UV-Vis spectrum reveals two primary wavelengths at 324 and 441 nm, signalling that the transition is of the (d-d) type.

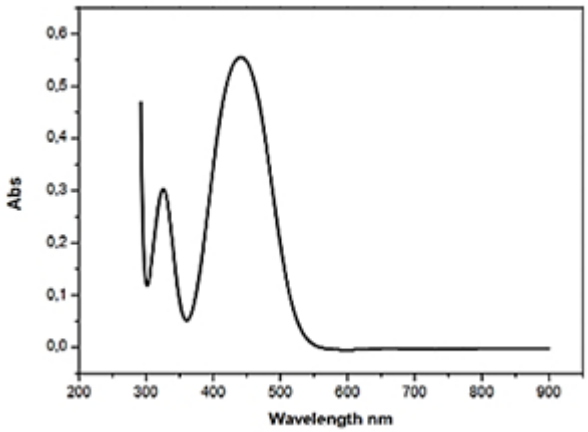

Figure I.15 : UV-VIS spectrum of a diluted ethanol solution of ferrocene.[18]

The ferrocene molecule's NMR 1H spectrum is quite straightforward, with a single peak at 4.15 ppm which refers to the ten protons of two cyclopentadienyl cycles.

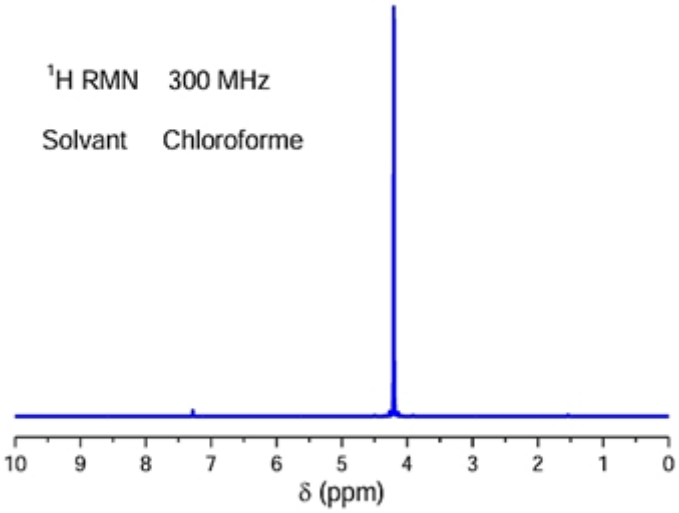

Figure I.16: NMR 1H spectrum of Ferrocene.[17]

Accordingly, a single peak at 68 ppm in ferrocene's NMR 13C spectrum represents the ten carbon atoms of two cyclopentadienyl rings.

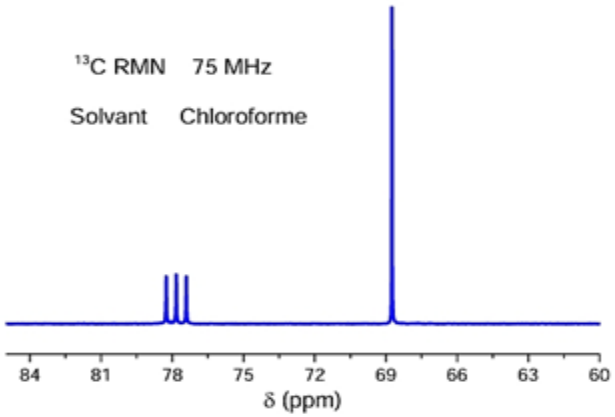

Figure I.17: NMR 13C spectrum of Ferrocene.[17]

5. Biological and Pharmacological Relevance of Ferrocene Derivatives

5.1 Pharmacological Activity

Ferrocenyl derivatives with low oxidation potentials are attracting attention due to their ability to catalyze the production of reactive oxygenated species under physiological conditions that generate cytotoxic effects.[22] Some ferrocene derivatives have shown cytotoxicity against lung tumors [23] and breast cancer,[24] antiproliferative effects in vitro,[25] and DNA detection [26] and antimalarial [27] activities.

5.1.1. Anticancer Activity

Interest in ferrocene for medicinal chemistry began around 1984, when certain salts of ferrocenium were found to have antitumor effects [28–29]. Based on this observation, it was proposed that ferrocene compounds could be oxidized inside the cell and that such oxidation could be responsible for these cytotoxic effects.

Furthermore, it was proposed that the activity of ferricenium ion derivatives could not be linked to direct intercalation into DNA. However, it was observed that these species were capable of generating HO• radicals in cancer cells and rapidly damaging their DNA. Subsequent studies have confirmed the ability of ferrocenium salts to produce reactive oxygen species (ROS) as a result of their degradation in water in the presence of oxygen [30]. In this way, the toxicity of these species leads to oxidative DNA damage through the production of ROS concurrent with their degradation. [31]

One of the most frequently cited examples in the literature of a biologically active ferrocene derivative that exhibits antitumor effects is the combination of ferrocene and tamoxifen. Tamoxifen is an antagonist of certain estrogen receptors located in the breast; it inhibits the proliferation of hormone-dependent breast cancer [32].

The source of the activity of these ferrocene derivative appears to be the redox properties of ferrocene, which allow for intramolecular oxidation, thereby producing a toxic metabolite. The simple replacement of the β-phenyl group with a ferrocenyl group and the homologation of the alkyl chain of the tamoxifen (TAM) molecule or its active metabolite, hydroxy tamoxifen (OHTAM), yielded the derivatives ferrocifene (FcTAM) and hydroxyferrocifene (FcOHTAM), respectively [33,34]

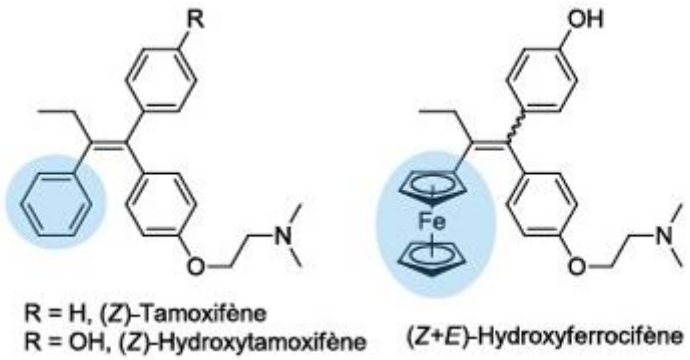

Figure I.18: L'hydroxyferrocifène, bioisostère de l'hydroxytamoxifène [35]

5.1.2. Antimalarial Agents

Malaria is one of the most problematic parasitic infections in the world. Chloroquine (CQ), mefloquine and quinine are the most effective drugs against malaria. [36–37] The most dangerous parasite.

Plasmodium falciparum, is however becoming resistant to these drugs. Therefore, synthesis of newly ferrocenyl anti malarial agents has attracted many authors. Ferroquine (FQ) derivatives 39, 40, 41 and 42 are novel antimalarial compounds currently in phase I clinical trials. FQ is a unique ferrocenyl compound designed to overcome the CQ resistance. Indeed, FQ was more potent than CQ in the inhibition of growth of P. falciparum in vitro and on P. berghei in vivo. Also, FQ showed 22-fold higher activity than chloroquine in vivo in mice infected with P.berghei and P. yoelii NS, and no significant evidence of toxicity of ferrocenes was detected. Synthesis of FQ was based on incorporation of ferrocenyl moiety with chloroquine to give FQ. [38]

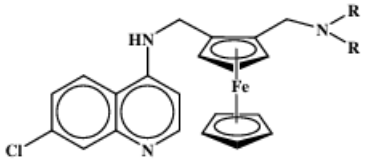

R = H, **39**; R = Me, **40**; R = Et, **41**; R = t-Bu, **42**

Figure I.19: Chemical structure of Ferroquine Derivatives with anti malarial activity [38]

Other ferrocenyl derivatives have been prepared from triazacyclononane and evaluated against chloroquine sensitive (HB3) and chloroquine-resistant (Dd2) Plasmodium falciparum. The most effective one was 7-chloro-4-[4-(7 chloro-4-quinolyl)-7-ferrocenylmethyl-1,4,7-triazacyclono nan-1-yl] quinoline. It showed potent antimalarial activity in vitro against the chloroquine-resistant strain Dd2.

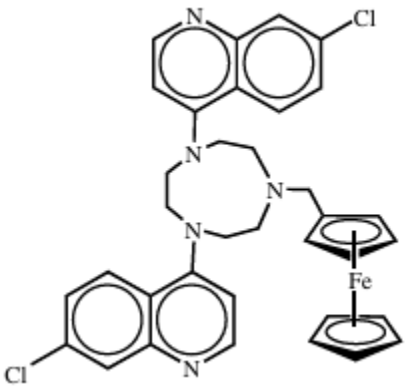

Figure I.20: 7-chloro-4-[4-(7 chloro-4-quinolyl)-7-ferrocenylmethyl-1,4,7-triazacyclono nan-1-yl] quinoline [38]

5.1.3. Anti-HIV Activity

Topoisomerases are enzymes that control the topological structure of DNA (including HIV DNA) by cleaving one (topoisomerase I) or both (topoisomerase II) of the DNA strands. They play a central role in cell division and transcription. Inhibition of topoisomerases is an important target in the discovery of anticancer drugs, as well as in anti-HIV therapy.

Indeed, it has also been shown that topoisomerase II activity is necessary for HIV-1 replication.

Kondapi and colleagues studied the impact of ferrocene azalactone and ferrocene thiomorpholide amidomethyl on cell proliferation and various phenomena of the HIV-1 replication cycle -1; they demonstrated that these compounds are selective topoisomerase I inhibitors, exhibiting IC50 values for the inhibition of catalytic activity of 50 and 100 µM, respectively.

The two topoisomerase II inhibitors demonstrated significant anti-HIV activity with inhibition of proviral DNA synthesis, as well as the formation of pre-integration complexes [39]

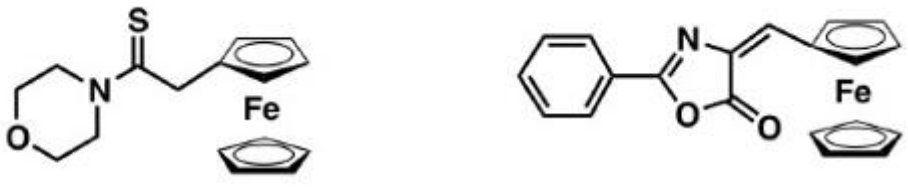

Figure I.21: Structure of ferrocenic derivatives with anti-HIV activity [40.41]

5.1.4. Antibacterial Activity

Ferrocene chemistry has had a huge impact in numerous applications, such as: pharmaceutical applications (the production of antibiotics such as penicillin, cephalosporins, and rifamycins). One of the first applications in this field was the development of ferrocene derivatives of antibiotics derived from the modification of β lactams by inserting a ferrocene moiety into their structure, such as (ferrocenyl penicillin and ferrocenyl-cephalosporin), synthesized by Edwards and colleagues to combat certain bacteria. This work was followed by numerous attempts to introduce ferrocene into antibiotics; some of these compounds demonstrated good activity and selectivity against Gram-positive bacteria [12].

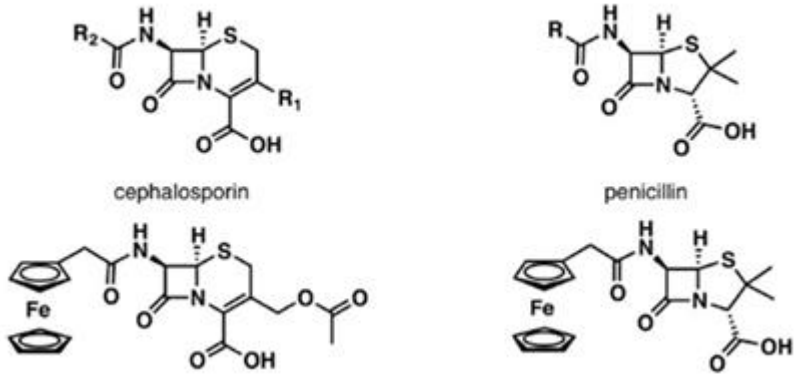

Figure I.I.22: Penicillin and cephalosporin structures and their corresponding ferrocene derivatives [12]

5.1.5. Antifungal Activity

Table I.1 summarizes the results of the evaluation of the antifungal activity of 3-nitrophenylferrocene against two pathogenic yeast species. Based on these results, it was found that the compound exhibits promising antifungal activity against two yeast strains (Aspergillus niger, Aspergillus flavus). These results suggest that the compound exhibits selective activity against the yeasts studied [42].

Fungal Type	Concentration (Mg/100ml)	Negative control growth DMSO	Culture length (cm)	Fungal growth length (cm)	%Inhibition of fungal growth
Aspergillus niger	3.00	11.00	12.50	7.50	40.00
	5.00	11.50	12.50	6.30	49.60
	20.00	11.00	12.50	2.20	82.40
Aspergillus flavus	3.00	10.00	12.50	7.00	50.70
	5.00	10.00	12.50	5.40	65.50
	20.00	10.00	12.50	1.50	89.50

Table I.1: Antifungal activity of 3-nitrophenylferrocene [42].

1.5.2. BIOLOGICAL Activity

1.5.2.1. Ferrocene-based topoisomerase II (Topo II) inhibitors

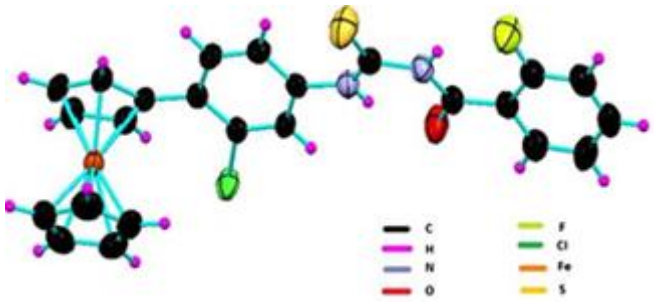

Figure I.23: Chemical and molecular structure of 1-(2-fluorobenzoyl)-3-(2 chloro-4-ferrocenylphenyl) thiourea [43]

1.5.2.2. Electrochemical gene detectors

The F4ND hybridization indicator, containing four ferrocene units, exhibits strong intercalation with double-stranded DNA and enables sensitive electrochemical discrimination between methylated and unmethylated gene sequences

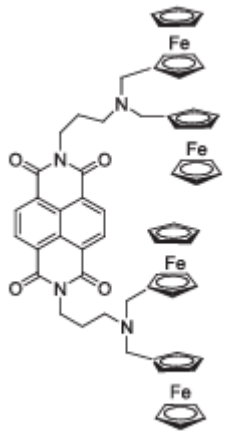

Figure I.I.24: Structure of the naphthalene diimide–ferrocene hybrid (F4ND) [43]

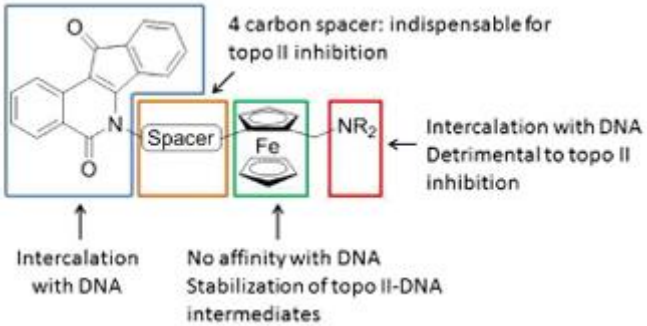

Figure I.I.25: Structure–activity relationships of ferrocenyl derivatives [43]

6. CONCLUSION

In conclusion, ferrocene and its derivatives represent a remarkable class of organometallic compounds distinguished by their unique structural features and outstanding redox properties. These characteristics have enabled their extensive application across multiple scientific domains, including materials science, catalysis, and medicinal chemistry. The versatility of ferrocenyl derivatives is particularly evident in their wide-ranging biological and pharmacological activities, where their incorporation into known drug frameworks often enhances efficacy and broadens therapeutic potential.

Notably, several ferrocenyl-based compounds have demonstrated promising results in biomedical applications, especially in anticancer and antimalarial therapies, with examples such as ferrocifens and ferroquine showing significant activity both in vitro and in vivo, alongside low toxicity profiles. Furthermore, the electrochemical properties of ferrocene have facilitated the development of advanced sensing systems for biological and environmental targets, highlighting their importance in modern analytical technologies.

Overall, the continuous progress in the synthesis, functionalization, and application of ferrocene derivatives underscores their growing significance in both fundamental research and applied sciences. This field remains highly dynamic and promising, offering vast opportunities for the design of novel compounds with enhanced properties, thereby paving the way for future innovations in chemistry and medicine [38.43].

Chapter 2: Computational Approaches in Molecular Modelling and Drug Design

1. INTRODUCTION

For centuries, natural products—particularly those derived from plants—have played a central role in the treatment of various diseases. Numerous bioactive compounds such as artemisinin, quinine, vinblastine, and taxol have demonstrated remarkable therapeutic efficacy against serious conditions including malaria and cancer. Despite these advances, many diseases such as cancer, HIV/AIDS, and metabolic disorders remain major global health challenges, highlighting the urgent need for the discovery of novel, safe, and effective therapeutic agents. Moreover, conventional drug discovery methods are often costly, time-consuming, and associated with high failure rates, typically requiring over a decade of research and substantial financial investment before reaching clinical application.

In response to these limitations, modern drug discovery has increasingly shifted toward the integration of computational approaches, commonly referred to as computer-aided drug design (CADD). These approaches combine advances in computational chemistry, bioinformatics, and artificial intelligence to accelerate and optimize the drug development process. CADD techniques enable researchers to identify biological targets, screen large libraries of compounds, and optimize lead molecules with improved efficiency and reduced cost. As a result, they play a crucial role in addressing global health challenges and contribute significantly to sustainable development goals related to health and innovation.

Among the various computational methods, Density Functional Theory (DFT) has emerged as a powerful quantum mechanical tool for investigating the electronic structure and physicochemical properties of molecules. DFT provides valuable insights into molecular reactivity, stability, and electronic descriptors such as HOMO–LUMO energies, which are essential for understanding drug–receptor interactions at the atomic level. These theoretical calculations support the rational design and optimization of potential drug candidates.

Complementing quantum mechanical approaches, molecular docking is widely used in structure-based drug design to predict the binding orientation and affinity of ligands within the active site of target proteins. This technique facilitates virtual screening and helps identify promising compounds by evaluating ligand–protein interactions. However, docking provides a static representation of molecular interactions; therefore, it is often coupled with molecular dynamics (MD) simulations, which offer a dynamic perspective by analyzing the stability, flexibility, and conformational changes of biomolecular systems over time under physiological conditions.

In addition to structural and interaction studies, the evaluation of pharmacokinetic and toxicological properties is essential for successful drug development. The prediction of

ADMET properties (Absorption, Distribution, Metabolism, Excretion, and Toxicity) allows early assessment of drug-likeness and safety profiles, thereby reducing the risk of failure in later stages of development. These in silico evaluations are crucial for prioritizing compounds with optimal biological activity and minimal adverse effects.

Overall, the integration of DFT calculations, molecular docking, molecular dynamics simulations, and ADMET prediction constitutes a comprehensive and synergistic framework for rational drug design. These computational approaches significantly enhance the efficiency, accuracy, and success rate of drug discovery processes. With continuous advancements in computational power and artificial intelligence, these methodologies are expected to play an increasingly vital role in the development of innovative therapeutic agents capable of addressing complex diseases and improving global health outcomes [44.45]

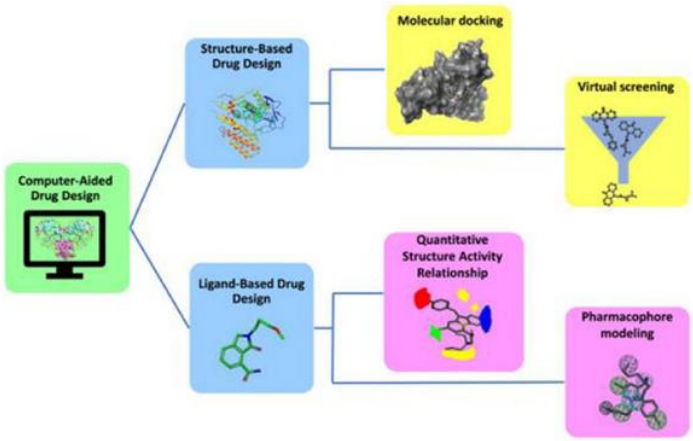

Figure I.26: Drug discovery process and identification using various computational methods [44]

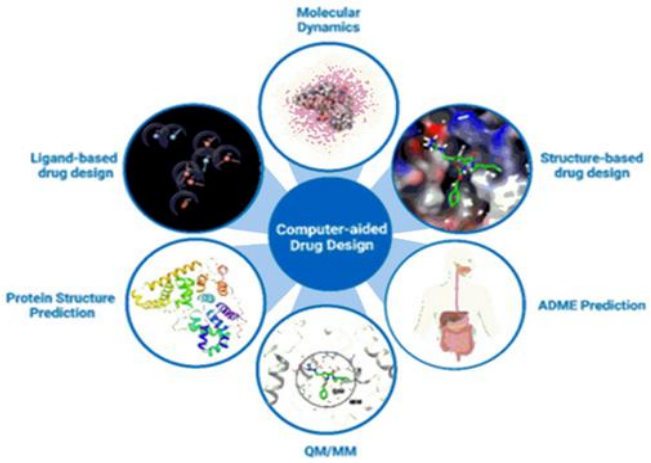

Figure I.27: The computation resources used in predicting molecules with potential therapeutic effects [44]

2.Density Functional Theory (DFT) Analysis

The Hartree–Fock (HF) methods exclude electron correlations and thus may not describe some properties of drug can didates precisely. Similarly, the post-HF methods, configuration interaction (CI) and Møller-Plesset perturbation (MPn) theory consider electron correlations flawed by high computational costs. DFT is cost-effective, with high computational accuracy and less computational time than MPn, HF, and CI methods. In view of this, DFT has inspired intense scholarly interest in studying molecular properties. DFT has demonstrated its efficacy in studying the geometries of smaller drug molecules, demonstrating its suitability in drug design. A crucial step in drug design using DFT is the study of energetic properties such as metal–ligand bond strengths, relative energies, ionization energies, and electron affinities. The properties and the interactions of drug molecules with their receptors are governed by their molecular structures. Therefore, the DFT technique has been conveniently used in computational drug design to predict relative conformational energies. Numerous studies have reported that possible interactions between a drug and a receptor include charge transfer, dipole–dipole interactions, ionic interactions, ion–dipole interactions, covalent bonds, hydrophobic interactions, and hydrogen bonding. DFT method (c.f Fig. 12) provides reasonable predictions for covalent, ionic, and hydrogen bonding; however, interactions for weaker bonds have been difficult to predict. Quantum chemistry software packages such as ADF employ DFT in electronic structure calculations and elucidate spectroscopic properties such as nuclear magnetic resonance (NMR), infrared (IR), and vibrational frequency spectra. Further, ADF can also be used for molecular geometry optimization, to explore the role of catalysis in reactions, and to study reaction channels and activation energies of systems being studied. There are a significant number of research reports that have shown that DFT has been used for structure elucidation and modelling the interactions between the drug and the receptor. This computational tool has also shown proficiency in modelling metal-containing biological systems in the study of inorganic therapeutics. Figure I.28 depicts a graphical representation of ligands' structural accuracy and binding affinity. The ligands are pre dicted using two DFT-based energy functionals, namely B3LYP and CAM-B3LYP. The predictions were then compared to experimental data. The x-axis represents the experimental binding affinity value, while the y-axis represents the calculated binding affinity value using the two DFT methods. Data points closer to the diagonal line indicate better structural accuracy and binding affinity prediction as they are more closely aligned with the experimental data. The graph demonstrates that both methods exhibit strong performance in predicting structural accuracy and binding affinity [44]

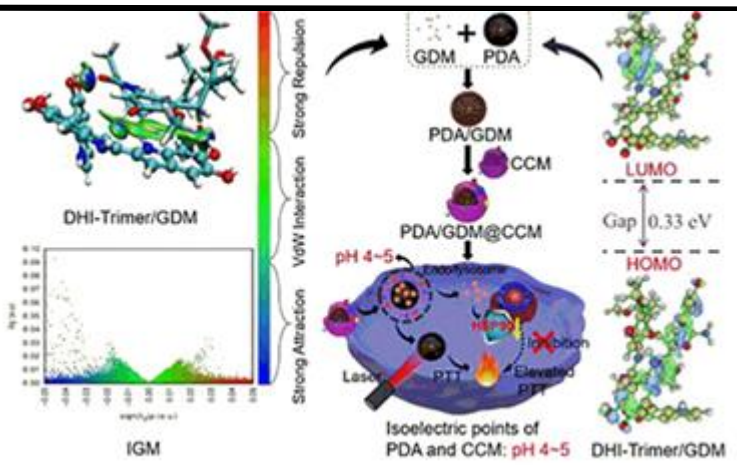

Figure I.28: The DFT method (B3LYP and CAM-B3YLP) in Drug Design [44]

We conducted a density functional theory (DFT) analysis to examine the electronic properties of the best-identified hit from virtual screening. We used the Gaussian 09 software tool to perform geometry optimisation and total energy calculations, utilising the Becke-3-Lee Yang–Parr (B3LYP) function with the standard 6–311 + + G (d,p) basis set. Visualisation of the structure and the analysis of the outputs were carried out with Gauss-View software. Frontier Molecular Orbital (FMO) studies can predict compounds' chemical reactivity and identify their stability. We calculated the energies of the highest occupied molecular orbital (HOMO), the lowest unoccupied molecular orbital (LUMO), and the gap between them to study the chemical stability of the identified molecule. We found out the new inhibitor's chemical potential (μ), chemical hardness (η), chemical soft ness (S), and global electrophilicity (ω). We derived the 'index' mathematically using Eq. (1), taking into account the frontier molecular orbitals LUMO and HOMO. The chemical hardness (η), chemical softness (S), and global electrophilicity (ω) were computed using the expressions (2), (3), and (4), respectively [45].

$$\mu = (E_{HOMO}+E_{LUMO})/2 \quad (1)$$

$$\eta = E_{LUMO}-E_{HOMO} \quad (2)$$

$$S=1/\eta \quad (3)$$

$$\omega=\mu 2/2\eta \quad (4)$$

3. Protein–Ligand docking

The protein–ligand docking study of the chosen protein–ligand complex was performed by using the virtual screening software interface PyRx (Autodock Vina) tools version v0.8. During docking analyses, protein structures were kept rigid and ligands were kept flexible [47]. The exhaustiveness was set at 8. The program performed energy minimization with the Universal Force Field (UFF) after uploading the chosen target proteins and ligands. The software's Open Babel tool then saved both ligands and protein structures in the 'pdbqt' format.

We generated a grid box around the active binding site. We adjusted the grid box's size and coordinates by tracking the box's boundary line. PyRx employs the Lamarckian genetic algorithm as its conformational search algorithm. The present work employed semi-flexible docking as the docking method. The software displayed the binding energy with different conformers after docking and saved it in the'.csv' format. Autodock Vina splits the docking results into individual conformers. Next, we analysed the docking output files using Discovery Studio Visualiser [46] to study the interactions between the ligands and the amino acid present at the active site of target proteins. We loaded each conformer and the protein into Discovery Studio Visualiser and observed the interactions. We selected the best conformer based on the docking score and better non-covalent bond interaction.

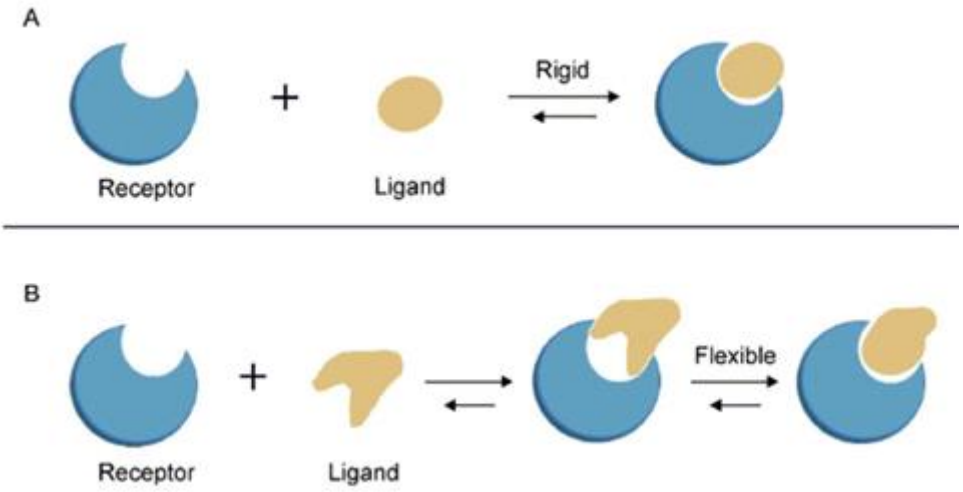

Figure I.29: Two models of molecu lar docking—(a) rigid-body and (b) flexible (induced-fit model) [44]

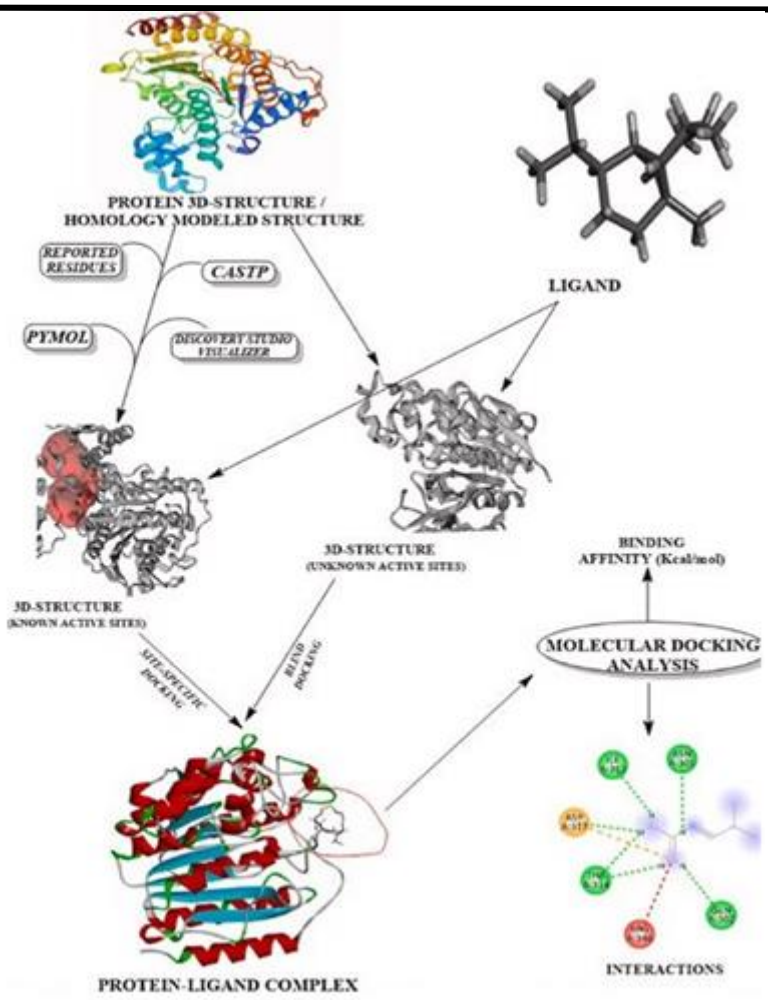

Figure I.30: Active site determination of 3D-receptors, protein ligand docking simulation (blind and site-specific docking), and analysis of docking complex [46]

4. Molecular Dynamic Simulation

The molecular dynamics (MD) simulation study is very important for finding new small compounds that could be used as biological drug targets because it shows how ligands and proteins interact at the atomic level. MD simulations help the researchers study the conformational changes, binding events, and structural stability of both protein targets and ligands. Molecular dynamics studies bridge the gap between structural information and the dynamic behaviour of target proteins, which aids in the rational design of potential drug candidates by providing a deeper understanding of their binding mechanisms and interactions with the various target proteins. The simulation study and generation of trajectory files were performed by GROningen Machine for Chemical Simulations (GROMAC) software. The best docking conformations of selected ligands with both the target proteins of PDB ID 2NSD and 4FDO were selected for the MD simulation study. The CHARMM27 force field and simple point charge (SPC) water solvation models were selected for study. A cubic boundary box and

the counter ion Na+ Cl− of concentration 0.15 M were added to neutralise the system. The energy minimisation was performed by selecting the steepest descent algorithm as an EM integrator with 5000 steps. Simulation was conducted under the equilibration parameters NPT and NVT at 300 k, 1 bar pressure, and a thermostat relaxation time of 100 ps. Leap frog was selected as simulator, and 100 ns under simulation time were executed using the mdrun program in GROMAC. Trajectories files were generated for analysing various dynamic parameters such as root mean square deviation (RMSD), root mean square fluctuation (RMSF), radius of gyration (RoG), solvent accessible surface area (SASA), binding free energy estimate (MM-PBSA), and H-bonds [45].

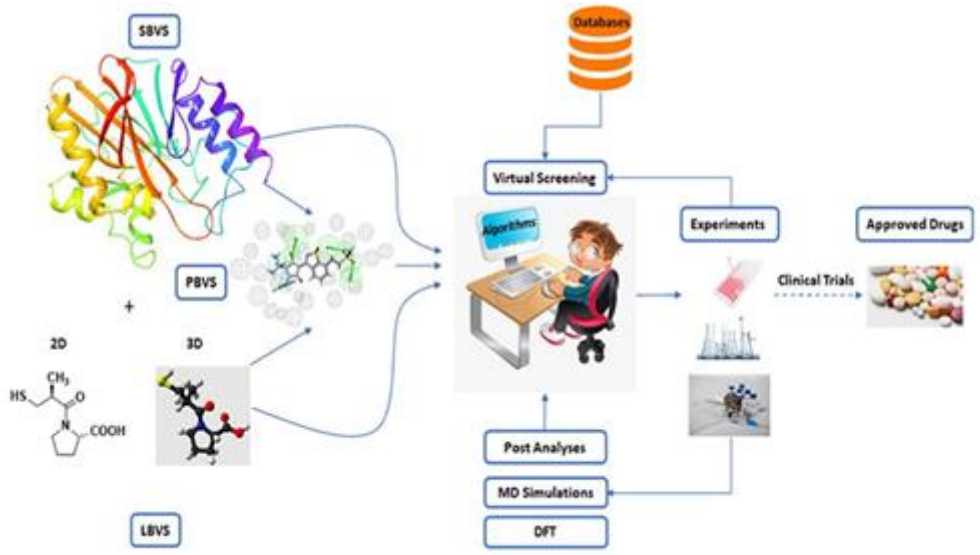

Figure I.31: Schematic representation of molecular dynamics simulations [45]

5. ADMET Prediction and Drug-Likeness Evaluation

In addition to the optimum binding affinities of the lead molecules with the target protein, the potency of the hit molecules is another driving factor in the drug development process. To become therapeutically successful and effective, the identified hits must possess high biological actions with low toxicity. Experimenting with ADMET (A: Absorption, D: Distribution, M: Metabolism, E: Excretion, T: Toxicity) properties on small molecules is expensive and time-consuming. Therefore, the computational evaluation of pharmacokinetic (PK) and toxicity profiles of small molecules has proven to be an effective and crucial element in evaluating small molecules as drug candidates during the initial stages of drug development. Nowadays, the study of ADME-Tox properties has become an essential field of drug discovery, which significantly reduces the clinical failure of lead compounds. We made ADME-Tox predictions for all the ligands selected from virtual screening using ADMET Lab 2.0, a user-friendly, freely available web server (https:// admetmesh. scbdd. com). The properties assessed during the study are partition coefficient, aqueous solubility, % of oral absorption, plasma protein binding, skin

permeability, blood–brain barrier, plasma protein binding, metabolism, and elimination. Additionally, we studied various toxicity aspects, including the maximum tolerated human dosage, hepatotoxic ity, skin reactivity, mutagenicity, and hERG inhibitor. For drug-likeness analysis, we also examined the number of rotatable bonds, molecular weight, number of hydrogen bond donors, number of hydrogen bond acceptors, and topological polar surface area. We further subjected the lead compounds to estimating their drug-like properties using the Lipinski rule of five [45].

6.Conclusion

Computational approaches have transformed drug discovery by providing efficient and cost-effective tools for predicting molecular behavior and biological activity.

The integration of DFT, molecular docking, MD simulations, and ADMET prediction offers a comprehensive framework for rational drug design.

PART II:

EXPERIMENTAL

Chapter 01:

Materials & Methods

1. General Introduction

This chapter outlines the experimental protocols and computational strategies adopted for the synthesis, structural elucidation, and in silico investigation of ferrocenyl acetylaniline derivatives. The overall methodology integrates synthetic organometallic chemistry with advanced spectroscopic, electrochemical, and molecular modelling techniques in order to establish a comprehensive correlation between molecular structure, electronic properties, and interaction behaviour towards acetylcholinesterase (AChE), a key target in Alzheimer's disease.

The synthesis of the target compounds was carried out at the Laboratory of Valorisation and Technology of Saharian Resources (VTRS), Faculty of Technology, University of El Oued, under controlled laboratory conditions. The same research facility was used to perform all computational investigations, including density functional theory (DFT) calculations, molecular docking, molecular dynamics simulations, and MM-PBSA analyses, thereby ensuring methodological consistency between experimental and theoretical results.

Spectroscopic characterisation was conducted in collaboration with the Centre de Recherche Scientifique et Technique en Analyses Physico-Chimiques (CRAPC), University of Ouargla. A combination of FT-IR, UV–Visible spectroscopy, and one- and two-dimensional NMR techniques was employed to confirm the molecular structures of the synthesised derivatives. In addition, cyclic voltammetry was used to explore the redox properties of the ferrocenyl core, which are directly related to its electronic behaviour.

Particular emphasis was placed on evaluating the interaction potential of these compounds with acetylcholinesterase (AChE), an essential enzyme responsible for the hydrolysis of acetylcholine and a well-established therapeutic target in Alzheimer's disease. To this end, molecular docking and molecular dynamics simulations were performed to investigate binding affinity, interaction mechanisms, and structural stability of the ligand–enzyme complexes.

Furthermore, in silico ADMET predictions were carried out to assess pharmacokinetic properties, drug-likeness, and potential toxicity, providing a preliminary evaluation of their suitability as anti-Alzheimer agents.

Overall, this integrated approach ensures the robustness and reliability of the obtained data and provides a solid framework for understanding the physicochemical behaviour and biological relevance of ferrocenyl derivatives in the context of neurodegenerative disease targeting.

2. Chemicals and Reagents

All reagents and solvents employed in this study were of analytical grade and used without further purification unless otherwise specified. The choice of chemicals was guided by their suitability for organometallic synthesis and compatibility with subsequent spectroscopic and electrochemical analyses.

Ferrocene (Fc, 99%) and orthophosphoric acid (85%) were supplied by Alfa Aesar. The o-, m-, and p-aminoacetophenone isomers (99%), along with tetrabutylammonium tetrafluoroborate (Bu_4NBF_4, electrochemical grade, 99%) used as supporting electrolyte, were obtained from Sigma-Aldrich. Iodomethane and anhydrous magnesium sulfate (97%) were purchased from Acros Organics, while acetic acid (99–100%) and ethanol (95%) were provided by Biochem Chemopharma.

The ferrocenylmethyl quaternary ammonium intermediate was synthesised according to previously reported procedures and used directly without additional purification [1]. All aqueous solutions were prepared using double-distilled water, and solvents used for analytical measurements were of appropriate purity to ensure reproducibility.

Stock solutions were freshly prepared when required and handled under standard laboratory conditions to minimise degradation and contamination.

3. Instrumentation and Experimental Conditions

3.1. Spectroscopic Analysis

3.1.1. FT-IR Spectroscopy

Fourier-transform infrared (FT-IR) spectra were recorded using a Shimadzu 8000S spectrophotometer over the range 4000–400 cm^{-1}. Solid samples were prepared as KBr pellets.

This technique enabled identification of key functional groups, including N–H stretching, carbonyl (C=O) vibrations and aromatic C–H bonds, thereby confirming the formation of the ferrocenyl acetylaniline framework [2].

3.1.2. UV–Visible Spectroscopy

Electronic absorption spectra were obtained using a Shimadzu UV-1800 spectrophotometer in the range 200–900 nm. Measurements were carried out in dimethyl sulfoxide (DMSO) using quartz cuvettes (1 cm path length).

The analysis provided information on electronic transitions within the molecules, including π–π*, n–π* and metal-centred transitions, reflecting the conjugation between the ferrocenyl unit and the aromatic system [3].

3.2. Nuclear Magnetic Resonance (NMR)

3.2.1. ^{1}H NMR Analysis

^{1}H NMR spectra were recorded on a Bruker ARX-500 spectrometer (400 MHz) using DMSO-d_6 as solvent. Chemical shifts (δ) were referenced to tetramethylsilane (TMS).

The spectra allowed clear identification of proton environments associated with the ferrocenyl rings, aromatic moiety, methylene bridge and acetyl group, confirming the expected molecular structures [4].

3.2.2. ^{13}C NMR Analysis

^{13}C NMR spectra were obtained under similar experimental conditions. The analysis provided detailed assignment of carbon atoms, including carbonyl carbons, aromatic carbons, cyclopentadienyl rings and methylene carbons.

These data confirmed the successful functionalisation of the ferrocenyl scaffold [5].

3.2.3. Two-Dimensional NMR (HSQC/HMBC)

Two-dimensional NMR experiments (HSQC and HMBC) were performed to establish proton–carbon correlations.

HSQC enabled direct one-bond correlations, while HMBC provided long-range connectivity, allowing unambiguous structural assignment and confirmation of substitution patterns on the aromatic ring [6].

3.3. Electrochemical Measurements (Cyclic Voltammetry)

Electrochemical measurements were carried out using a PGZ301 potentiostat/galvanostat (Radiometer Analytical, France) in dimethyl sulfoxide (DMSO) under nitrogen atmosphere at 298 K.

A conventional three-electrode system was employed, consisting of a glassy carbon working electrode (0.013 cm^2), a platinum counter electrode (0.05 cm^2) and a saturated Hg/Hg_2Cl_2 reference electrode. Tetrabutylammonium tetrafluoroborate (0.1 M) was used as supporting electrolyte.

Prior to each experiment, the solution was purged with nitrogen to eliminate dissolved oxygen and ensure stable electrochemical conditions.

Cyclic voltammetry measurements were performed within a defined potential window to investigate the Fe(II)/Fe(III) redox behaviour of the ferrocenyl derivatives. The obtained electrochemical parameters provided insight into electron-transfer processes and the intrinsic electronic properties of the compounds [7].

4. Synthesis of Ferrocenyl Acetylaniline Derivatives

This section outlines the synthetic route adopted for the preparation of the ferrocenyl acetylaniline derivatives. The methodology is based on a nucleophilic substitution strategy involving a ferrocenylmethyl quaternary ammonium intermediate, allowing efficient formation of the C–N bond under relatively mild reaction conditions. This approach ensures good selectivity, operational simplicity and reproducibility in obtaining the three regioisomeric derivatives.

The overall synthetic pathway is illustrated in Figure II.15, which depicts the generation of the ferrocenylmethyl intermediate followed by its coupling with the corresponding aminoacetophenone isomers.

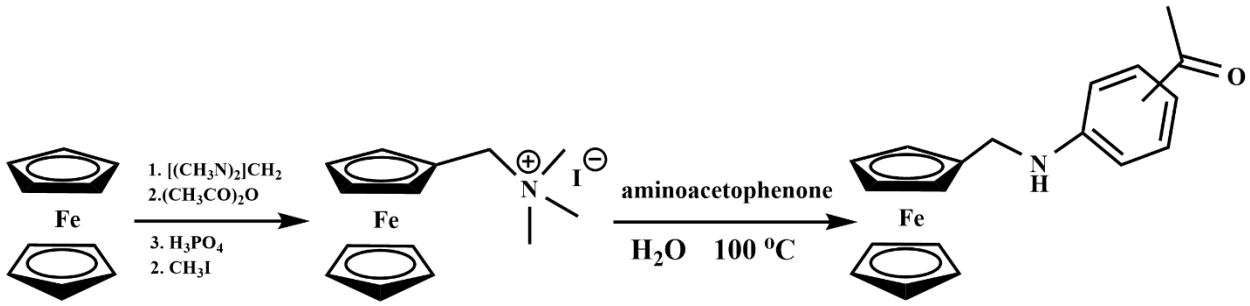

Figure II. 1. Synthetic route for the preparation of N-[(ferrocenyl)methyl]acetylaniline derivatives (FcMe2Ac, FcMe3Ac and FcMe4Ac).

4.1. General Synthetic Procedure

The target compounds were synthesised via nucleophilic substitution between trimethylferrocenylmethylammonium iodide and the corresponding aminoacetophenone isomers (ortho, meta and para), as shown in Figure II.15.

In a typical experiment, the selected aminoacetophenone (3.84 mmol) was progressively introduced into a stirred aqueous solution of trimethylferrocenylmethylammonium iodide (2.56 mmol) dissolved in distilled water (60 mL). The reaction mixture was maintained under reflux for 4 hours to ensure complete conversion.

After completion, the mixture was cooled to ambient temperature, resulting in the formation of a yellow precipitate. The crude product was recovered by vacuum filtration and washed thoroughly with distilled water to eliminate residual salts and unreacted reagents.

Purification was achieved by recrystallisation from a 90% ethanol/water mixture. For the meta-substituted derivative, an additional purification step using column chromatography (chloroform/methanol, 99:1 v/v) was required to obtain a higher purity product.

This synthetic protocol offers several advantages, including the use of an aqueous medium, straightforward experimental handling and avoidance of harsh conditions, making it well-suited for the reproducible synthesis of ferrocenyl derivatives [8].

4.2. Synthesis of Individual Compounds

4.2.1. N-[(ferrocenyl)methyl]-2-acetylaniline (FcMe2Ac)

Yield: 650 mg (77%).

Appearance: Yellow crystalline solid.

Melting point: 148–150 °C.

^{1}H NMR (500 MHz, DMSO-d_6): δ 2.60 (3H, m, CH_3), 3.40 (2H, t, α-C_5H_4), 4.05 (2H, t, β-C_5H_4), 4.15 (5H, s, C_5H_5), 4.30 (2H, d, CH_2N), 6.62 (1H, m, Ar-H), 6.84 (1H, d, Ar-H), 7.40 (1H, m, Ar-H), 7.85 (1H, d, Ar-H), 9.01 (1H, s, NH).

^{13}C NMR (500 MHz, DMSO-d_6): δ 29 (CH_3), 42 (CH_2N), 67, 68 (C_5H_4), 69 (C_5H_5), 87 (ipso-C), 112, 116, 118, 134, 138, 150 (aromatic carbons), 210 (C=O).

FT-IR (KBr, ν, cm^{-1}): 3426, 3291 (N–H), 3082 (Ar–C–H), 1647 (C=O), 1566, 1516 (C=C), 1454, 1416, 1146, 1003, 617.

UV–Vis (DMSO): λmax = 259 nm (π–π*), 380 nm (d–d).

Cyclic voltammetry (DMSO, Fc^{+}/Fc): Ipa = 29.13 μA, Ipc = −28.52 μA, Epa = 2.17 mV, Epc = −85.60 mV, ΔE = 87.8 mV, E° = 43.9 mV, Ipa/Ipc = 1.02.

4.2.2. N-[(ferrocenyl)methyl]-3-acetylaniline (FcMe3Ac)

Yield: 480 mg (48%).

Appearance: Yellow–orange crystalline solid.

Melting point: 138–140 °C.

^{1}H NMR (500 MHz, DMSO-d_6): δ 2.45 (3H, s, CH_3), 3.42 (2H, t, α-C_5H_4), 4.08 (2H, t, β-C_5H_4), 4.18 (5H, s, C_5H_5), 4.32 (2H, d, CH_2N), 6.70–7.20 (3H, m, Ar-H), 7.65 (1H, d, Ar-H), 8.95 (1H, s, NH).

^{13}C NMR (500 MHz, DMSO-d_6): δ 28 (CH_3), 43 (CH_2N), 66, 68 (C_5H_4), 69 (C_5H_5), 86 (ipso-C), 114, 118, 125, 131, 136, 152 (aromatic carbons), 205 (C=O).

FT-IR (KBr, ν, cm^{-1}): 3432, 3338 (N–H), 2925, 1650 (C=O), 1582, 1510, 1450, 1365, 1170, 820.

UV–Vis (DMSO): λmax = 268 nm, 402 nm.

Cyclic voltammetry (DMSO, Fc^{+}/Fc): Ipa = 52.4 μA, Ipc = −51.9 μA, Epa = 10 mV, Epc = −92 mV, ΔE = 102 mV, E° = 51.0 mV, Ipa/Ipc = 1.01.

4.2.3. N-[(ferrocenyl)methyl]-4-acetylaniline (FcMe4Ac)

Yield: 690 mg (80%).

Appearance: Deep yellow crystalline solid.

Melting point: 162–164 °C.

^{1}H NMR (500 MHz, DMSO-d_6): δ 2.35 (3H, m, CH_3), 3.41 (2H, t, α-C_5H_4), 4.10 (2H, t, β-C_5H_4), 4.20 (5H, s, C_5H_5), 4.31 (2H, d, CH_2N), 6.65 (2H, d, Ar-H), 6.78 (1H, t, NH), 7.76 (2H, d, Ar-H).

^{13}C NMR (500 MHz, DMSO-d_6): δ 28 (CH_3), 43 (CH_2N), 66 (C_5H_4), 68 (C_5H_5), 87 (ipso-C), 112, 125, 132, 154 (aromatic carbons), 194 (C=O).

FT-IR (KBr, ν, cm^{-1}): 3445, 3345 (N–H), 2932, 1651 (C=O), 1589, 1562, 1369, 1281, 1173, 822.

UV–Vis (DMSO): λmax = 432 nm.

Cyclic voltammetry (DMSO, Fc^{+}/Fc): Ipa = 71.07 μA, Ipc = −71.66 μA, Epa = 16 mV, Epc = −99 mV, ΔE = 115 mV, E° = 57.5 mV, Ipa/Ipc = 0.99.

5. Computational Methodology

Computational analyses were undertaken to elucidate the electronic characteristics and interaction potential of the synthesised ferrocenyl acetylaniline derivatives in relation to their inhibitory activity against acetylcholinesterase (AChE), a key enzyme involved in cholinergic neurotransmission and a validated therapeutic target in Alzheimer's disease. The adopted in silico framework integrates density functional theory (DFT), molecular docking, molecular dynamics (MD) simulations, and MM-PBSA free energy calculations, complemented by ADMET prediction tools.

This integrated methodology enables the establishment of correlations between molecular structure, electronic distribution, and binding behaviour towards acetylcholinesterase, thereby providing mechanistic insight into ligand–enzyme recognition and inhibition potential.

5.1. Electronic Structure Calculations (DFT)

Quantum chemical calculations were performed using Gaussian 16 [9] to investigate the electronic properties of FcMe2Ac, FcMe3Ac and FcMe4Ac.

Geometry optimisation was carried out at the B3LYP level using the 6-311++G(d,p) basis set for light atoms (C, H, N, O), while the Stuttgart–Dresden (SDD) effective core potential was applied to the iron centre [10]. Vibrational frequency calculations confirmed that all optimised structures correspond to true minima.

The optimised geometries were used to evaluate frontier molecular orbitals (HOMO and LUMO), energy gaps and global reactivity descriptors, including electronegativity, hardness, softness and electrophilicity index. These parameters provide insight into the reactivity profile and potential interaction capability of the molecules with biological targets.

In addition, molecular electrostatic potential (MEP), electron localisation function (ELF), localised orbital locator (LOL) and reduced density gradient (RDG) analyses were performed to characterise charge distribution and weak intramolecular interactions. Visualisation was carried out using GaussView and Multiwfn [11].

5.2. Molecular Docking Simulations

Molecular docking studies were conducted to evaluate the binding affinity and interaction mechanisms of the ferrocenyl derivatives with acetylcholinesterase (AChE), a key enzyme involved in cholinergic neurotransmission. The crystallographic structures used in this study were PDB ID: 4EY7 (human acetylcholinesterase complexed with an inhibitor) and PDB ID: 1EVE (Torpedo californica acetylcholinesterase), both widely used as reference models for AChE inhibition studies.

5.2.1. Receptor Preparation

The three-dimensional structures of the selected AChE targets are illustrated in Figure II.16, highlighting the architecture of the catalytic gorge and active site region.

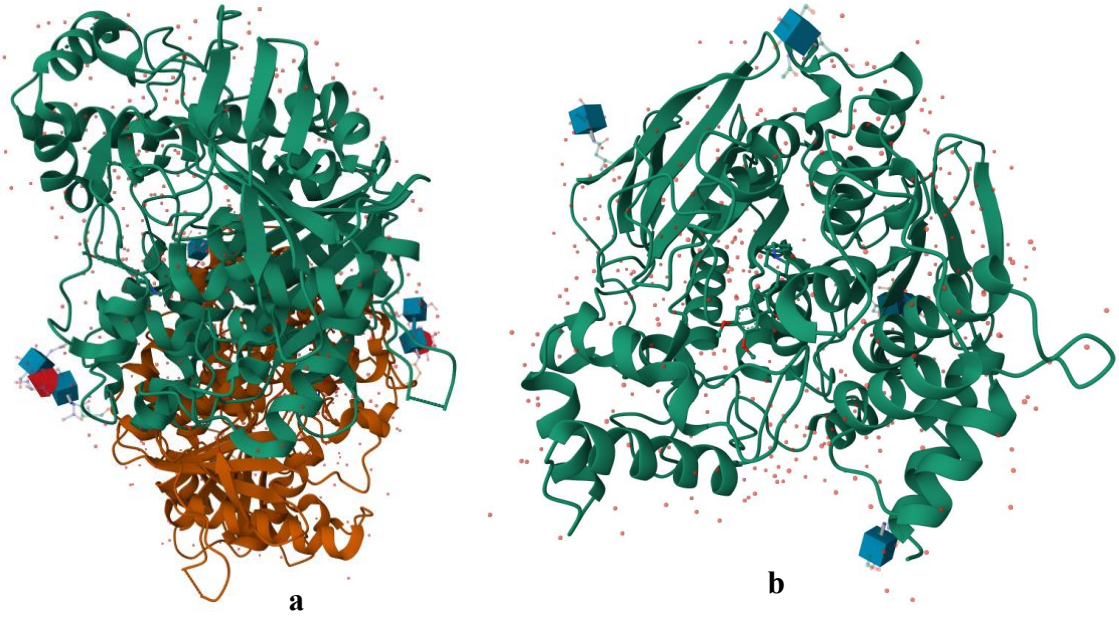

Figure II. 2. Three-dimensional structures of acetylcholinesterase targets used in docking studies: (a) human AChE (PDB ID: 4EY7) and (b) *Torpedo californica* AChE (PDB ID: 1EVE).

The crystallographic structures were retrieved from the Protein Data Bank (https://www.rcsb.org/) [12] and prepared using AutoDock Tools (ADT 1.5.7) [13]. All crystallographic water molecules, co-crystallised ligands, and non-essential heteroatoms were removed to avoid interference with ligand binding. Polar hydrogen atoms were added, and Kollman charges were assigned. The prepared receptors were then converted into PDBQT format.

5.2.2. Ligand Preparation

The optimised geometries of FcMe2Ac, FcMe3Ac, and FcMe4Ac were used as input structures (Figure II. 17).

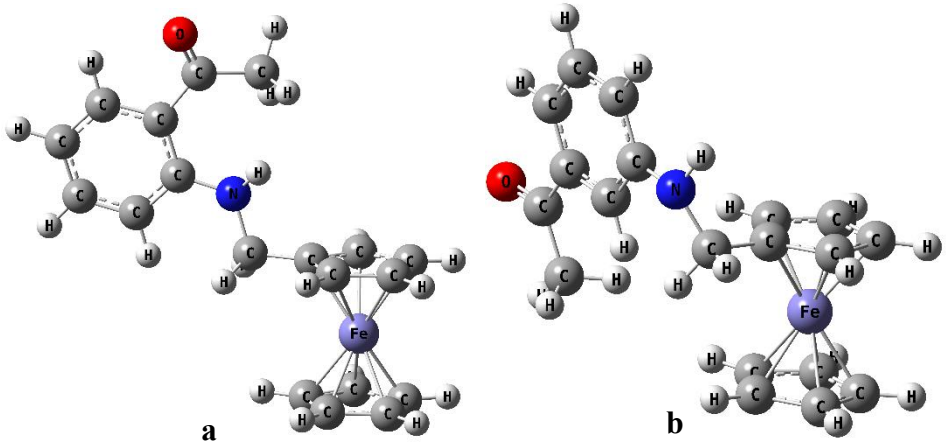

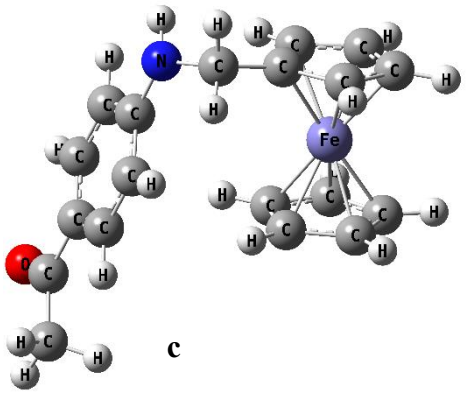

Figure II. 3. Optimised molecular structures of ferrocenyl derivatives used as ligands: FcMe2Ac (a), FcMe3Ac (b), and FcMe4Ac (c).

Ligands were prepared using AutoDock Tools by assigning Gasteiger charges and defining rotatable bonds, followed by conversion into PDBQT format.

5.2.3. Docking Protocol and Validation

The docking workflow is presented in Figure II.18, summarising receptor preparation, ligand preparation, grid generation and docking analysis.

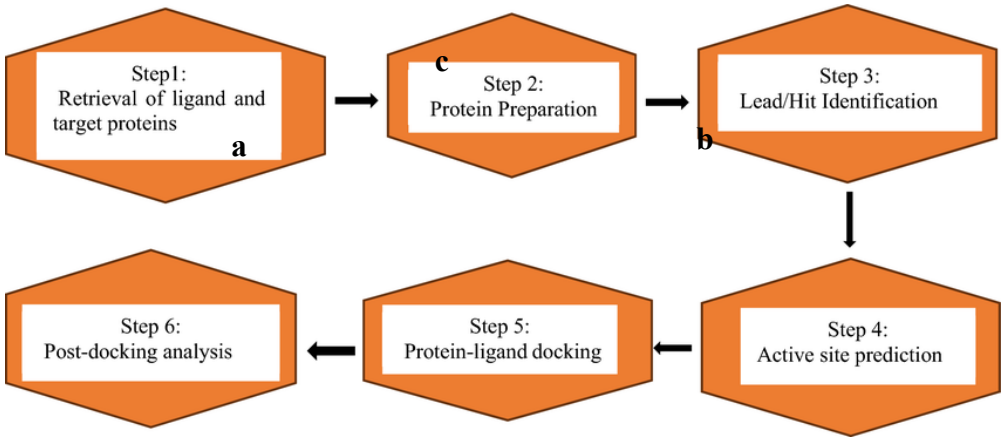

Figure II. 4. Molecular docking workflow illustrating protein and ligand preparation, grid generation, docking execution and interaction analysis.

Docking simulations were performed using AutoDock 4.2 with the Lamarckian genetic algorithm. A grid box of 60 × 60 × 60 Å with a spacing of 0.375 Å was centred on the active site of acetylcholinesterase, encompassing both the **catalytic active site (CAS)** and the **peripheral anionic site (PAS)**, which are essential for substrate recognition and inhibitor binding.

A total of 100 independent docking runs were performed for each ligand–target system. The best binding pose was selected based on the lowest binding energy and the most populated cluster.

Validation of the docking protocol was achieved by redocking the co-crystallised ligand into the active site and calculating the RMSD between experimental and predicted conformations. An RMSD value below 2.0 Å confirmed the reliability and accuracy of the docking procedure [14].

5.3. Molecular Dynamics (MD) Simulations

Molecular dynamics (MD) simulations were carried out to assess the stability and dynamic behaviour of the selected ligand–acetylcholinesterase (AChE) complexes using GROMACS [15].

5.3.1. System Setup and Solvation

The solvated system is illustrated in Figure II.19, showing the protein–DNA–ligand complex embedded in an explicit water box.

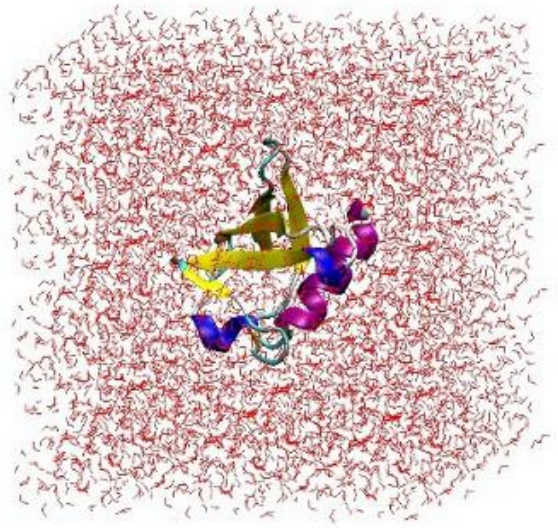

Figure II. 5. Solvated protein–ligand complex showing the explicit water box used for molecular dynamics simulations.

The CHARMM36 force field was employed for protein parameterisation [16], while ligand parameters were generated using the CGenFF protocol [17]. Each system was placed in a cubic simulation box with a minimum distance of 10 Å between the protein surface and the box boundary and solvated using the TIP3P water model. Counter ions were added to neutralise the system and ensure electrostatic stability.

5.3.2. Energy Minimisation and Equilibration

The general molecular dynamics simulation protocol, including minimisation, equilibration, and production stages, is summarised in Figure II. 20.

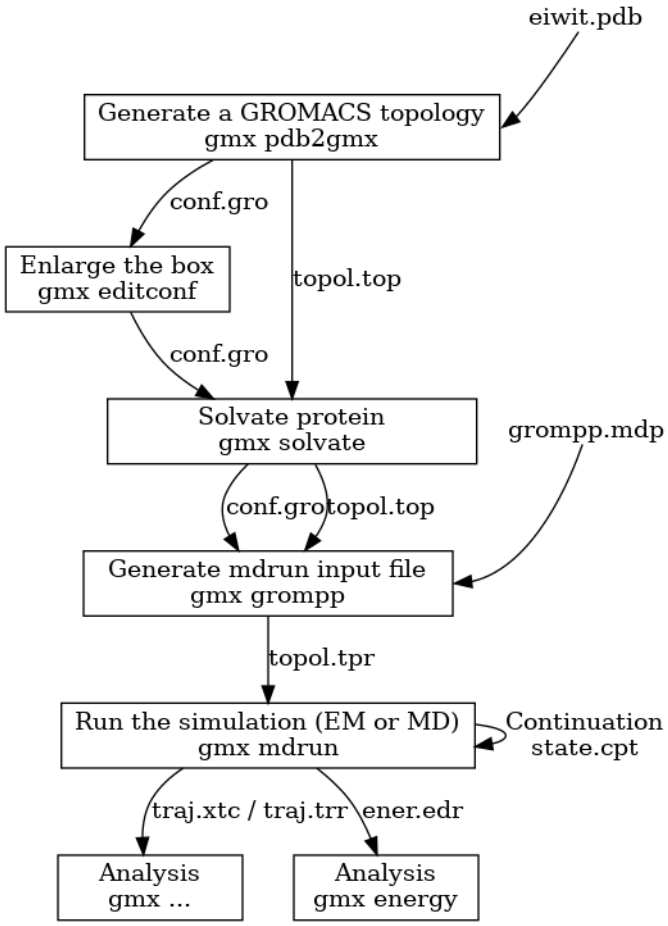

Figure II. 6. Molecular dynamics simulation workflow including system preparation, energy minimisation, equilibration and production phases.

Energy minimisation was performed using the steepest descent algorithm to eliminate steric clashes and optimise the system geometry. The system was subsequently equilibrated under NVT conditions (300 K, 500 ps), followed by NPT conditions (1 atm, 500 ps), using the V-rescale thermostat and Parrinello–Rahman barostat.

5.3.3. Production Run Parameters

Production simulations were conducted for 100 ns with a time step of 2 fs. Periodic boundary conditions were applied in all directions, and long-range electrostatic interactions were treated using the Particle Mesh Ewald (PME) method. Covalent bonds involving hydrogen atoms were constrained using the LINCS algorithm.

Trajectory analyses were carried out using GROMACS built-in tools, including RMSD, RMSF, radius of gyration (Rg), and solvent surface accessibility area (SASA).

5.4. MM-PBSA Binding Free Energy Calculations

Binding free energy calculations were performed using the g_mmpbsa tool [18]. Snapshots extracted from the last 20 ns of equilibrated trajectories were used.

The total binding free energy (ΔG_bind) was estimated as the sum of van der Waals, electrostatic, polar solvation and non-polar solvation contributions.

5.5. ADMET Prediction

Pharmacokinetic and toxicity properties were predicted using ADMETlab 2.0 [19] and ProTox-II [20].

Key parameters included gastrointestinal absorption, blood–brain barrier permeability, cytochrome P450 interactions, plasma protein binding, and toxicity indicators (hepatotoxicity, mutagenicity, and LD_{50}), providing an initial assessment of the suitability of the compounds as anti-Alzheimer agents.

Chapter 02:

Results & Discussion

1. General Introduction

This chapter presents a comprehensive analysis of the experimental and computational results obtained for the synthesised ferrocenyl acetylaniline derivatives. The objective is to establish clear correlations between molecular structure, electronic properties, and their interaction behaviour towards acetylcholinesterase (AChE), a key enzymatic target in Alzheimer's disease.

The discussion begins with an evaluation of the synthetic outcomes, including reaction efficiency and substituent effects, followed by an in-depth structural characterisation using FT-IR, UV–visible spectroscopy, nuclear magnetic resonance (^{1}H, ^{13}C, and 2D NMR), and cyclic voltammetry. These complementary techniques provide robust confirmation of molecular structures and valuable insight into the electronic properties of the ferrocenyl core.

Subsequently, computational investigations are presented to extend the experimental findings. Density functional theory calculations are employed to analyse electronic descriptors and charge distribution, while molecular docking and molecular dynamics simulations are used to explore the interaction of the synthesised compounds with acetylcholinesterase. Finally, MM-PBSA and ADMET analyses are discussed to evaluate binding stability and pharmacokinetic suitability in the context of anti-Alzheimer drug development.

2. Synthesis of Ferrocenyl Acetylaniline Derivatives

The ferrocenyl acetylaniline derivatives (FcMe2Ac, FcMe3Ac and FcMe4Ac) were successfully obtained through a nucleophilic substitution strategy involving a ferrocenylmethyl quaternary ammonium intermediate and the corresponding aminoacetophenone isomers. The adopted synthetic route demonstrated high reliability and reproducibility, affording the desired products as yellow to orange crystalline solids under relatively mild experimental conditions.

The reaction pathway is depicted in Figure II. 21, which outlines the key mechanistic steps leading to the formation of the C–N bond at the ferrocenylmethyl position.

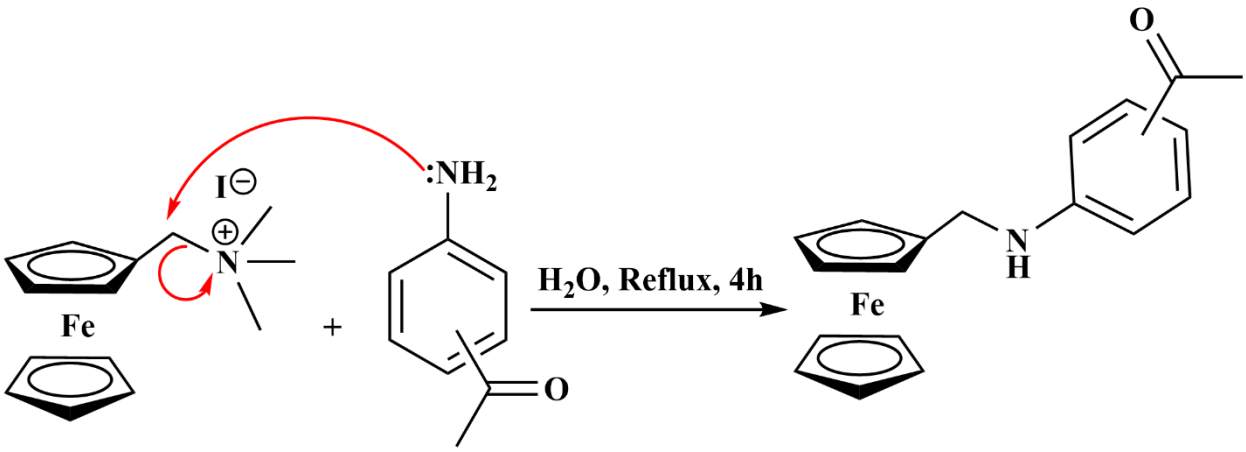

Figure II. 7. Proposed reaction mechanism for the formation of N-[(ferrocenyl)methyl]acetylaniline derivatives via nucleophilic substitution.

As illustrated in Figure II. 21, the transformation proceeds via a bimolecular nucleophilic substitution (SN2) mechanism, where the lone pair of the amino group attacks the electrophilic methylene carbon bonded to the quaternary ammonium centre. This process results in the displacement of trimethylamine as a leaving group and the formation of the ferrocenylmethylamine linkage [21].

The efficiency of this reaction can be rationalised by both electronic and structural factors. The ferrocenyl moiety exhibits electron-donating properties, which facilitate stabilisation of the transition state and enhance the reactivity of the methylene carbon [22]. In parallel, the quaternary ammonium group acts as an excellent leaving group, enabling smooth bond cleavage under aqueous conditions. Such behaviour is consistent with previously reported reactivity patterns of ferrocenylmethyl derivatives, where favourable electronic delocalisation and structural flexibility promote nucleophilic substitution processes [23,24].

The chemical structures of the obtained compounds are presented in Figure II.22, highlighting the positional variation of the acetyl substituent on the aromatic ring.

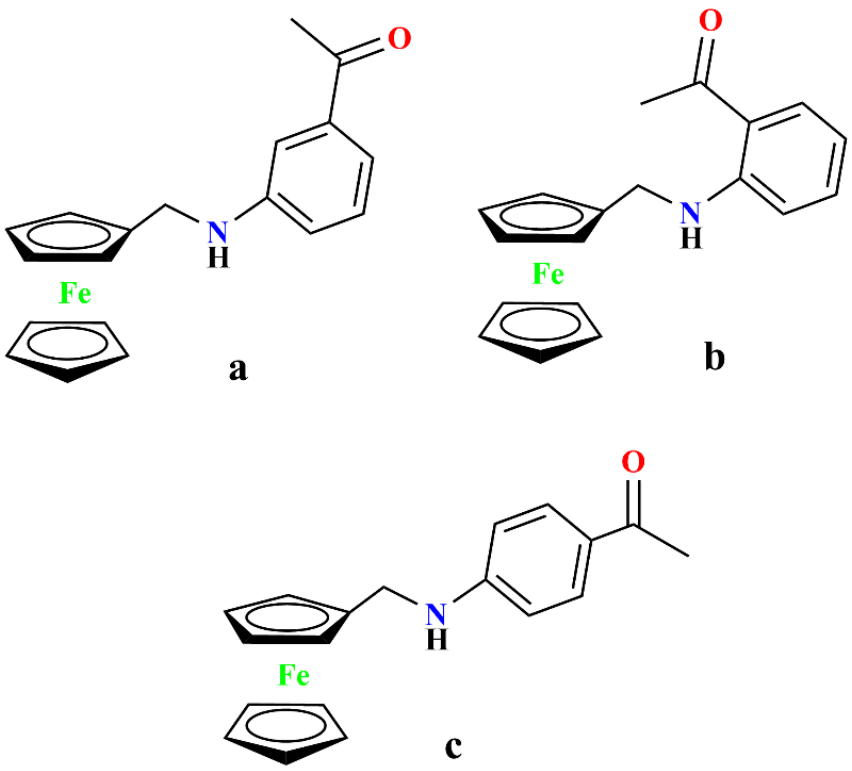

Figure II. 8. Chemical structures of the synthesised ferrocenyl acetylaniline derivatives: (a) FcMe2Ac (ortho), (b) FcMe3Ac (meta), and (c) FcMe4Ac (para).

As shown in Figure II. 22, the three derivatives differ solely by the position of the acetyl group, which significantly influences steric accessibility and electronic distribution within the molecule. These factors are known to play a critical role in modulating the nucleophilicity of the amino group and, consequently, the efficiency of the substitution reaction [25].

To further evaluate the synthetic performance, the yields and physical characteristics of the obtained compounds are summarised in Table II.1.

Table II.1. Yields and physical properties of the synthesised ferrocenyl acetylaniline derivatives.

Compound	Substituent Position	Yield (%)	Appearance	Melting Point (°C)
FcMe2Ac	Ortho	77	Yellow crystalline solid	148–150
FcMe3Ac	Meta	48	Yellow–orange solid	138–140
FcMe4Ac	Para	80	Deep yellow solid	162–164

As shown in **Table II.1**, the reaction yields follow the order: FcMe4Ac > FcMe2Ac > FcMe3Ac

This trend can be rationalised by considering both steric and electronic effects, which are known to govern nucleophilic substitution reactions in aromatic amines. The para-substituted derivative (FcMe4Ac) exhibited the highest yield (80%), reflecting minimal steric hindrance and favourable resonance interaction between the acetyl group and the amino functionality. This electronic delocalisation enhances the nucleophilicity of the amine, thereby facilitating the substitution process [26].

In contrast, the meta derivative (FcMe3Ac) showed a significantly lower yield (48%), which can be attributed to the absence of resonance interaction between the substituents. In the meta position, the acetyl group exerts mainly an inductive electron-withdrawing effect, reducing the electron density on the amino group and consequently its nucleophilicity.

The ortho derivative (FcMe2Ac) presented intermediate behaviour (77%), where steric hindrance between adjacent substituents partially limits the accessibility of the nucleophilic site, despite favourable electronic effects.

These observations are in good agreement with previously reported studies on substituted aniline derivatives, where both steric congestion and electronic factors significantly influence reactivity. Furthermore, the results confirm that the adopted synthetic strategy is robust and well adapted for the preparation of ferrocenyl derivatives with controlled structural variation [27].

3. FT-IR Spectral Analysis

The structural features of the synthesised ferrocenyl acetylaniline derivatives were initially investigated by Fourier-transform infrared (FT-IR) spectroscopy. The recorded spectra for FcMe2Ac, FcMe3Ac and FcMe4Ac are presented in Figure II. 23, while the principal absorption bands and their corresponding assignments are summarised in Table II.2.

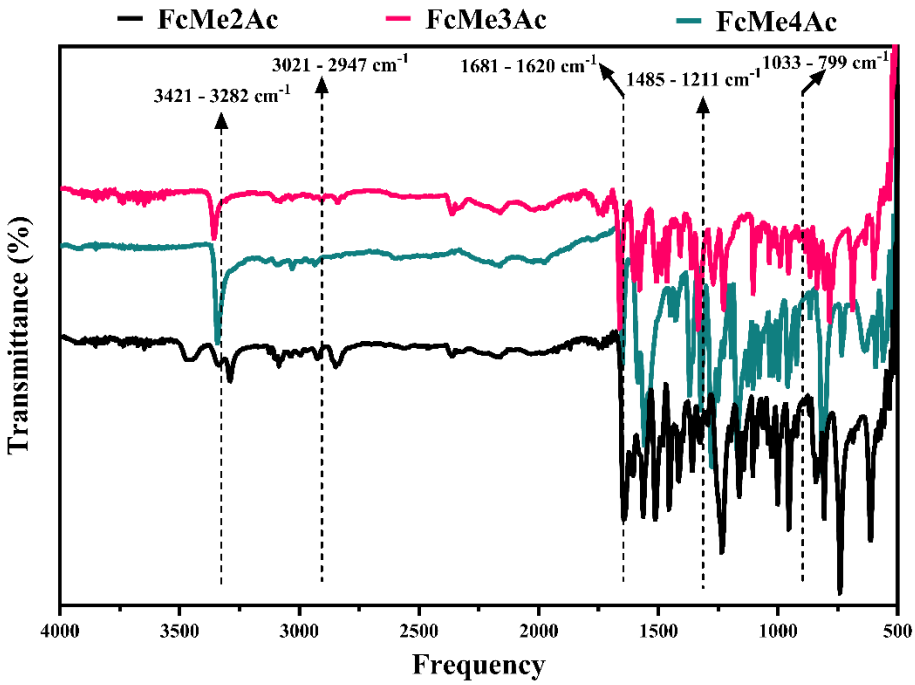

Figure II. 9. FT-IR spectra of the synthesised ferrocenyl acetylaniline derivatives.

Table II.2. Characteristic FT-IR absorption bands (cm^{-1}) and their assignments for the synthesised compounds.

Assignment	FcMe2Ac (cm^{-1})	FcMe3Ac (cm^{-1})	FcMe4Ac (cm^{-1})	Description
N–H stretching	3426, 3291	3432, 3338	3445, 3345	Secondary amine vibration
Ar–C–H stretching	3082	—	—	Aromatic C–H
C=O stretching	1647	1650	1651	Acetyl carbonyl group
C=C (aromatic)	1566, 1516	1582, 1510	1589, 1562	Aromatic ring vibrations
C–N stretching	1146	1170	1173	Amine linkage
C–H bending	1454, 1416	1450, 1365	1369	Methyl/aromatic bending
Out-of-plane C–H	1003, 617	820	822	Aromatic substitution pattern

As shown in Figure II.23, all compounds display closely related spectral profiles, confirming the preservation of the ferrocenyl acetylaniline framework across the series. Minor

variations in band positions and intensities are observed and can be attributed to the different substitution patterns on the aromatic ring [28].

Broad absorption bands in the region 3445–3291 cm^{-1} are assigned to N–H stretching vibrations, confirming the presence of secondary amine functionality formed during the nucleophilic substitution reaction. The slight shifts observed between the derivatives reflect variations in hydrogen bonding interactions and local electronic environments [29].

The strong and well-defined bands located at 1651–1647 cm^{-1} correspond to the stretching vibration of the carbonyl (C=O) group of the acetyl substituent. The consistency of this band across all compounds confirms that the carbonyl functionality remains intact during synthesis.

Aromatic C=C stretching vibrations are observed in the region 1589–1510 cm^{-1}, providing clear evidence for the presence of the substituted benzene ring. Additionally, the bands detected between 1173–1146 cm^{-1} are attributed to C–N stretching vibrations, confirming the successful formation of the ferrocenylmethyl–aniline linkage.

Particularly informative are the out-of-plane C–H bending vibrations observed between 820 and 617 cm^{-1}, which are highly sensitive to substitution patterns. The differences in these bands among the ortho, meta and para derivatives provide strong evidence for the positional variation of the acetyl group on the aromatic ring.

Overall, the FT-IR data provide clear confirmation of the successful synthesis of the target compounds. The observed spectral features are fully consistent with the proposed structures and align well with reported data for related ferrocenyl and substituted aniline systems [30].

4. UV–Visible Spectral Analysis

The electronic absorption properties of the synthesised ferrocenyl acetylaniline derivatives were investigated using UV–visible spectroscopy in DMSO. The corresponding spectra are presented in Figure II. 24, and the absorption maxima are summarised in Table II.3.

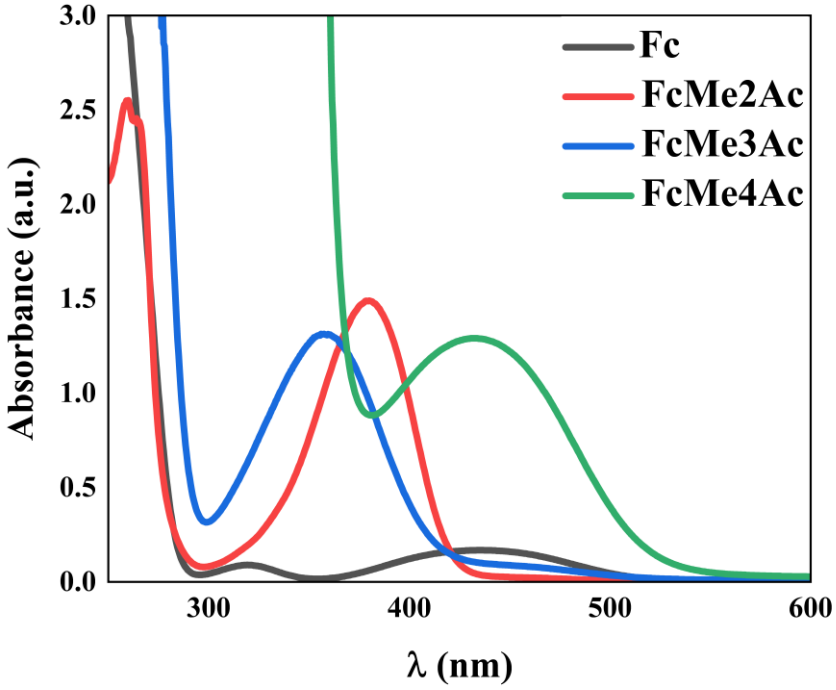

Figure II. 10. UV–visible absorption spectra of the synthesised ferrocenyl acetylaniline derivatives.

Table II.3. UV–visible absorption maxima (λmax) of the synthesised ferrocenyl acetylaniline derivatives.

Compound	λmax (nm)	Assignment
FcMe2Ac	259	π → π* (aromatic system)
	380	d–d (Fe^{2+} centre)
FcMe3Ac	268	π → π*
	402	d–d transition
FcMe4Ac	432	d–d / charge transfer

As illustrated in Figure II.24, all compounds exhibit characteristic absorption bands associated with both the aromatic system and the ferrocenyl moiety. Intense bands in the ultraviolet region (**259–268 nm**) are attributed to π → π* transitions within the conjugated aromatic system, corresponding to electronic excitation within the benzene ring [31].

In the visible region, absorption bands between **380 and 432 nm** are observed, corresponding to transitions involving the ferrocenyl iron centre. These transitions can be assigned to metal-centred d–d transitions and, in some cases, ligand-to-metal charge transfer

(LMCT), reflecting the interaction between the iron centre and the surrounding π-electron system [32].

A pronounced bathochromic shift is observed from FcMe2Ac (380 nm) to FcMe4Ac (432 nm), indicating an increase in electronic delocalisation in the para-substituted derivative. This behaviour arises from enhanced conjugation between the acetyl substituent and the aromatic system, which lowers the energy gap between molecular orbitals and facilitates lower-energy electronic transitions.

The meta derivative (FcMe3Ac) exhibits intermediate behaviour due to the absence of effective resonance interaction between substituents, limiting electron delocalisation. In contrast, the ortho derivative (FcMe2Ac), although capable of resonance interaction, may experience steric effects that slightly distort molecular planarity and reduce conjugation efficiency.

These observations highlight the significant influence of substituent position on the electronic structure of ferrocenyl derivatives. Such variations in electronic distribution are expected to play a key role in modulating molecular recognition and interaction behaviour with biological targets [33].

5. NMR Spectral Analysis

The structural elucidation of the synthesised ferrocenyl acetylaniline derivatives was comprehensively achieved using one-dimensional (^{1}H and ^{13}C) and two-dimensional (HSQC and HMBC) NMR techniques. These complementary analyses enabled precise assignment of all proton and carbon environments and provided unambiguous confirmation of the molecular structures. To facilitate interpretation, the spectra are presented individually for each compound, allowing direct correlation between spectral features and structural elements.

5.1. ^{1}H NMR Analysis

The ^{1}H NMR spectra of FcMe2Ac, FcMe3Ac and FcMe4Ac are presented in Figure II. 25.

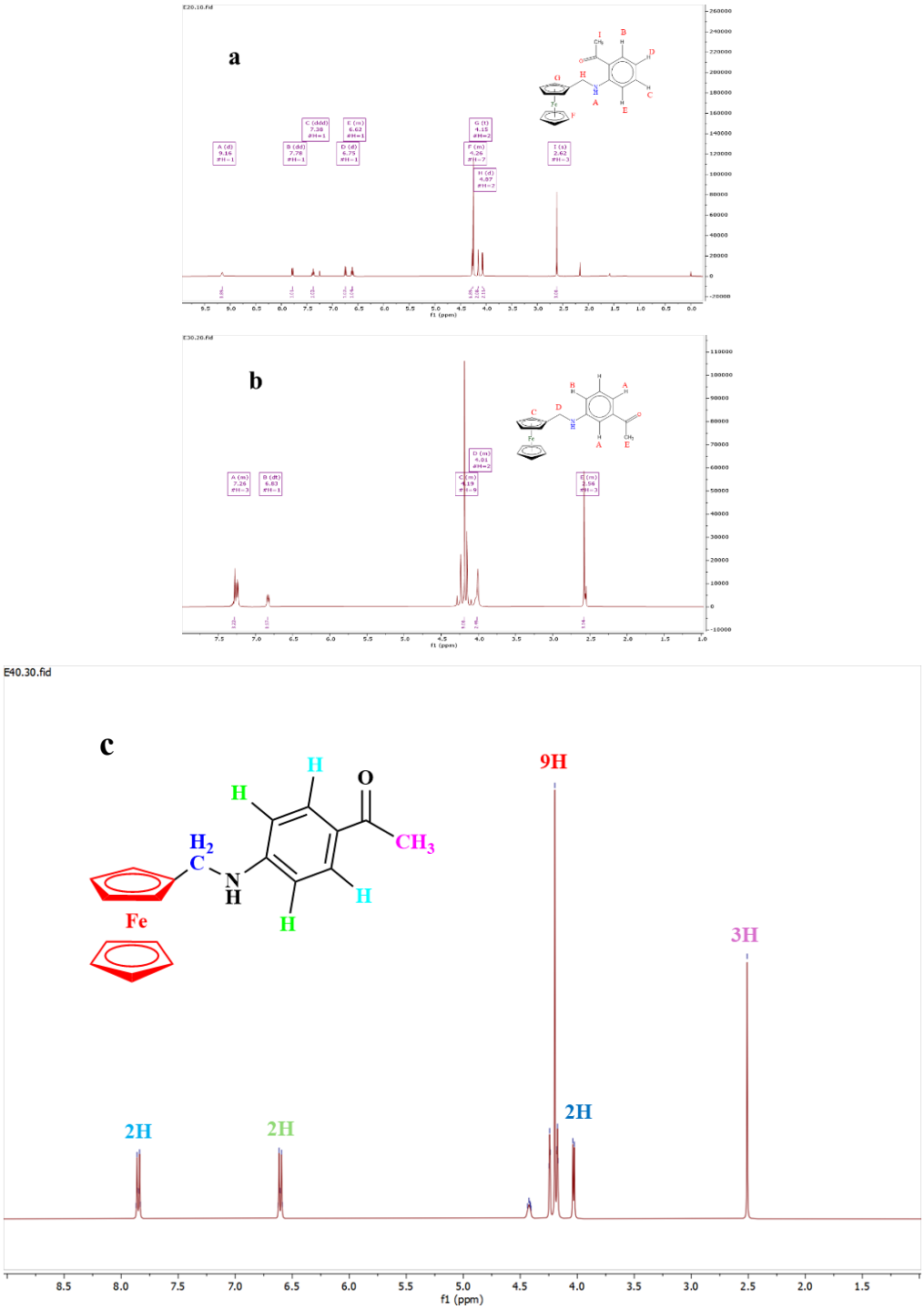

Figure II. 11. ^{1}H NMR spectra of the synthesised ferrocenyl acetylaniline derivatives: (a) FcMe2Ac, (b) FcMe3Ac, and (c) FcMe4Ac.

As illustrated in Figure II. 25, all compounds exhibit well-resolved signals consistent with the proposed molecular structures.

The methyl group of the acetyl functionality (–$COCH_3$) appears as a singlet in the region **2.35–2.60 ppm**, confirming its isolated chemical environment. The methylene bridge (–CH_2–

N–), linking the ferrocenyl unit to the aromatic ring, is observed as a doublet at approximately **4.30 ppm**, providing clear evidence for the formation of the C–N bond [34].

The ferrocenyl moiety displays its characteristic spectral features. The unsubstituted cyclopentadienyl ring (C_5H_5) appears as a sharp singlet around **4.15–4.20 ppm**, reflecting its high symmetry. In contrast, the substituted cyclopentadienyl ring (C_5H_4) gives rise to multiplet signals in the region **3.40–4.10 ppm**, indicative of reduced symmetry upon substitution. This splitting pattern is a well-established signature of monosubstituted ferrocenyl systems.

Aromatic protons are detected between **6.6 and 7.8 ppm**, exhibiting distinct splitting patterns depending on the substitution position. The ortho, meta and para isomers can be clearly differentiated based on their coupling patterns and signal multiplicity, reflecting differences in electronic distribution and proton–proton interactions within the aromatic ring.

The NH proton appears as a downfield singlet around **8.9–9.0 ppm** for FcMe2Ac and FcMe3Ac, suggesting involvement in intermolecular or intramolecular hydrogen bonding. In FcMe4Ac, a slight upfield shift is observed, which may be attributed to enhanced electronic delocalisation in the para-substituted system, reducing deshielding effects [35].

5.2. ^{13}C NMR Analysis

The ^{13}C NMR spectra of the synthesised compounds are shown in Figure II. 26.

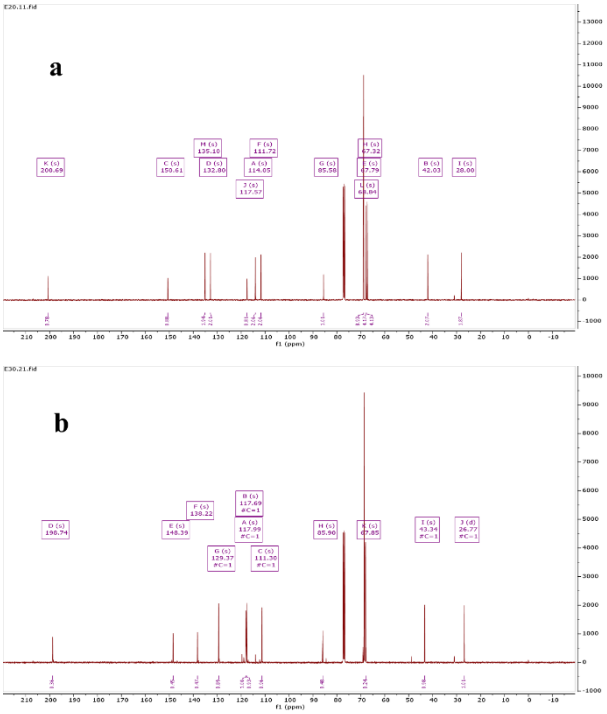

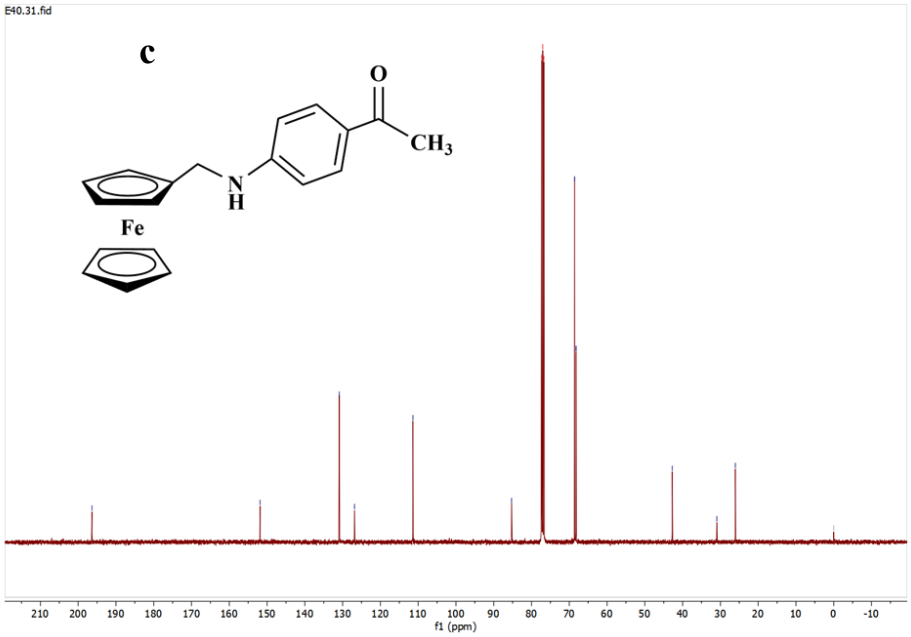

Figure II. 12. ^{13}C NMR spectra of the synthesised ferrocenyl acetylaniline derivatives: (a) FcMe2Ac, (b) FcMe3Ac, and (c) FcMe4Ac.

As illustrated in Figure II. 26, the spectra provide clear evidence for the carbon framework of the compounds.

The carbonyl carbon (C=O) is observed in the downfield region between 194 and 210 ppm, confirming the presence of the acetyl group. The variation in chemical shift among the three derivatives reflects differences in electronic environment due to substituent position.

The methylene carbon (CH_2–N) appears consistently around 42–43 ppm, confirming the linkage between the ferrocenyl moiety and the aromatic system.

The ferrocenyl carbons are detected in the range 66–69 ppm, corresponding to the cyclopentadienyl rings. The ipso carbon bonded to the substituent appears slightly downfield due to its distinct electronic environment.

Aromatic carbons are distributed between 112 and 154 ppm, with slight variations depending on substitution pattern, which is consistent with substituted benzene derivatives [36].

5.3. Two-Dimensional NMR Analysis (HSQC and HMBC)

Two-dimensional NMR spectroscopy was employed to achieve unambiguous structural assignment and to confirm the connectivity within the synthesised ferrocenyl acetylaniline derivatives. The HSQC and HMBC spectra are presented separately to allow a clear interpretation of both direct and long-range correlations.

The HSQC spectra of FcMe2Ac, FcMe3Ac and FcMe4Ac are shown in Figure II.27, while the corresponding HMBC spectra are presented in Figure II.28.

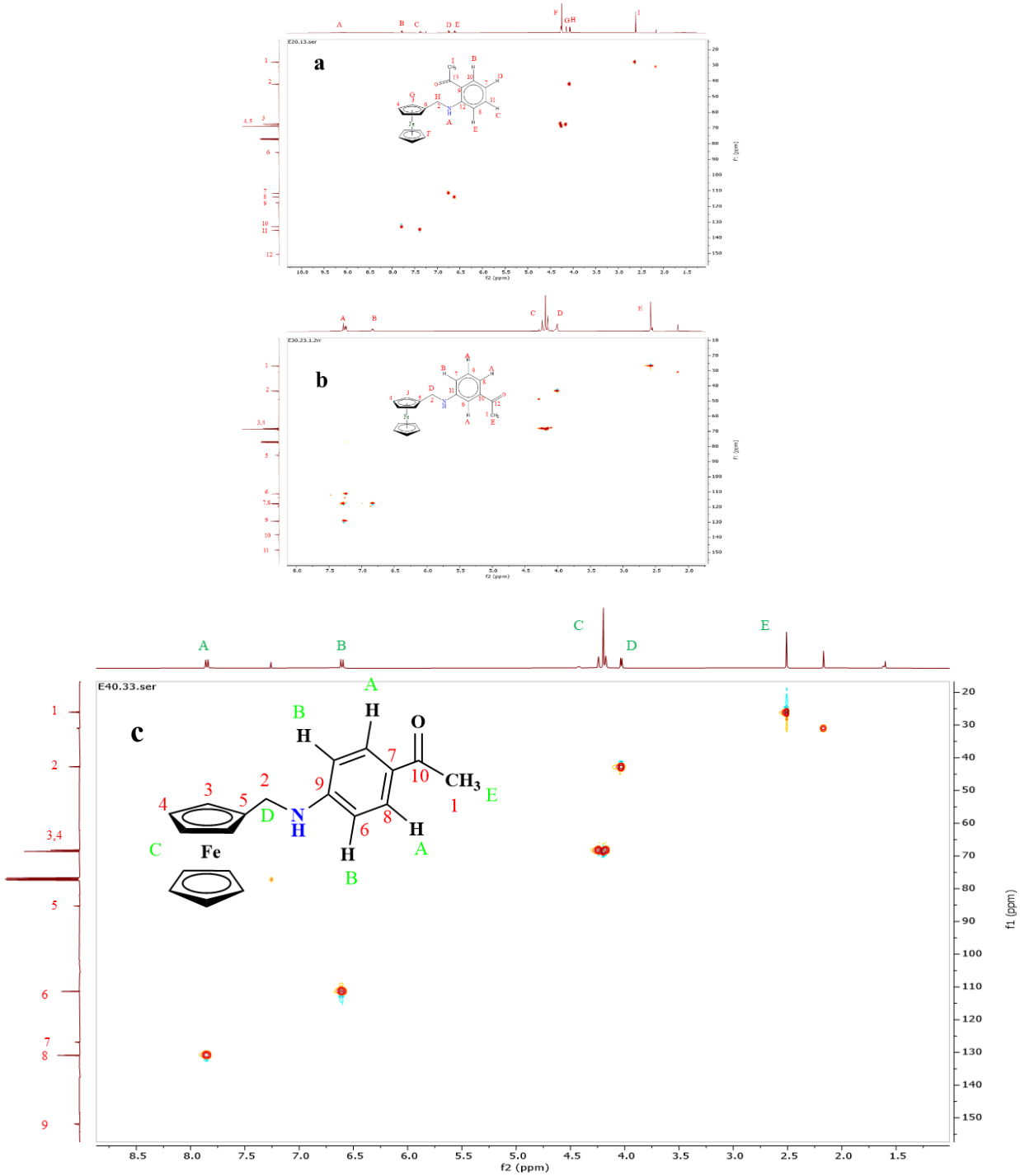

Figure II. 13. HSQC spectra of the synthesised ferrocenyl acetylaniline derivatives: (a) FcMe2Ac, (b) FcMe3Ac, and (c) FcMe4Ac.

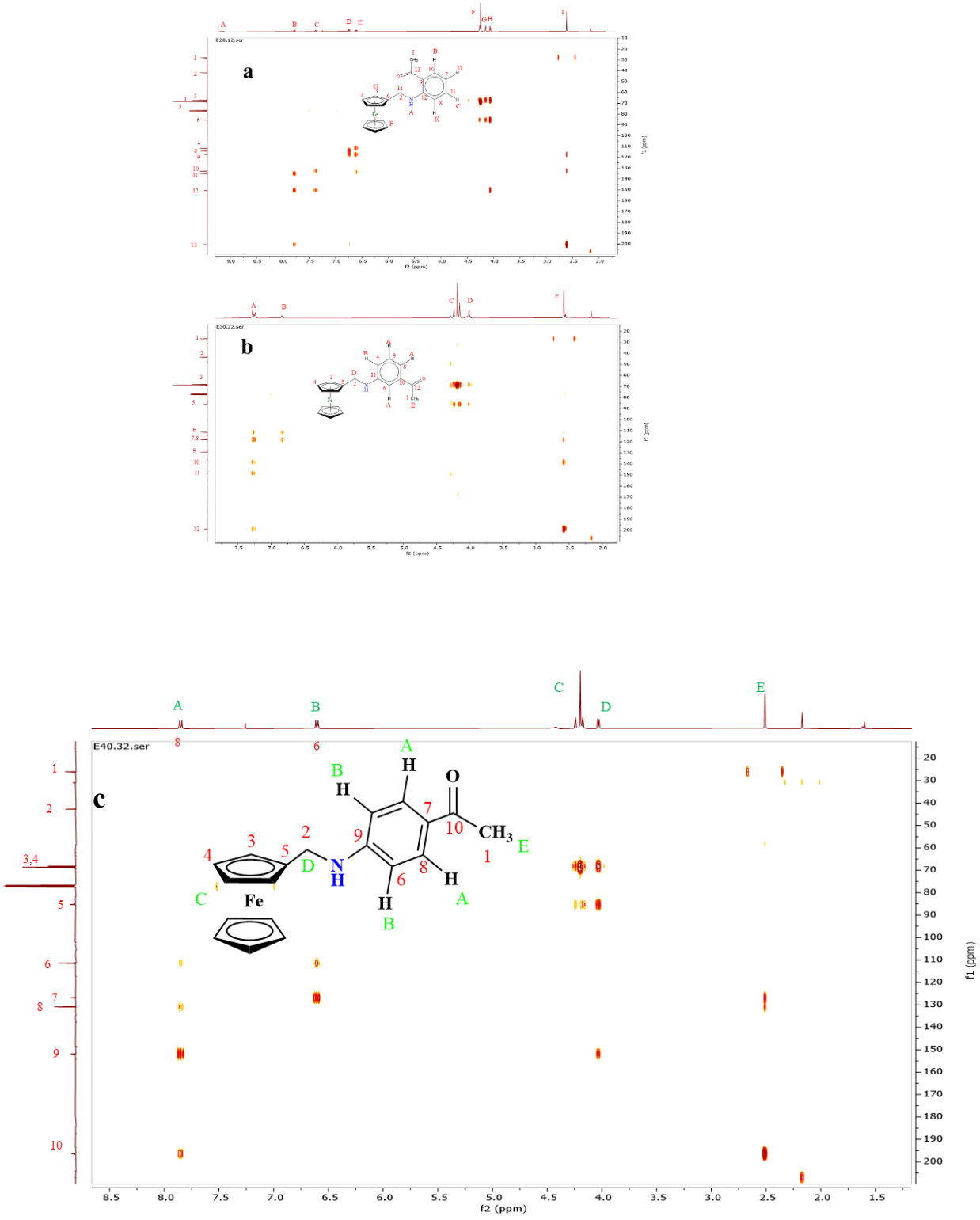

Figure II. 14. HMBC spectra of the synthesised ferrocenyl acetylaniline derivatives: (a) FcMe2Ac, (b) FcMe3Ac, and (c) FcMe4Ac.

As illustrated in Figure II.27, the HSQC spectra provide direct one-bond correlations between proton and carbon nuclei (^{1}JCH), allowing precise assignment of all protonated carbon atoms. The methylene protons (–CH$_2$–N–), observed around 4.30 ppm in the ^{1}H NMR spectra,

show clear cross-peaks with their corresponding carbon signals at approximately 42–43 ppm, confirming the presence of the ferrocenylmethyl linkage.

Similarly, the signals corresponding to the cyclopentadienyl rings exhibit well-defined correlations. The unsubstituted Cp ring (C_5H_5) shows a single correlation pattern consistent with its symmetry, whereas the substituted Cp ring (C_5H_4) displays multiple correlations reflecting the loss of equivalence upon substitution. These observations are characteristic of monosubstituted ferrocenyl systems and further confirm the structural integrity of the organometallic core.

The aromatic proton signals also show distinct HSQC correlations with their corresponding carbon atoms in the region 112–140 ppm, enabling clear assignment of the benzene ring protons. The differences observed between the ortho, meta and para derivatives further support the positional variation of the acetyl substituent [37,38].

In contrast, the HMBC spectra (Figure II.28) provide long-range correlations (^{2}JCH and ^{3}JCH), which are essential for confirming the connectivity between different fragments of the molecule. In particular, strong correlations are observed between the methylene protons (–CH_2–N–) and the aromatic carbons, confirming the formation of the C–N bond linking the ferrocenyl unit to the aniline moiety.

Additional long-range correlations between aromatic protons and the carbonyl carbon (C=O) are observed, allowing precise localisation of the acetyl group on the aromatic ring. These correlations are especially important for distinguishing between the regioisomers, as the HMBC patterns differ significantly depending on the substitution position (ortho, meta or para).

Furthermore, correlations involving the ferrocenyl carbons provide additional confirmation of the substitution pattern on the cyclopentadienyl ring. The combined HSQC and HMBC data therefore establish a complete mapping of proton–carbon connectivity within the molecules [39,40].

Overall, the two-dimensional NMR analysis provides definitive structural confirmation of the synthesised ferrocenyl acetylaniline derivatives. The observed correlation patterns are fully consistent with the proposed structures and are in excellent agreement with literature reports on related ferrocenyl compounds, where HSQC and HMBC techniques are commonly used to validate substitution patterns and molecular connectivity.

6. Cyclic Voltammetry Characterization

6.1. Redox Properties and Voltammetric Response

The electrochemical properties of FcMe2Ac, FcMe3Ac and FcMe4Ac were investigated by cyclic voltammetry in DMSO (1 mM) containing 0.1 M Bu_4NBF_4 as supporting electrolyte, using Hg/Hg_2Cl_2 as reference electrode. Measurements were performed within a potential window of −0.60 to +0.60 V at a scan rate of 100 $mV \cdot s^{-1}$, with the Fc/Fc^+ redox couple used as an internal reference.

The corresponding voltammograms are presented in Figure II.29, where the responses of the substituted derivatives are compared with that of ferrocene.

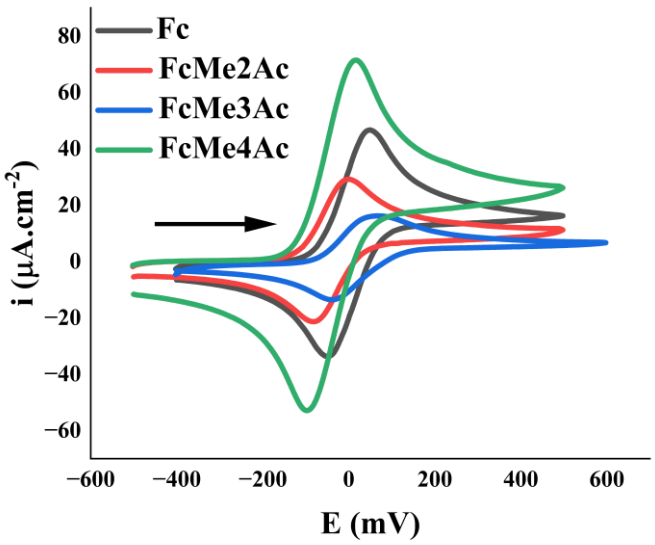

Figure II. 15. Cyclic voltammograms of Fc, FcMe2Ac, FcMe3Ac and FcMe4Ac recorded in DMSO containing 0.1 M Bu_4NBF_4 at a scan rate of 100 $mV \cdot s^{-1}$ (referenced to Fc^+/Fc).

As shown in Figure II.29, all derivatives exhibit a single well-defined redox couple corresponding to the Fe(II)/Fe(III) transition, confirming that the ferrocenyl unit retains its electroactivity after functionalization [41].

A systematic anodic shift in formal potential is observed following the order: **FcMe2Ac (43.9 mV) < FcMe3Ac (51.0 mV) < FcMe4Ac (57.5 mV)**

This trend reflects the influence of the acetylaniline substituent on the electronic environment of the ferrocenyl centre. The positive shift indicates a decrease in electron density at the iron centre, suggesting that oxidation becomes progressively less favourable. This

behaviour can be attributed to the electron-withdrawing nature of the acetyl group, which modulates the electron-donating ability of the ferrocenyl moiety through inductive and resonance effects [42].

The anodic-to-cathodic peak current ratios (Ipa/Ipc ≈ 1) indicate that the redox process is chemically reversible. However, the observed peak-to-peak separation (ΔEp = 87.8–115 mV) exceeds the theoretical value expected for an ideal reversible one-electron process (59 mV), indicating a **quasi-reversible electron transfer** [43].

This deviation suggests the presence of kinetic limitations, which may arise from:

- finite heterogeneous electron-transfer rates
- uncompensated ohmic resistance in the non-aqueous medium
- structural reorganisation accompanying oxidation of the ferrocenyl unit

6.2. Scan Rate Dependence and Mass Transport Regime

The influence of scan rate on the electrochemical response was examined in the range 100–500 mV·s⁻¹. The resulting voltammograms are shown in Figure II.30, while the dependence of anodic peak current on the square root of scan rate is presented in Figure II.31.

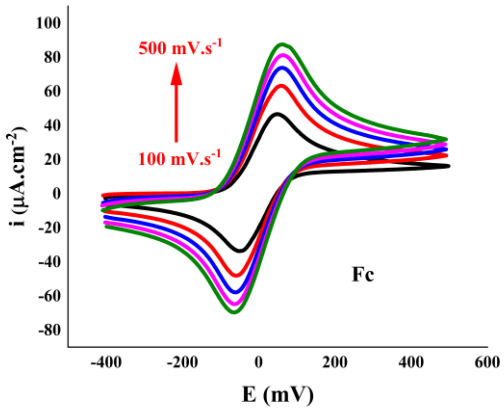

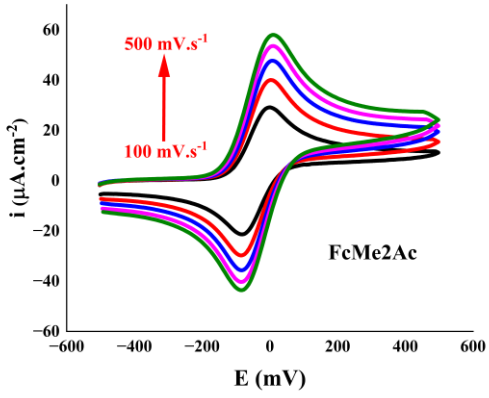

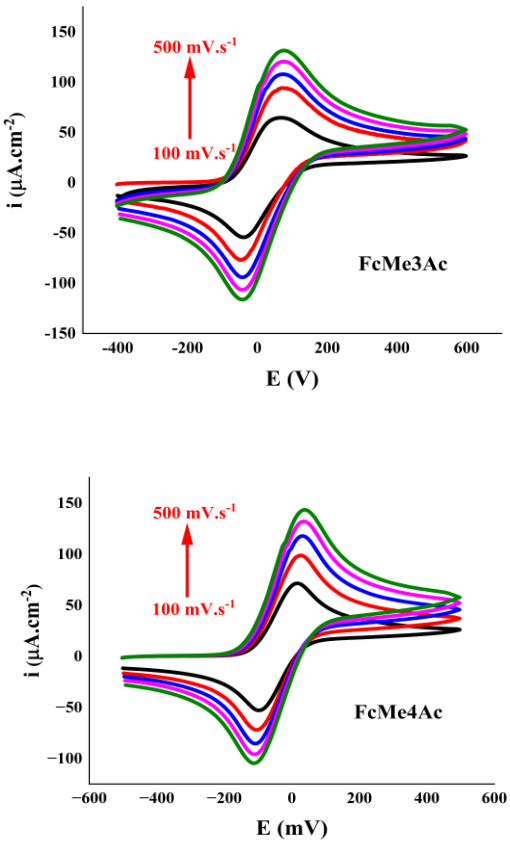

Figure II. 16. Cyclic voltammograms of Fc, FcMe2Ac, FcMe3Ac and FcMe4Ac at different scan rates (100–500 mV·s^{-1}).

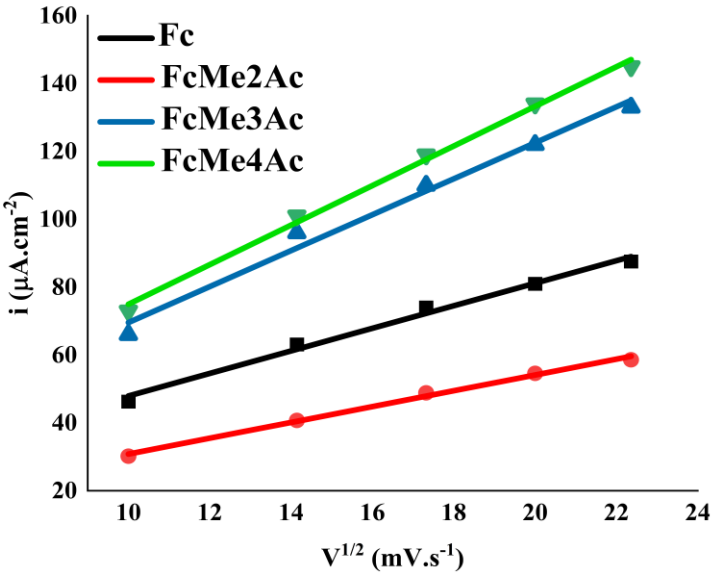

Figure II. 17. Linear variation of anodic peak current (i_{pa}) as a function of the square root of scan rate ($\nu^{1/2}$).

As illustrated in Figure II.30, increasing the scan rate results in a proportional increase in both anodic and cathodic peak currents, without significant distortion of peak shape. This behaviour indicates that the redox process is not governed by adsorption phenomena [44].

A linear relationship between anodic peak current (i_{pa}) and $v^{1/2}$ is clearly observed in Figure II.31 for all compounds. The corresponding linear regression equations (Table II.4) exhibit high correlation coefficients (R^2 = 0.980–0.994), confirming excellent linearity [45].

The high R^2 values demonstrate that the experimental data closely follow the Randles–Ševčík model, thereby confirming that the electron transfer process is diffusion-controlled. Slight deviations from ideal linearity, particularly for FcMe3Ac (R^2 = 0.980), may reflect minor contributions from kinetic limitations or increased solution resistance [46].

6.3. Diffusion Coefficients and Transport Properties

The diffusion coefficients of the electroactive species were determined using the Randles–Ševčík Equation 1 for a reversible system, which relates the peak current to the square root of the scan rate:

$$ip_a = 2.69\times10^5 \left(\sqrt{n}\right)^3 SC\sqrt{D}\sqrt{v}$$

Equation 1

where i_p is the peak current (A), $n$is the number of electrons transferred, A is the electrode surface area (cm^2), C is the concentration of the electroactive species ($mol.cm^{-3}$), D is the diffusion coefficient ($cm^2 \cdot s^{-1}$), and v is the scan rate ($V \cdot s^{-1}$).

The diffusion coefficients (D) were calculated using the Randles–Ševčík equation, and the results are presented in Table II.4.

Table II.4. Diffusion coefficients and linear regression parameters obtained from Randles–Ševčík analysis.

Compound	Equation	R^2	D × 10^{-7} ($cm^2 \cdot s^{-1}$)
Fc	y = 3.321x + 14.727	0.987	6.952
FcMe2Ac	y = 2.328x + 7.539	0.993	1.108
FcMe3Ac	y = 5.298x + 16.578	0.980	5.738
FcMe4Ac	y = 5.831x + 16.638	0.994	2.255

As shown in Table II.4, the diffusion coefficients of the substituted derivatives are significantly lower than that of ferrocene. This decrease can be attributed to several physicochemical factors:

- Increased molecular volume, leading to reduced translational mobility
- Enhanced solute–solvent interactions in polar DMSO medium
- Greater structural complexity and conformational flexibility

FcMe2Ac exhibits the lowest diffusion coefficient (1.11×10^{-7} $cm^2 \cdot s^{-1}$), suggesting stronger intermolecular interactions and possibly a more hindered diffusion pathway. In contrast, FcMe3Ac retains a relatively higher diffusion coefficient, which may be associated with a more favourable molecular geometry and reduced steric constraints [47,48].

6.4. Electron Transfer Kinetics

The heterogeneous electron-transfer rate constants were estimated using Nicholson's method, which relates the peak-to-peak separation to the kinetic parameter Ψ and the standard rate constant as described in Equation 2:

$$\psi = \frac{K_s}{\sqrt{\pi D \frac{nFv}{RT}}}$$

Equation 2

where k_s is the standard heterogeneous electron-transfer rate constant ($cm.s^{-1}$), D is the diffusion coefficient ($cm^2.s^{-1}$), n is the number of electrons transferred, F is the Faraday constant (96,500 $C.mol^{-1}$), v is the scan rate ($V.s^{-1}$), R is the gas constant (8.314 $J.mol^{-1}.K^{-1}$), and T is the absolute temperature (K).

The heterogeneous electron-transfer rate constants (k_s) were estimated using Nicholson's method, and the results are summarised in Table II.5.

Table II.5. Nicholson kinetic parameters (Ψ, ΔEp) and heterogeneous electron-transfer rate constants (k_s).

Compound	Ψ	ΔEp (mV)	$k_s \times 10^3$ ($cm \cdot s^{-1}$)
Fc	1.51	73	2.88
FcMe2Ac	0.323	124	0.62
FcMe3Ac	0.074	263	0.14
FcMe4Ac	0.100	223	0.19

The obtained kinetic parameters clearly indicate a decrease in electron-transfer rates upon substitution. The order: Fc > FcMe2Ac > FcMe4Ac > FcMe3Ac, reflects the increasing complexity of the molecular structure and its impact on electron-transfer dynamics [49].

The relatively high k_s value for ferrocene confirms its well-known fast and reversible electron-transfer behaviour. In contrast, the substituted derivatives exhibit slower kinetics, which can be explained by:

- Increased **steric hindrance**, limiting effective interaction with the electrode surface
- Higher **reorganisation energy** associated with structural changes during oxidation
- Reduced **electronic coupling** between the ferrocenyl centre and the electrode

The particularly low k_s value for FcMe3Ac suggests that the meta substitution pattern is least favourable for efficient electron transfer, likely due to suboptimal electronic communication within the molecule [50].

7. Density Functional Theory (DFT) Analysis

Density functional theory (DFT) calculations were performed to gain detailed insight into the electronic structure, reactivity and physicochemical properties of the synthesised ferrocenyl acetylaniline derivatives. These theoretical investigations provide a molecular-level interpretation of electronic distribution and complement the experimental findings, allowing a more comprehensive understanding of structure–property relationships [51].

7.1. Frontier Molecular Orbitals and Electronic Structure

The frontier molecular orbitals (HOMO and LUMO) are key descriptors governing the reactivity of molecular systems, as they define electron-donating and electron-accepting capacities. The calculated orbital energies are summarised in Table II.6, while their spatial distributions are presented in Figure II.32.

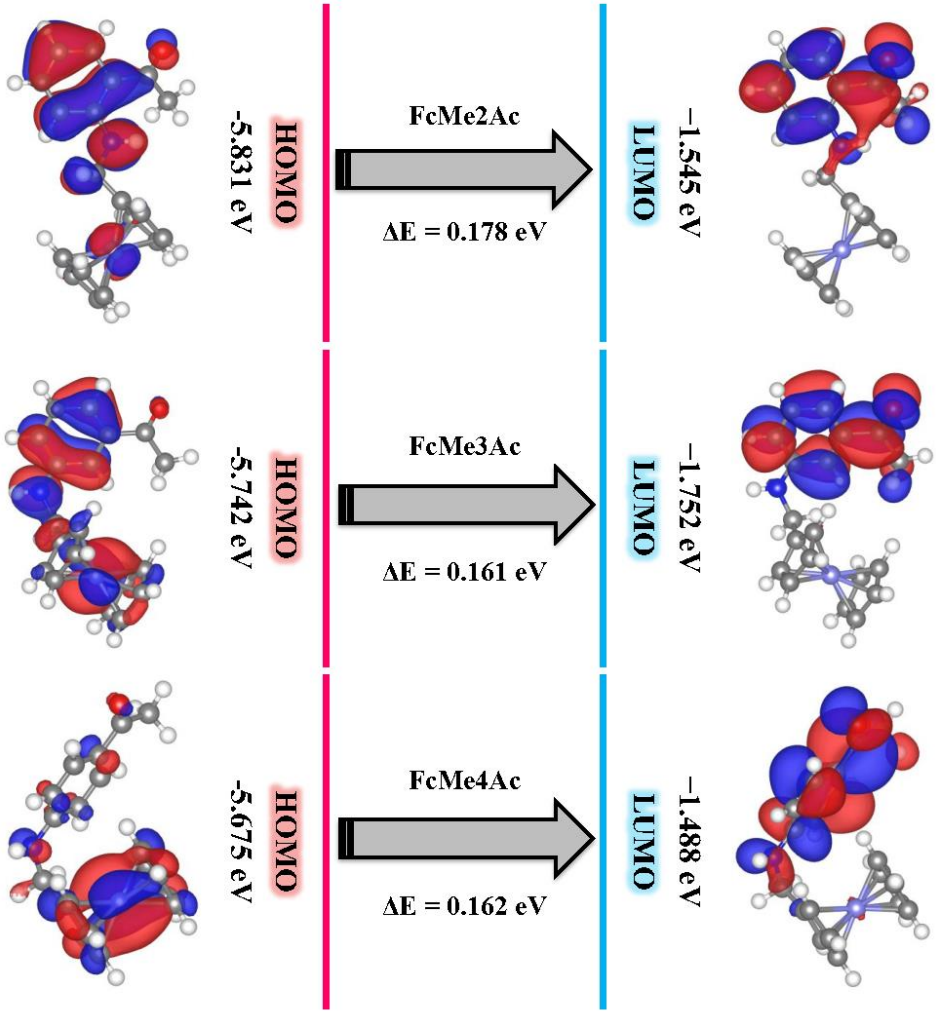

Figure II. 18. Frontier molecular orbitals of ferrocenyl acetylaniline derivatives: HOMO and LUMO surfaces.

Table II.6. Frontier molecular orbital energies (eV) of the synthesised compounds.

Compound	EHOMO (eV)	ELUMO (eV)	ΔE (eV)
FcMe2Ac	−5.8306	−1.5453	4.285
FcMe3Ac	−5.7421	−1.7521	3.990
FcMe4Ac	−5.6752	−1.4882	4.187

The results reveal a gradual increase in HOMO energy from FcMe2Ac (−5.8306 eV) to FcMe4Ac (−5.6752 eV), indicating an enhancement of electron-donating character across the series. This trend reflects the influence of the substitution pattern on the electronic density of the ferrocenyl core, where improved conjugation promotes electron delocalisation.

The HOMO–LUMO energy gap (ΔE) ranges between **3.990 and 4.285 eV**, suggesting that all compounds possess moderate chemical stability combined with sufficient electronic flexibility. Among the derivatives, FcMe3Ac exhibits the lowest energy gap (3.990 eV),

indicating increased softness and higher reactivity, whereas FcMe2Ac displays the highest gap, reflecting comparatively greater stability [52].

The orbital distribution (Figure II.32) shows a clear donor–acceptor separation within the molecular framework. The HOMO is predominantly localised over the ferrocenyl moiety and partially extends towards the amine bridge, identifying this region as the principal electron donor. In contrast, the LUMO is mainly distributed over the aromatic ring and the carbonyl group, designating these sites as electron-accepting regions.

This spatial separation suggests an **intramolecular charge-transfer character**, whereby electron density is transferred from the ferrocenyl unit towards the aromatic substituent. Such donor–acceptor behaviour is particularly relevant for molecular recognition processes, as it facilitates electronic adaptation upon interaction with biological macromolecules [53].

7.2. Global Reactivity Descriptors and Thermodynamic Parameters

To further quantify molecular reactivity, global descriptors derived from frontier orbital energies were calculated and are summarised in Table II.7.

Table II.7. Global reactivity descriptors and thermodynamic parameters of the synthesised derivatives at 298.15 K.

Parameter	FcMe2Ac	FcMe3Ac	FcMe4Ac
Hardness, η (eV)	2.143	1.995	2.094
Electronegativity, χ (eV)	3.688	3.747	3.582
Chemical potential, μ (eV)	−3.688	−3.747	−3.582
Softness, S (eV^{-1})	0.233	0.251	0.239
Electrophilicity, ω (eV)	3.174	3.519	3.064
Nucleophilicity, N	2.829	2.918	2.985
Dipole moment (D)	3.82	4.46	5.12
Polarizability ($Å^3$)	38.5	42.7	47.3
Enthalpy ($kJ \cdot mol^{-1}$)	−1245.6	−1388.2	−1531.4
Entropy ($J \cdot mol^{-1} \cdot K^{-1}$)	412.5	448.9	486.7
Heat capacity ($J \cdot mol^{-1} \cdot K^{-1}$)	236.4	258.7	281.3

The hardness (η) values confirm that all compounds exhibit moderate stability, consistent with their HOMO–LUMO gaps. FcMe3Ac presents the lowest hardness (1.995 eV) and highest softness (0.251 eV^{-1}), reinforcing its greater electronic flexibility and reactivity.

The electrophilicity index (ω) follows the order: **FcMe3Ac > FcMe2Ac > FcMe4Ac**, indicating that FcMe3Ac has the strongest electron-accepting capability. In contrast, FcMe4Ac exhibits the highest nucleophilicity index, suggesting enhanced electron-donating potential. This duality reflects the delicate balance between donor and acceptor characteristics within the series.

The negative values of chemical potential (μ) for all compounds indicate thermodynamic stability and a natural tendency towards charge redistribution. Additionally, a progressive increase in dipole moment from FcMe2Ac to FcMe4Ac is observed, reflecting enhanced molecular polarity and asymmetry [54].

Similarly, polarizability increases across the series, indicating that the electronic cloud becomes more easily deformable. This property is particularly important for intermolecular interactions, as it enhances the ability of the molecule to adapt to external electrostatic environments.

Thermodynamic parameters, including entropy and heat capacity, also show an increasing trend, suggesting greater molecular flexibility and a higher number of accessible vibrational states. This behaviour is consistent with increasing structural complexity and conformational freedom in the substituted derivatives [55].

7.3. Molecular Electrostatic Potential (MEP) Analysis

The molecular electrostatic potential maps provide valuable insight into charge distribution and reactive sites. The calculated MEP surfaces are presented in Figure II.33.

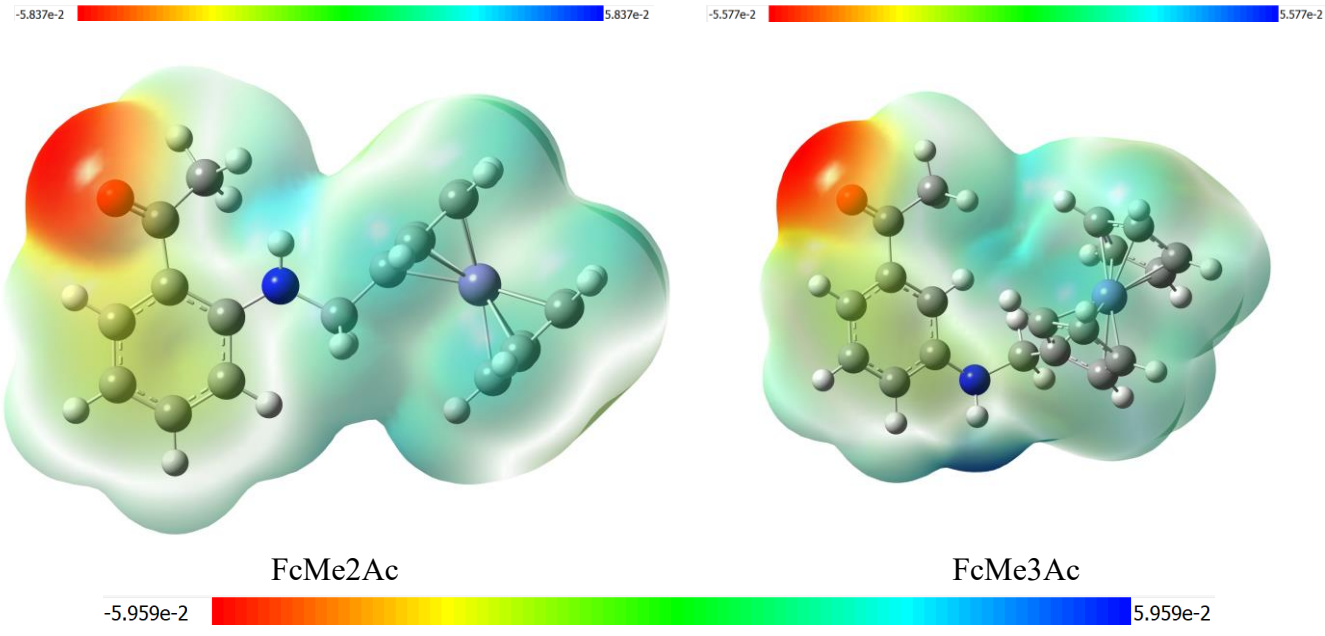

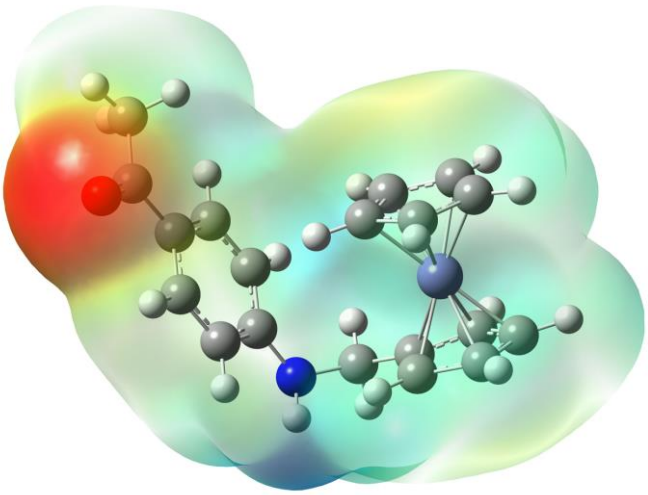

FcMe4Ac

Figure II. 19. Molecular electrostatic potential (MEP) maps of ferrocenyl acetylaniline derivatives showing charge distribution.

The MEP analysis reveals that regions of highest negative potential are localised around the carbonyl oxygen atoms, indicating areas of high electron density and strong nucleophilic character. These regions are therefore likely to serve as preferential sites for intermolecular interactions, including hydrogen bonding and electrostatic interactions.

In contrast, positive electrostatic potential regions are primarily located around hydrogen atoms and partially over the ferrocenyl unit, corresponding to electron-deficient zones [56].

Although the overall electrostatic distribution remains similar across the three derivatives, subtle differences are observed, particularly in the para-substituted compound (FcMe4Ac), which exhibits a more delocalised charge distribution. This enhanced delocalisation may contribute to improved interaction capabilities with biological targets [57].

7.4. Electron Localisation and Non-Covalent Interaction Analysis

To further investigate electronic behaviour, ELF, LOL and RDG analyses were performed. Representative maps are presented in Figure II.34 and II.35.

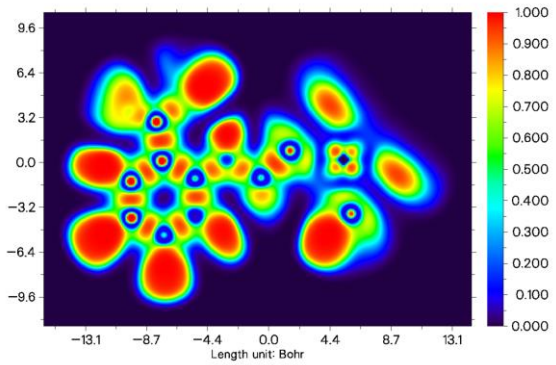

ELF_ **FcMe2Ac**

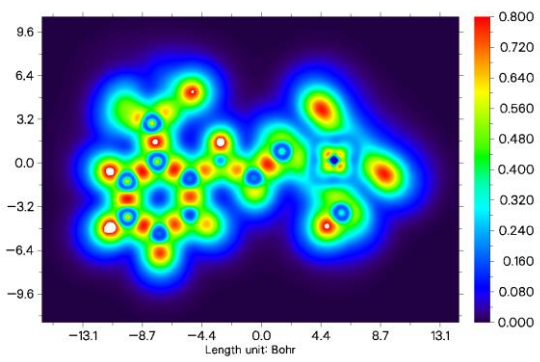

LOL_ **FcMe2Ac**

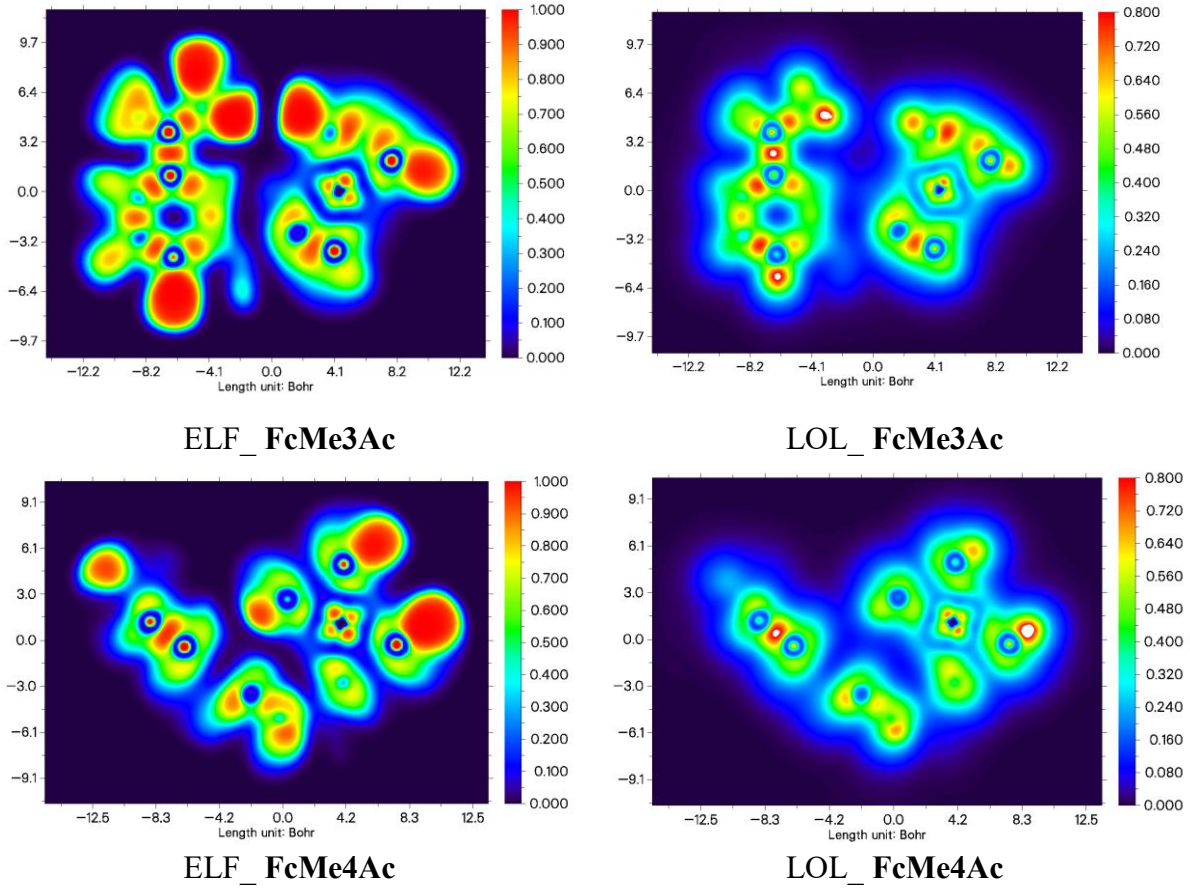

ELF_ **FcMe3Ac** LOL_ **FcMe3Ac**

ELF_ **FcMe4Ac** LOL_ **FcMe4Ac**

Figure II. 20. Electron localisation (ELF and LOL) analyses of FcMeAc.

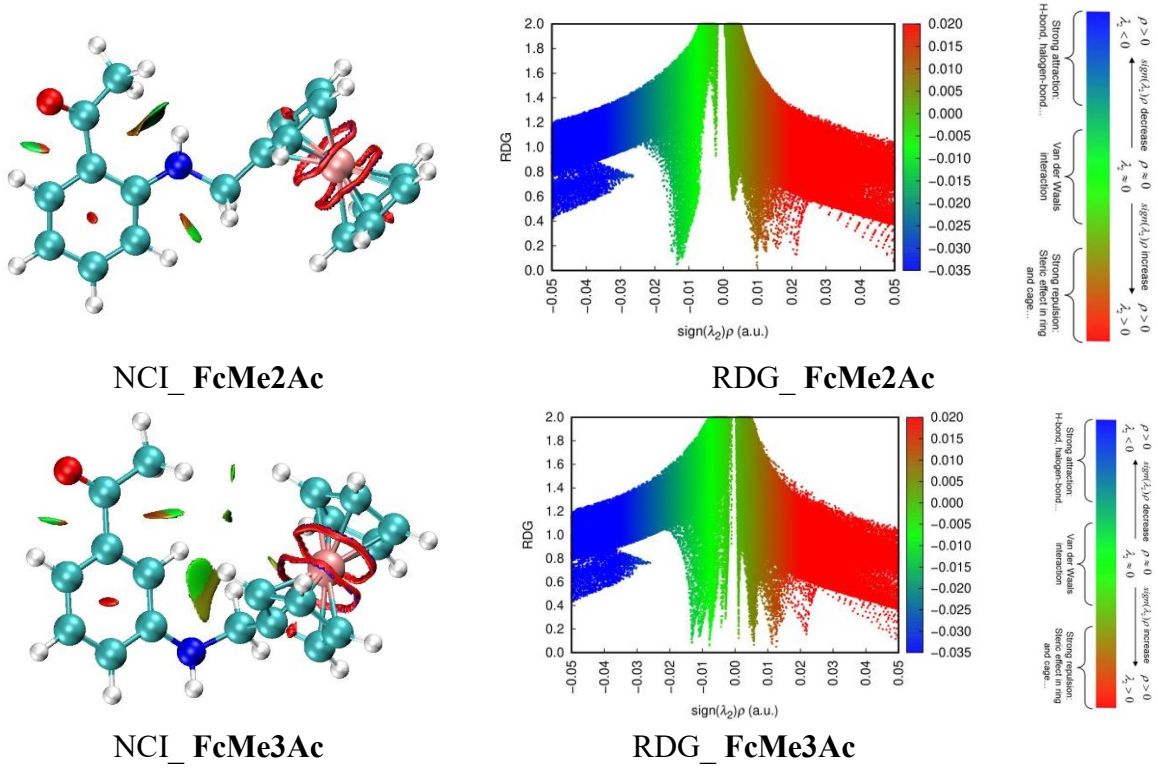

NCI_ **FcMe2Ac** RDG_ **FcMe2Ac**

NCI_ **FcMe3Ac** RDG_ **FcMe3Ac**

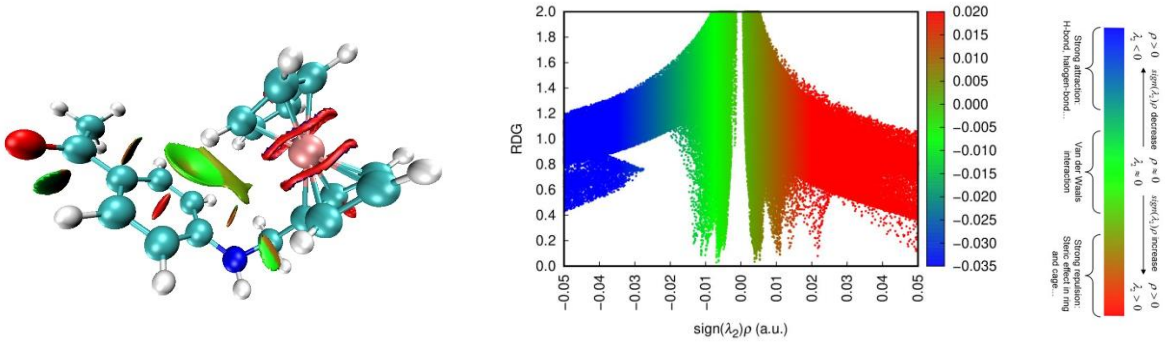

NCI_ **FcMe4Ac** RDG_ **FcMe4Ac**

Figure II. 21. Non-covalent interaction (RDG/NCI) analyses of FcMeAc.

The ELF and LOL maps clearly show strong electron localisation within the cyclopentadienyl rings and the aromatic system, reflecting extensive π-electron delocalisation. Localised electron density around nitrogen and oxygen atoms corresponds to lone-pair regions, which are important for intermolecular interactions.

The RDG analysis highlights weak non-covalent interactions, including van der Waals contacts and steric repulsion zones. These interactions contribute to the overall stability and conformational behaviour of the molecules.

The consistency of these features across the series indicates that the fundamental electronic structure of the ferrocenyl core is preserved, while substitution mainly modulates peripheral electronic properties [58,59].

8. Molecular Docking Study

To investigate the molecular recognition and binding behaviour of the synthesised ferrocenyl acetylaniline derivatives, molecular docking simulations were performed. The study aimed to evaluate the affinity, binding modes, and interaction patterns of the compounds within the binding sites of acetylcholinesterase (AChE), a key enzyme involved in cholinergic neurotransmission.

8.1. Docking Protocol Validation

Prior to analysing ligand–protein interactions, the reliability of the docking protocol was assessed through a redocking procedure of the co-crystallised ligand into the active site of acetylcholinesterase. The superposition between the crystallographic and predicted binding conformations is presented in Figure II.36.

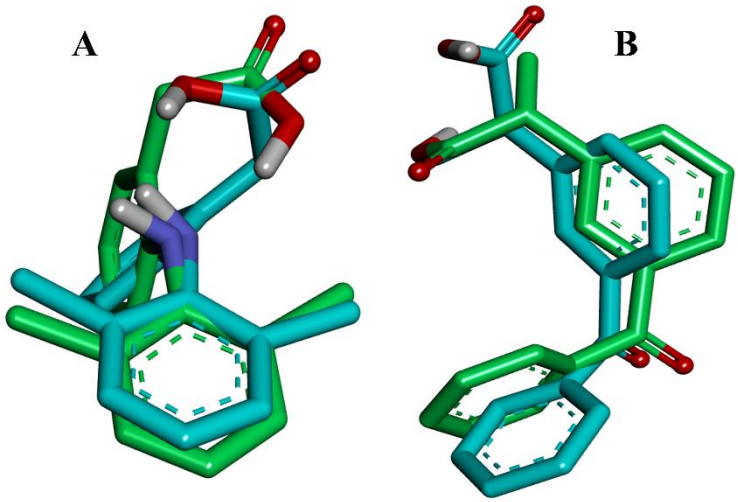

Figure II. 22. Superposition of the co-crystallised ligand and the redocked pose within the active site (validation of docking protocol).

The calculated root-mean-square deviation (RMSD) between the experimental and redocked conformations was found to be 0.339 Å, which is significantly lower than the commonly accepted threshold of 2.0 Å. This result demonstrates excellent agreement between predicted and experimental ligand orientations, confirming the accuracy of the docking parameters, grid definition, and scoring function.

The low RMSD value indicates that the adopted docking protocol is highly reliable for reproducing the native binding mode and can therefore be confidently applied to the ferrocenyl derivatives for subsequent interaction analysis with acetylcholinesterase [60].

8.2. Binding Affinity and Energetic Analysis

The molecular docking results obtained for the ferrocenyl acetylaniline derivatives against acetylcholinesterase are summarised in Table II.8. The calculated binding energies and energetic contributions provide insight into the strength and nature of ligand–enzyme interactions.

Table II.8. Molecular docking results of ferrocenyl acetylaniline derivatives against acetylcholinesterase.

Compound	Intermolecular Energy (kcal·mol⁻¹)	Internal Energy (kcal·mol⁻¹)	Torsional Energy (kcal·mol⁻¹)	Binding Energy (kcal·mol⁻¹)
FcMe2Ac	−7.96	−0.58	+0.74	−7.34
FcMe3Ac	−8.48	−0.71	+0.88	−7.92

FcMe4Ac	−9.42	−0.83	+0.96	−8.58
Reference ligand	—	—	—	−7.65

As shown in Table II.8, all compounds exhibit negative binding energies, indicating spontaneous and thermodynamically favourable interactions within the AChE active site. Among the studied derivatives, FcMe4Ac displays the most favourable binding energy (−8.58 kcal·mol^{-1}), suggesting the strongest inhibitory potential.

A clear affinity trend is observed: **FcMe4Ac > FcMe3Ac > FcMe2Ac**, highlighting the influence of substitution pattern on ligand–enzyme complementarity and binding strength.

The intermolecular energy contribution dominates the binding process, indicating that stabilisation arises primarily from van der Waals interactions, electrostatic forces, and hydrogen bonding within the AChE catalytic gorge. The low internal energy values suggest minimal conformational strain upon binding, while the limited torsional contributions indicate that the ligands adopt energetically favourable conformations within the enzyme environment [61].

8.3. Binding Mode and Interaction Analysis

The three-dimensional binding conformation of the most active compound (FcMe4Ac) within the acetylcholinesterase active site is illustrated in Figure II.37.

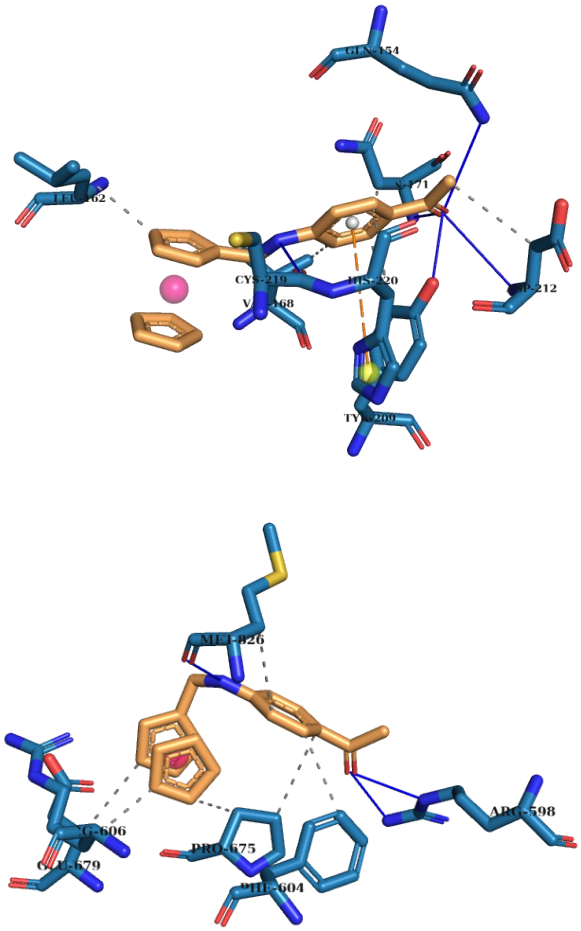

Figure II. 23. Three-dimensional binding mode of FcMe4Ac within the active site of acetylcholinesterase.

The docking results reveal that all ferrocenyl derivatives are stabilised within the **deep hydrophobic catalytic gorge of AChE**, where the ferrocenyl core plays a key role in anchoring the ligand through non-polar interactions.

The interaction profile is characterised by a combination of:

- Hydrophobic interactions with key residues of the gorge (e.g., **TRP86, TYR337, PHE338**)
- π–π stacking interactions between the aromatic ring and aromatic residues (e.g., **TRP86, TYR124, TYR337**)
- Hydrogen bonding interactions involving the carbonyl oxygen and catalytic residues (e.g., **SER203, HIS447, GLU334**)
- Additional electrostatic interactions contributing to binding stabilisation

The binding behaviour differs among the derivatives:

- **FcMe2Ac** exhibits a limited interaction network, with fewer stabilising contacts, resulting in weaker binding affinity.
- **FcMe3Ac** shows improved stabilisation through additional hydrogen bonds and enhanced aromatic interactions.
- **FcMe4Ac** demonstrates the most optimal binding configuration, characterised by:
    - Extensive hydrophobic contacts along the catalytic gorge
    - Stable hydrogen bonding with catalytic residues
    - Strong π–π stacking interactions with aromatic residues
    - Optimal orientation spanning both the **catalytic active site (CAS)** and the **peripheral anionic site (PAS)**

This cooperative interaction network results in enhanced stabilisation of the ligand–enzyme complex and explains its superior binding affinity compared to the other derivatives and the reference ligand [62].

8.4. Structure–Interaction Relationship

The observed differences in binding affinity and interaction behaviour can be rationalised based on structural and electronic considerations.

The **para-substituted derivative (FcMe4Ac)** exhibits the most favourable behaviour due to its extended and more symmetrical structure, allowing optimal insertion into the AChE catalytic gorge. This configuration enhances steric complementarity and maximises intermolecular interactions.

Additionally, the higher dipole moment and increased polarizability of FcMe4Ac contribute to stronger electrostatic and dispersion interactions with the enzyme environment. Enhanced electronic delocalisation further facilitates effective interaction with key active site residues.

In contrast, the **ortho derivative (FcMe2Ac)** is affected by steric hindrance, limiting its ability to adopt an optimal conformation within the binding pocket. The **meta derivative (FcMe3Ac)** exhibits intermediate behaviour due to less efficient electronic delocalisation.

Overall, these findings demonstrate that substitution pattern plays a critical role in modulating ligand–enzyme interactions within acetylcholinesterase. The results clearly identify **FcMe4Ac as the most promising candidate** for AChE inhibition and potential anti-Alzheimer activity [63].

9. Molecular Dynamics Simulation

Molecular dynamics (MD) simulations were performed to investigate the stability and dynamic behaviour of FcMe4Ac in complex with acetylcholinesterase (AChE), using representative crystallographic structures (e.g., PDB ID: 4EY7 and 1EVE). These systems provide a reliable framework for evaluating ligand binding within the catalytic gorge of AChE under dynamic conditions.

9.1. System Stability: RMSD Analysis

The temporal evolution of backbone RMSD for both apo and FcMe4Ac-bound AChE systems is presented in Figure II.38.

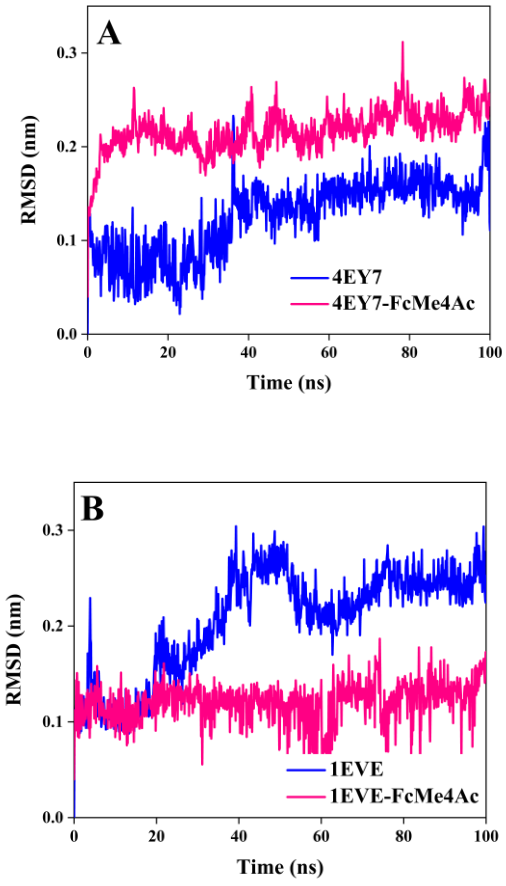

Figure II. 24. RMSD evolution of acetylcholinesterase systems: (A) **4EY7** and (B) **1EVE** over 100 ns.

As shown in Figure II.38, the apo AChE stabilises within ~0.10–0.15 nm after an initial equilibration phase, indicating an intrinsically stable protein conformation. Upon binding of FcMe4Ac, the RMSD increases moderately and stabilises in the range of ~0.18–0.24 nm.

This slight increase reflects ligand-induced conformational adaptation within the catalytic gorge, particularly around the active site residues. Importantly, the absence of large fluctuations confirms that the FcMe4Ac–AChE complex remains structurally stable throughout the simulation.

Overall, the RMSD analysis demonstrates that FcMe4Ac forms a stable complex with AChE, with minor structural rearrangements associated with ligand accommodation [64].

9.2. Residue Flexibility: RMSF Analysis

The root-mean-square fluctuation (RMSF) profiles, presented in Figure II.39, provide insight into residue-level flexibility within the AChE complexes.

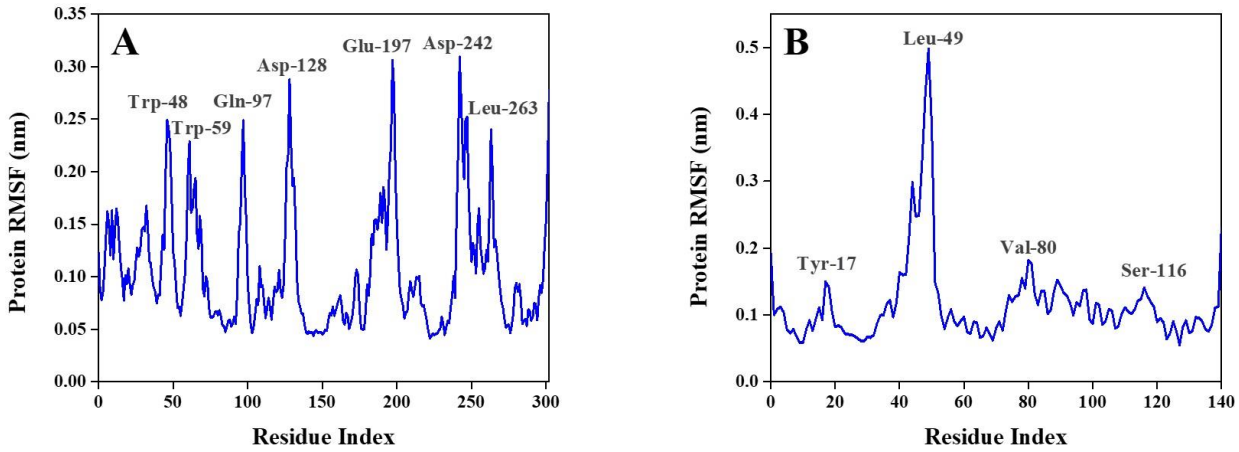

Figure II. 25. RMSF profiles of AChE residues in complex with FcMe4Ac.

The RMSF analysis reveals that most residues exhibit low fluctuations (<0.15 nm), indicating a stable protein backbone. Higher fluctuations are mainly observed in loop regions and solvent-exposed residues, which are inherently flexible.

Importantly, residues located within the **catalytic active site (CAS)** and **peripheral anionic site (PAS)**—including **TRP86, TYR124, TYR337, PHE338, SER203, HIS447, and GLU334**—display minimal fluctuations. This behaviour indicates that FcMe4Ac establishes stable interactions within the binding gorge, contributing to local rigidity.

Overall, the reduction in residue mobility in key functional regions confirms the stabilising effect of ligand binding on AChE structure.

9.3. Ligand Stability: Ligand RMSF Analysis

The conformational stability of FcMe4Ac within the AChE binding pocket was evaluated through ligand RMSF analysis (Figure II.40).

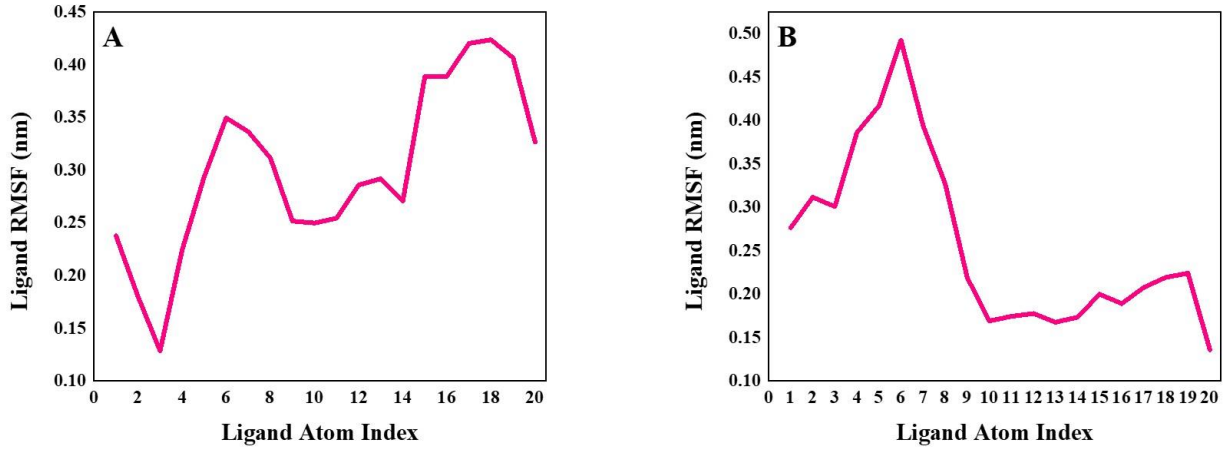

Figure II. 26. Ligand RMSF profile of FcMe4Ac in complex with AChE.

FcMe4Ac exhibits moderate fluctuations (~0.15–0.25 nm), primarily in peripheral substituents, while the ferrocenyl core remains highly stable. This behaviour indicates that the central scaffold is firmly anchored within the catalytic gorge, whereas terminal groups retain limited flexibility.

The relatively low ligand RMSF values confirm a well-confined binding mode and strong interaction with the enzyme.

9.4. Interaction Profile Analysis

The interaction profiles between FcMe4Ac and AChE residues during the simulation are shown in Figure II.41.

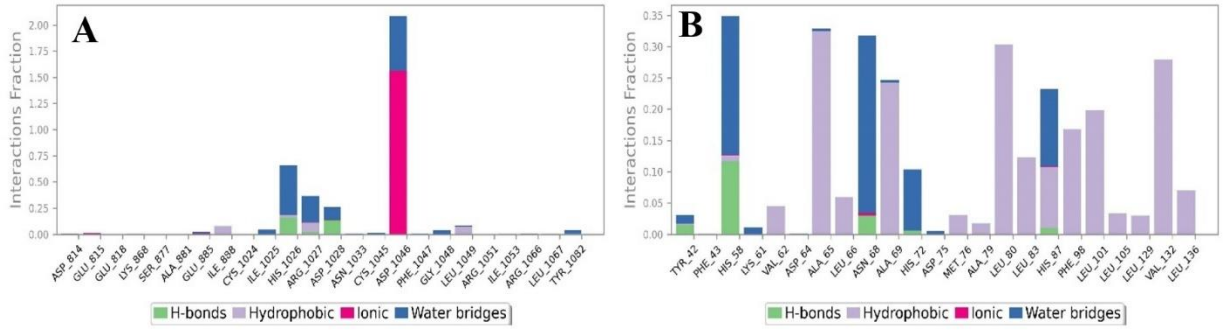

Figure II. 27. Interaction fraction analysis showing hydrogen bonds, hydrophobic interactions, π–π stacking, and water bridges in the AChE complex.

The stabilisation of the complex is governed by:

- Hydrophobic interactions with residues such as **TRP86, PHE338, and TYR337**
- π–π stacking interactions with aromatic residues (**TRP86, TYR124**)
- Hydrogen bonding interactions involving catalytic residues (**SER203, HIS447, GLU334**)

- Water-mediated bridges contributing to interaction persistence

These interactions form a stable and cooperative network within the AChE catalytic gorge, ensuring strong ligand retention throughout the simulation.

9.5. Global Structural Properties (Rg, SASA, PSA)

The evolution of global structural parameters is presented in Figure II.42.

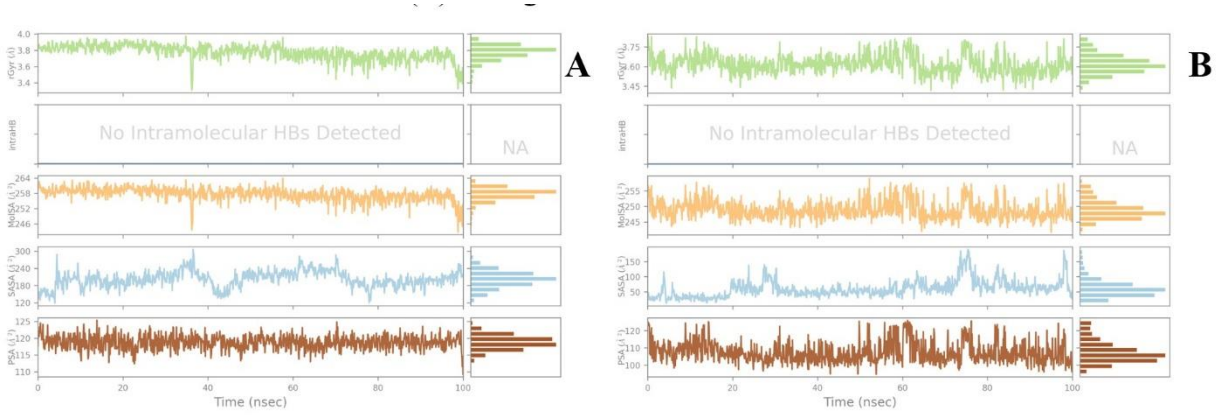

Figure II. 28. Time evolution of radius of gyration (Rg), molecular surface area (MolSA), solvent-accessible surface area (SASA), and polar surface area (PSA) for the AChE complex.

The radius of gyration (Rg) remains stable (~2.2–2.4 nm), indicating that no significant unfolding or structural collapse occurs during the simulation. The SASA values show moderate fluctuations, reflecting normal solvent exposure without major conformational changes.

Similarly, the polar surface area (PSA) remains nearly constant, suggesting that ligand binding does not significantly alter the global polarity of the enzyme.

These results confirm that FcMe4Ac binding does not disrupt the structural integrity of AChE and contributes to maintaining a stable protein conformation [65].

10. ADMET Prediction and Pharmacokinetic Evaluation

To complement the structural, electronic, and dynamic investigations, the pharmacokinetic behaviour and toxicity profile of the synthesised ferrocenyl acetylaniline derivatives were assessed using in silico ADMET prediction tools. This analysis provides critical insight into drug-likeness, absorption, distribution, metabolism, excretion, and safety characteristics, which are essential for evaluating their suitability as potential **anti-Alzheimer agents**.

10.1. Drug-Likeness and Physicochemical Properties

The fundamental physicochemical parameters governing drug-likeness are summarised in Table II.9.

Table II.9. Predicted physicochemical properties and drug-likeness parameters of ferrocenyl derivatives.

Parameter	FcMe2Ac	FcMe3Ac	FcMe4Ac
Molecular weight (g·mol⁻¹)	335.2	335.2	335.2
LogP (consensus)	3.12	3.28	3.45
Lipinski violations	0	0	0

All compounds comply with Lipinski's rule of five, indicating favourable characteristics for oral bioavailability. Their molecular weights (~335 g·mol⁻¹) remain well below the 500 g·mol⁻¹ threshold, while LogP values (3.12–3.45) indicate balanced lipophilicity.

This moderate lipophilicity is particularly advantageous for compounds targeting AChE, as it supports membrane permeability while maintaining adequate solubility [66].

10.2. Absorption and Distribution Properties

The predicted absorption and distribution profiles are presented in Table II.10.

Table II.10. Predicted absorption and distribution properties of the studied compounds**.**

Parameter	FcMe2Ac	FcMe3Ac	FcMe4Ac
Gastrointestinal absorption	High	High	High
Blood–brain barrier permeability	No	No	No

All derivatives exhibit high gastrointestinal absorption, suggesting favourable oral bioavailability.

Notably, the predicted absence of blood–brain barrier (BBB) permeability may represent a limitation for central nervous system targeting. However, this behaviour can be modulated through future structural optimisation to enhance CNS penetration, which is desirable for Alzheimer's disease therapy [67].

10.3. Toxicological Profile

The toxicity predictions are summarised in Table II.11.

Table II.11. Predicted toxicity profiles of ferrocenyl acetylaniline derivatives.

Parameter	FcMe2Ac	FcMe3Ac	FcMe4Ac
Ames toxicity	No	No	No
Hepatotoxicity	No	No	No
Skin sensitisation	Low risk	Low risk	Low risk

All derivatives are predicted to be non-mutagenic (Ames test negative) and non-hepatotoxic, indicating a favourable safety profile. Additionally, the low risk of skin sensitisation further supports their potential as biologically compatible compounds [68].

10.4. Structure–Property Relationship and Comparative Analysis

The ADMET results reveal a consistent and favourable pharmacokinetic profile:

FcMe4Ac exhibits the highest lipophilicity, which may enhance membrane permeability and binding interactions

Increased substitution improves polarizability and interaction potential

All compounds maintain a balanced profile without excessive lipophilicity

Importantly, the absence of toxicity alerts and compliance with drug-likeness rules confirm that modification of the ferrocenyl scaffold does not compromise safety [69].

CONCLUSION

General Conclusion

The present work was devoted to the rational design, synthesis, comprehensive characterisation, and advanced computational evaluation of a series of ferrocenyl acetylaniline derivatives, with particular emphasis on their potential as modulators of acetylcholinesterase (AChE), a key enzymatic target in Alzheimer's disease. The adopted multidisciplinary strategy enabled a coherent integration of experimental and theoretical approaches, providing a robust framework for understanding structure–property–activity relationships.

The synthetic methodology successfully yielded three regioisomeric derivatives (FcMe2Ac, FcMe3Ac, and FcMe4Ac) under mild and reproducible conditions. Structural elucidation, achieved through FT-IR, UV–Visible spectroscopy, and one- and two-dimensional NMR techniques, unequivocally confirmed the formation of the target compounds and validated the substitution patterns on the aromatic ring. The consistency of the spectroscopic data demonstrates the reliability of the synthetic route and the structural integrity of the ferrocenyl framework.

Electrochemical investigations revealed that all derivatives preserve the characteristic redox behaviour of the ferrocenyl core, exhibiting quasi-reversible Fe(II)/Fe(III) transitions. The observed modulation of redox potentials across the series highlights the influence of acetylaniline substitution on the electronic environment of the metal centre. Furthermore, diffusion-controlled electron-transfer processes and variations in kinetic parameters underline the sensitivity of electrochemical behaviour to molecular structure and substitution pattern.

From a theoretical perspective, density functional theory calculations provided detailed insight into the electronic structure and reactivity of the compounds. Frontier molecular orbital analysis demonstrated a pronounced donor–acceptor character, with electron density predominantly localised on the ferrocenyl unit and partially delocalised towards the aromatic moiety. The calculated global descriptors, together with MEP, ELF, and RDG analyses, confirmed the presence of well-defined reactive regions and emphasised the role of substitution in modulating electronic distribution, polarity, and intermolecular interaction potential.

Molecular docking investigations against acetylcholinesterase revealed favourable binding affinities for all derivatives, governed by a combination of hydrophobic interactions, hydrogen bonding, and π–π stacking within the enzyme catalytic gorge. Among the series, FcMe4Ac consistently exhibited superior binding performance, reflecting optimal steric complementarity, enhanced electronic delocalisation, and an extended interaction network spanning both the catalytic active site and the peripheral anionic site.

The dynamic stability of the ligand–enzyme complexes was further validated through molecular dynamics simulations, which confirmed the persistence and robustness of the interactions under simulated physiological conditions. Notably, FcMe4Ac demonstrated reduced structural fluctuations, increased conformational rigidity, and a highly stable interaction profile, indicating a strong and sustained binding mode within the acetylcholinesterase active site.

In parallel, in silico ADMET analysis revealed that all compounds possess favourable pharmacokinetic and safety profiles, characterised by compliance with drug-likeness criteria, high predicted gastrointestinal absorption, and absence of significant toxicity alerts. However, the limited predicted blood–brain barrier permeability suggests that further structural optimisation may be required to enhance central nervous system availability, which is essential for effective anti-Alzheimer activity.

Collectively, the results obtained in this work demonstrate that structural modulation of ferrocenyl derivatives through acetylaniline substitution significantly influences their electronic properties, interaction behaviour, and pharmacokinetic profile. The strong agreement between experimental observations and computational predictions further validates the reliability of the integrated methodological approach.

Among the investigated compounds, FcMe4Ac emerges as the most promising candidate, combining optimal electronic characteristics, strong binding affinity, dynamic stability, and favourable ADMET properties. This derivative represents a valuable lead scaffold for further optimisation aimed at improving acetylcholinesterase inhibition and central nervous system penetration.

In conclusion, this study provides a comprehensive and scientifically rigorous contribution to the field of organometallic medicinal chemistry, highlighting the potential of ferrocenyl derivatives as versatile scaffolds for the development of novel anti-Alzheimer agents and paving the way for future experimental and biological investigations.

REFERENCES

BIBLIOGRAPHY

References for the Theoretical part :

[1] C.-W. Wei *et al.*, 'Synthesis and evaluation of ferrocenoyl pentapeptide (Fc-KLVFF) as an inhibitor of Alzheimer's Aβ1–42 fibril formation in vitro', *Bioorg. Med. Chem. Lett.*, vol. 21, no. 19, pp. 5818–5821, Oct. 2011, doi: 10.1016/j.bmcl.2011.07.111.

[2] P. Štěpnička, *Ferrocenes: Ligands, Materials and Biomolecules*. 2008, p. 655. doi: 10.1002/9780470985663.

[3] K. Heinze and H. Lang, 'Ferrocene—Beauty and Function', *Organometallics*, vol. 32, pp. 5623–5625, Oct. 2013, doi: 10.1021/om400962w.

[4] 1-Azinyl-1′-Alkenylferrocenes with Anticholinesterase, Antioxidant, and Antiaggregating Activities as Multifunctional Agents for Potential Treatment of Alzheimer's Disease'. Available: https://www.mdpi.com/1424-8247/18/12/1862

[5] R. Hamera, 'Ferrocene', Synlett, vol. 26, no. 14, pp. 2047–2048, Jul. 2015, doi: 10.1055/s-0034-1381099.

[6] H. Benamara, 'Synthèse, caractérisation, étude de l'activité antimutagène et antioxydante et détermination des paramètres de liaison de quelques ferrocénylnitrobenzènes et ferrocénylbenzonitriles avec les radicaux O_2^(-^.)et', thesis, Universty of Eloued , 2022. Available: https://archives.univ-eloued.dz/handle/123456789/10845

[7] A. Khennoufa, 'Evaluation of the antioxidant activity and in vitro and in silico study of the interaction of some N-(ferrocenylmethyl)anilines with hemoglobin and serum albumin', thesis, University of Kasdi Merbah Ouargla, 2023. Available: https://dspace.univ-ouargla.dz/jspui/handle/123456789/33646

[8] M. Tazi, 'Nouvelles fonctionnalisations de ferrocènes', thesis, Universty of Rennes 1, 2019. Available: https://theses.fr/2019REN1S124

[9] D. Astruc, 'Why is Ferrocene so Exceptional?', Eur. J. Inorg. Chem., vol. 2017, no. 1, pp. 6–29, 2017, doi: 10.1002/ejic.201600983.

[10] N. Dwadnia, 'Ligands ferrocéniqes hybrides (P, N) : synthèse, coordination aux métaux et applications en catalyse de couplage d'arylation', thesis, Universty of Bourgogne Franche-Comté, 2017. Available: https://theses.fr/2017UBFCK050

[11] U. Rauf, G. Shabir, S. Bukhari, F. Albericio, and A. Saeed, 'Contemporary Developments in Ferrocene Chemistry: Physical, Chemical, Biological and Industrial Aspects', Molecules, vol. 28, no. 15, p. 5765, Jul. 2023, doi: 10.3390/molecules28155765.

[12] A. Adaika, 'Synthèse, caractérisation, étude in vitro de l'activité biologique et analyse in silico et in vivo de quelques dérivés N-ferrocénylméthyltrishydroxyméthylaminométhanes et

N-ferrocénylméthyltrifluoromethylanilines', thesis, University of Eloued, 2021. Available : https://archives.univ-eloued.dz/handle/123456789/8171

[13] S. Benabdesselam, 'Synthèse, activité antioxydante et antibactérienne de quelques dérivés ferrocéniques obtenus par l'arylation de ferrocène', thesis, Universty of Kasdi Merbah Ouargla 2017. Available: https://dspace.univ-ouargla.dz/jspui/handle/123456789/15784

[14] A. Thomas, 'Innovative ferrocene-based molecular switch and trichloroacetic acid fueled eco-compatible amine purifications', thesis, University of Aix-Marseille, 2021. Available: https://theses.fr/2021AIXM0639

[15] A. Singh, I. Lumb, V. Mehra, and V. Kumar, 'Correction: Ferrocene-appended pharmacophores: an exciting approach for modulating the biological potential of organic scaffolds', Dalton Trans., vol. 48, no. 9, p. 3146, Feb. 2019, doi: 10.1039/c9dt90027f.

[16] Y.-H. Gong, 'Etudes de synthèse électrochimiques et de fluorescence de nouveaux dérivés de la 1,2,4,5-tétrazines en tant que sondes moléculaires pour des anions et des composés riches en électrons et étude de synthèses électrochimiques de sels de ferrocène à base de pyridinium.', thesis, École normale supérieure de Cachan - ENS Cachan, 2007. Available : https://theses.hal.science/tel-00160587

[17] K. Abdellatif, 'Theoretical and comparative study of some N-ferrocenylmethylamines using the density function theory DFT and determination of their biological activity', thesis, Universty of Eloued, 2022. Available: http://hdl.handle.net/123456789/32406

[18] N. Zegheb, 'Etude par la modélisation moléculaire, analyse in vitro et in silico de l'activité anticancer du sein de quelques N-ferrocénylméthylanilines', thesis, Universty of Eloued, 2022. Available: https://archives.univ-eloued.dz/handle/123456789/10846

[19] A. Khelef, 'Synthèse et étude du comportement anodique de quelques N-ferrocenyl-N-phenylalkanamides et N'-ferrocenyl-N'-phenylalkanehydrazides et étude structurale de leurs phases cristallines', thesis, University of Mohamed Khider Biskra, 2014. Available: http://thesis.univ-biskra.dz/943/

[20] M. Platon, 'Propriétés et performances de phosphines ferrocéniques dans le couplage C-O, C-S et C-N : nouvelles méthodologies de synthèse au palladium', thesis, Universty of Bourgogne, 2012. Available: https://theses.hal.science/tel-00818998

[21] N. Salah and T. Lanez, 'Electrochemical properties of ferrocene in aqueous and organic mediums at glassy carbon electrode', Recent Trends Phys. Chem., vol. 1, pp. 1–3, Jan. 2013.

[22] E. W. Neuse, 'Ferrocene', Synlett, vol. 26, no. 14, pp. 2047–2048, Jul. 2015, doi: 10.1055/s-0034-1381099.

[23] V. N. Babin, P. M. Raevskii, K. G. Shchitkov, L. V. Snegur, S. Y. Nekrasov, Mendeleev Chem., 1995, 39, 17.

[24] L. Snegur, V. Babin, A. Simenel, Y. S. Nekrasov, L. Ostrovskaya, N. Sergeeva, Russ. Chem. B, 2010, 59, 2167.

[25] D. Plazuk, A. Vessieres, E. A. Hillard, O. Buriez, E. Labbe, P. Pigeon, M. A. Plamont, C. Amatore, J. Zakrzewski, G. Jaouen, J. Med. Chem., 2009, 52, 4967.

[26] S. Sato, M. Tsueda, S. Takenaka, J. Organomet. Chem., 2010, 695, 1858.

[27] N. Chavain, E. D. Charvet, X. Trivelli, L. Mbeki, M. Rottmann, R. Brun, C. Biot, Bioorg. Med. Chem., 2009, 17, 8059.

[28] P. Köpf-Meyer, H. Köpf, W. Neuse, 'Ferricenium complexes: a new type of water soluble antitumor agent', J Cancer Res Clin Oncol, 108, pp. 336–340, 1984.

[29] D. Osella, M. Ferrali, P. Zanello, F. Laschi, M. Fontani, C. Nervi, G. Cavigiolo, 'On the mechanism of the antitumor activity of ferrocenium derivative', Inorg Chim Acta, 306, pp. 42–48, 2000.

[30] C. Y. Acevedo-Morantes, E. Meléndez, S. P. Singh, J. E. Ramírez-Vick, 'Cytotoxicity and Reactive Oxygen Species Generated by Ferrocenium and Ferrocene on MCF7 and MCF10A Cell Lines', J Cancer Sci Ther, 4(9), 2012.

[31] G. Tabbi, C. Cassino, G. Cavigliolio, D. Colangelo, A. Ghiglia, I. Vivano, D. Osella, 'Water stability and cytotoxic activity relationship of a series of ferrocenium derivatives', J Med Chem, 45, pp. 5786–5796, 2002.

[32] Sansook, S. (2017). Biological Evaluation of Ferrocene Derivatives. Doctorat thesis, University of Sussex, pp. 06–09.

[33] S. Top, J. Tang, A. Vessières, D. Carrez, C. Provote, G. Jaouen, 'Ferrocenyl hydroxytamoxifen: a prototype for a new range of oestradiol receptor site-directed cytotoxics', Chem Commun, pp. 955–956, 1996.

[34] S. Top, A. Vessières, G. Leclercq, J. Quivy, J. Tang, J. Vaissermann, M. Huché, G. Jaouen, 'Synthesis, biochemical properties and molecular modeling studies of organometallic SERMs', 2003.

[35] P. Köpf-Meyer, H. Köpf, W. Neuse, 'Ferricenium complexes: a new type of water-soluble antitumor agent', J Cancer Res Clin Oncol, 108, pp. 336–340, 1984.

[36] A. Salmon, P. Jutzi, J. Organomet. Chem., 2001, 637, 595.

[37] P. Chinapang, V. Ruangpornvisuti, M. Sukwattanasinitt, P. Rashatasakhon, Dyes Pigm., 2015, 112, 236.

[38] Fouda, M. F. R., Abd-Elzaher, M. M., Abdelsamaia, R. A., & Labib, A. A. (2007). On the medicinal chemistry of ferrocene. Applied Organometallic Chemistry, 21(8), 613–625. https://doi.org/10.1002/aoc.1253

[39] A. K. Kondapi, N. S. Rayana, A. D. Saikrishna, 'A study of the topoisomerase II activity in HIV-1 replication using ferrocene derivatives as probes', Archives of Biochemistry and Biophysics, 450, pp. 123–132, 2006.

[40] Monserrat, J. P. (2012). Synthèse, caractérisation et criblage biologique de nouveaux dérivés ferrocèniques des flavonoïdes. Thèse de doctorat, Université Pierre et Marie Curie (Paris VI).

[41] Afzal, S. (2010). Redox Behavior and DNA Binding Studies of Some Electroactive Compounds. Doctorat thesis, Quaid-i-Azam University Islamabad, pp. 60–61.

[42] Benabdesselam, S. (2017). Synthèse, activité antioxydante et antibactérienne de quelques dérivés ferrocéniques obtenus par l'arylation de ferrocène (Thèse de doctorat, Université Kasdi Merbah Ouargla, Algérie).

[43] Larik, F. A., Saeed, A., Abdul Fattah, T., Muqadar, U., & Channar, P. A. (2017). Recent advances in the synthesis, biological activities and various applications of ferrocene derivatives. Applied Organometallic Chemistry, 31(3), e3664. https://doi.org/10.1002/aoc.3664

[44] Ouma, R. B. O., Ngari, S. M., & Kibet, J. K. (2024). A review of the current trends in computational approaches in drug design and metabolism. Discover Public Health, 21, Article 108. https://doi.org/10.1186/s12982-024-00229-3

[45] Panigrahi, D., & Sahu, S. K. (2025). Computational approaches: Atom-based 3D-QSAR, molecular docking, ADME-Tox, MD simulation and DFT to find novel multi- targeted anti-tubercular agents targeted anti-tubercular agents. BMC Chemistry, 19, Article 1. https://doi.org/10.1186/s13065-024-01357-2

[46] Mun, C. S., Hui, L. Y., Sing, L. C., Karunakaran, R., & Ravichandran, V. Multi-targeted molecular docking, pharmacokinetics, and drug-likeness evaluation of coumarin based compounds targeting proteins involved in development of COVID-19. Saudi J Biol Sci, 2022, 29, 103458. https://doi.org/10.1016/j.sjbs.2022.103458

[47] Edache, E. I., Uzairu, A., Mamza, P. A., & Shallangwa, G. A. Structure-based simulated scanning of rheumatoid arthritis inhibitors: 2D-QSAR, 3D-QSAR, docking, molecular dynamics simulation, and lipophilicity indices calculation. Sci Afr, 2022. https://doi.org/10.1016/j.sciaf.2021.e01088

References for the Experimental part:

[1] I.U. Khand, T. Lanez, P.L. Pauson, Ferrocene derivatives. Part 24. Synthesis of dihydro-2-pyrindines and dihydro-3 H-2-cyclopent [c] azepines by photolysis of their cyclopentadienyliron derivatives, J. Chem. Soc. Perkin 1 (1989) 2075–2078.

[2] E. Lanez, L. Bechki, T. Lanez, Antioxidant Activities, Binding Parameters, and Electrochemical Behavior of Superoxide Anion Radicals Twords 1-Ferrocenylmethylthymine and 1-Ferrocenylmethylcytosine, Curr. Phys. Chem. 10 (2020) 10–22.

[3] E. Lanez, L. Bechki, T. Lanez, Ferrocenylmethylnucleobases: Synthesis, dft calculations, electrochemical and spectroscopic characterisation, Chemistry (Easton). 14 (2020) 146–153.

[4] E. Lanez, M. Saidi, T. Lanez, Assessment of antioxidant and DPPH free radical scavenging activity of 1,2-dithiole-3-thione derivatives by using cyclic voltammetry, spectroscopic, and molecular docking studies, Journal of Sulfur Chemistry 44 (2023) 542–558. https://doi.org/10.1080/17415993.2023.2200142.

[5] H. Benamara, T. Lanez, E. Lanez, Bsa-binding studies of 2-and 4-ferrocenylbenzonitrile: Voltammetric, spectroscopic and molecular docking investigations, Journal of Electrochemical Science and Engineering 10 (2020) 335–346. https://doi.org/10.5599/jese.861.

[6] E. Lanez, L. Bechki, T. Lanez, Antioxidant Activities, Binding Parameters, and Electrochemical Behavior of Superoxide Anion Radicals Twords 1-Ferrocenylmethylthymine and 1-Ferrocenylmethylcytosine, Curr. Phys. Chem. 10 (2019) 10–22. https://doi.org/10.2174/1877946809666190424143752.

[7] E. Lanez, L. Bechki, T. Lanez, Ferrocenylmethylnucleobases: Synthesis, dft calculations, electrochemical and spectroscopic characterisation, Chemistry and Chemical Technology 14 (2020) 146–153. https://doi.org/10.23939/chcht14.02.146.

[8] E. Lanez, L. Bechki, T. Lanez, N6, 9-bis (ferrocenylmethyl) adenine: synthesis, cyclic voltammetric, spectroscopic characterization, and DFT calculations, Scientific Study & Research. Chemistry & Chemical Engineering, Biotechnology, Food Industry 20 (2019) 509–519.

[9] M.J. Frisch, G.W. Trucks, H.B. Schlegel, G.E. Scuseria, M.A. Robb, J.R. Cheeseman, G. Scalmani, V. Barone, B. Mennucci, G.A. Petersson, Gaussian 09. Wallingford, CT: Gaussian, 2009.

[10] M.P. Andersson, P. Uvdal, New scale factors for harmonic vibrational frequencies using the B3LYP density functional method with the triple-ζ basis set 6-311+ G (d, p), J. Phys. Chem. A 109 (2005) 2937–2941.

[11] T. Lu, F. Chen, Multiwfn: A multifunctional wavefunction analyzer, J. Comput. Chem. 33 (2012) 580–592.

[12] P.W. Rose, A. Prlić, A. Altunkaya, C. Bi, A.R. Bradley, C.H. Christie, L. Di Costanzo, J.M. Duarte, S. Dutta, Z. Feng, R.K. Green, D.S. Goodsell, B. Hudson, T. Kalro, R. Lowe, E. Peisach, C. Randle, A.S. Rose, C. Shao, Y.P. Tao, Y. Valasatava, M. Voigt, J.D. Westbrook, J. Woo, H. Yang, J.Y. Young, C. Zardecki, H.M. Berman, S.K. Burley, The RCSB protein data bank: Integrative view of protein, gene and 3D structural information, Nucleic Acids Res. 45 (2017) D271–D281.

[13] C. Steffen, K. Thomas, U. Huniar, A. Hellweg, O. Rubner, A. Schroer, AutoDock4 and AutoDockTools4: Automated Docking with Selective Receptor Flexibility, J. Comput. Chem. 31 (2010) 2967–2970.

[14] T. Lanez, M. Lanez, R. Lanez, E. Lanez, B. Talbi-Lanez, Computational Screening of Novel Nitroimidazole Candidates: Targeting Key Enzymes of Oral Anaerobes for Anti-Parasitic Potential, Curr. Drug Discov. Technol. (2024).

[15] E. Lanez, N. Zegheb, T. Lanez, In silico ADME, toxicological analysis, molecular docking studies and Molecular dynamics simulation of Afzelin with potential antibacterial effects against Staphylococcus aureus, Turkish Computational and Theoretical Chemistry 7 (2023) 10–16. https://doi.org/10.33435/TCANDTC.1196422.

[16] J. Huang, A.D. Mackerell, CHARMM36 all-atom additive protein force field: Validation based on comparison to NMR data, J. Comput. Chem. 34 (2013) 2135–2145. https://doi.org/10.1002/jcc.23354.

[17] K. Vanommeslaeghe, A.D. MacKerell, Automation of the CHARMM general force field (CGenFF) I: Bond perception and atom typing, J. Chem. Inf. Model. 52 (2012) 3144–3154. https://doi.org/10.1021/ci300363c.

[18] R. Kumari, R. Kumar, A. Lynn, G-mmpbsa -A GROMACS tool for high-throughput MM-PBSA calculations, J. Chem. Inf. Model. 54 (2014) 1951–1962. https://doi.org/10.1021/ci500020m.

[19] J. Dong, N.N. Wang, Z.J. Yao, L. Zhang, Y. Cheng, D. Ouyang, A.P. Lu, D.S. Cao, Admetlab: A platform for systematic ADMET evaluation based on a comprehensively collected ADMET database, J. Cheminform. 10 (2018) 1–11. https://doi.org/10.1186/s13321-018-0283-x.

[20] P. Banerjee, A.O. Eckert, A.K. Schrey, R. Preissner, ProTox-II: A webserver for the prediction of toxicity of chemicals, Nucleic Acids Res. 46 (2018) W257–W263. https://doi.org/10.1093/nar/gky318.

[21] Y. Ouennoughi, H.E. Karce, D. Aggoun, T. Lanez, R. Ruiz-Rosas, B. Bouzerafa, A. Ourari, E. Morallon, A novel ferrocenic copper (II) complex Salen-like, derived from 5-chloromethyl-2-hydroxyacetophenone and N-ferrocenmethylaniline: Design, spectral approach and solvent effect towards electrochemical behavior of Fc+/Fc redox couple, J. Organomet. Chem. 848 (2017) 344–351.

[22] M. Chebbah, E. Lanez, S. Bouacida, H. Athmani, M.L. Ben Amor, R. Hafidi, A. Bouchemma, Synthesis, Characterization, Structural Analysis, Hirshfeld Surface Studies, and Molecular Docking of 1, 3, 5-Tris (P-Bromophenyl)-1, 3, 5-Triazacyclohexane, Hirshfeld Surface Studies, and Molecular Docking Of 1 (n.d.).

[23] M. Hanane, T. Lanez, I. Zafar, M.S. Afghan, N. Zegheb, N'-Ferrocenylmethyl-N'-phenylbenzohydrazide as a potential DNA binding compound: a combined experimental and computational study, J. Coord. Chem. 76 (2023) 1984–1998. https://doi.org/10.1080/00958972.2023.2275247.

[24] A. Adaika, Y. Bekkar, S. Youmbai, L. Bourougaa, E. Lanez, M.L. Ben Amor, K. Nesba, T. Lanez, L. Bechki, Synthesis, Antioxidant, and Antidiabetic Potential of Ferrocenylmethylnucleobase Compounds: In Vitro, In Silico Molecular Docking, DFT Calculation, and Molecular Dynamic Simulations, Appl. Organomet. Chem. 39 (2025) e7988.

[25] E. LANEZ, D. BENKHELIFA, F.Z. CHERIET, K. GORI, C. SLIMANI, S. KEBACHE, R. OUAKOUAK, O. ABDELLAOUI, Y. DJOUGHI, M.L. BENAMOR, Theoretical Investigation of Mitomycin Derivatives as Dual Inhibitors of HER2 and ER-α: Prospects for Novel Breast Cancer Treatment Strategies, Algerian Journal of Biosciences 6 (2025) 1–20.

[26] E. Lanez, Y. Bekkar, L. Bourougaa, M.L. Benamor, R. Bouraoui, O. Boudebia, A. Adaika, K. Nesba, H. Chaoua, L. Bechki, Antidiabetic potential of mentha piperita essential oil: GC-MS profiling, in vitro, in vivo and in silico analyses, J. Mol. Struct. (2025) 144239.

[27] C. Benine, D.A. Boutlelis, L.A. Touhami, E. Lanez, D.G. Amara, G. Rim, N. Hanen, W. Zahnit, M. Messaoudi, Green synthesis, characterization, antioxidant, interaction with DNA/BSA, and investigation of cytotoxicity against MCF-7 cancer cells of zinc oxide nanoparticles using Hammada scoparia (Pomel) Iljin extract, Int. J. Biol. Macromol. 295 (2025) 139709.

[28] M.L. Tlili, I. Laib, K. Salemi, I. Chetehouna, I. BenMoussa, E. Lanez, Phytochemical Analysis and Evaluation of the Antioxidant, Anti-Inflammatory, Hemolytic, and Antibacterial Effects of Astragalus gombo (L.) Leaves., Acta Chim. Slov. 71 (2024).

[29] M.L. Tlili, F. Alia, E. Bahri, T. Beyat, K. Redouan, E. Lanez, In vivo evaluations of the antidiabetic and antioxidant effects of Olea europaea L.(Chemlali variety) leaves, Acta Periodica Technologica (2025) 3.

[30] S. Khamouli, S. Belaidi, M. Ouassaf, T. Lanez, S. Belaaouad, S. Chtita, Multi-combined 3D-QSAR, docking molecular and ADMET prediction of 5-azaindazole derivatives as LRRK2 tyrosine kinase inhibitors, J. Biomol. Struct. Dyn. 40 (2022) 1285–1298.

[31] N. Zouaghi, E. Lanez, M.L. Benamor, S.N. Nacer, T. Lanez, Y. Bekkar, H. Haddad, K. Al-Abdallat, M. Zihlif, Y. Al-Abdallat, Targeting Alzheimer's Disease via Phytochemicals from Artemisia campestris L.: GC/MS Analysis with an Integrated Computational Approach, Food Biosci. (2025) 108128.

[32] N. Zegheb, C. Boubekri, T. Lanez, E. Lanez, T.T. Küçükkılınç, E. Öz, A. Khennoufa, S. Khamouli, S. Belaidi, In Vitro and In Silico Determination of Some N-ferrocenylmethylaniline Derivatives as Anti-Proliferative Agents Against MCF-7 Human Breast Cancer Cell Lines, Anticancer Agents Med. Chem. 22 (2021) 1426–1437. https://doi.org/10.2174/1871520621666210624141712.

[33] M.L.B.E.N. AMOR, E. LANEZ, Y. Bekkar, A. ADAIKA, T. LANEZ, K. NESBA, L. BECHKI, Exploring the Interactions of Ferrocenylmethylnucleobase Derivatives With BSA and HHb: Insights From Electrochemical, Spectroscopic, ADMET, in Silico Docking, and MD Simulations, ChemistrySelect 10 (2025) e202404678.

[34] A. Rebiai, T. Lanez, M.L. Belfar, Total polyphenol contents, radical scavenging and cyclic voltammetry of algerian propolis, Int. J. Pharm. Pharm. Sci. 6 (2014) 395–400.

[35] M.L. Ben Amor, E. Lanez, Y. Bekkar, A. Adaika, T. Lanez, K. Nesba, L. Bechki, EVALUATION OF FERROCENYLMETHYLNUCLEOBASES DERIVATIVES INTERACTING WITH DNA: INSIGHTS FROM ELECTROCHEMICAL, SPECTROSCOPIC, DFT CALCULATION, MOLECULAR DOCKING AND MOLECULAR DYNAMIC SIMULATIONS., Studia Universitatis Babes-Bolyai, Chemia 70 (2025).

[36] S. Khamouli, S. Belaidi, T. Lanez, Molecular doking and ADMET studies of amino-pyrimidine derivaties as mycobacterium tuberculosis Ser/Thr protein kinases B inhibitors, Journal of Fundamental and Applied Sciences 11 (2019) 914–939.

[37] H. Mouada, T. Lanez, I. Zafar, ROS scavenging, DNA binding and NADPH oxidase inhibition potential of N'-Ferrocenylmethyl-N'-phenylpropionohydrazide using cyclic voltammetry and molecular docking, J. Organomet. Chem. 1007 (2024) 123026.

[38] T. Lanez, M. Henni, H. Hemmami, Development of cyclic voltammetric method for the study of the interaction of antioxidant standards with superoxide anion radicals case of α-tocopherol, Scientific Study and Research: Chemistry and Chemical Engineering, Biotechnology, Food Industry 16 (2015) 161–168.

[39] Y. Bekkar, E. Lanez, T. Lanez, L. Bourougaa, A. Adaika, Z. Saada, A. Benine, Antidiabetic Potential of Synthesized Ferrocenylmethylaniline Derivatives: Insights From In Vitro Studies, Molecular Docking, ADMET, DFT Calculations, and Molecular Dynamics Simulation, Biotechnol. Appl. Biochem. (2025).

[40] Y. Bekkar, E. Lanez, T. Lanez, L. Bourougaa, A. Adaika, A. Benine, Z. Saada, Combined In Vitro and In Silico analysis of ferrocenylmethylaniline derivatives: Antibacterial potential, DFT calculations, and molecular dynamics insights, J. Organomet. Chem. (2025) 123618.

[41] E. Lanez, L. Zerrouk, L. Bechki, T. Lanez, A. Adaika, N. Zegheb, K. Nesba, Synthesis, molecular docking, drug-likeness analysis, and ADMET prediction of nickel and zinc tetraphenyl-porphyrin complexes as possible antioxidant agents, Journal of the Chinese Chemical Society (n.d.).

[42] S.N. Nacer, T. Lanez, Electrochemical properties of N'-ferrocenylmethyl-N'-phenylbenzohydrazide in aqueous and organic mediums, International Letters of Chemistry, Physics and Astronomy 5 (2013) 76–85.

[43] H. Laraoui, E. Lanez, N. Zegheb, A. Adaika, T. Lanez, M. Benkhaled, Anti-Diabetic Activity of Flavonol Glucosides From Fumana montana Pomel: In vitro Analysis, In Silico Docking, ADMET Prediction, and Molecular Dynamics Simulations, ChemistrySelect 8 (2023) e202204512. https://doi.org/10.1002/slct.202204512.

[44] T. Lanez, M. Henni, Dual Anti-Inflammatory and Antidiabetic Potential of Ferrocenylmethylcyanophenyl Derivatives: Integrated In Vitro and In Silico Evaluation, J. Organomet. Chem. (2025) 123956.

[45] A. Khelef, T. Lanez, In vitro assays of the antioxidant activities of ferrocene derivatives bearing amine, amide or hydrazine groups, . 7 (2015) 318–323.

[46] T. Zaiz, T. Lanez, Corrosion inhibition of carbon steel XC70 in H_2SO_4 solution by ferrocene derivative 3-(ferrocenylmethylamine)benzonitrile, Journal of Fundamental and Applied Sciences 4 (2015) 182. https://doi.org/10.4314/jfas.v4i2.8.

[47] T. Lanez, H. Hemmami, Antioxidant Activities of N-ferrocenylmethyl-2- and -3-nitroaniline and Determination of their Binding Parameters with Superoxide Anion Radicals, Curr. Pharm. Anal. 13 (2016) 110–116. https://doi.org/10.2174/1573412912666160831145524.

[48] N. Benyza, F. Allouche, S.W. Dammak, E. Lanez, T. Lanez, Chemical Reactivity, Topological Analysis, and Second-Order Nonlinear Optical Responses of M3O@ Al12N12: A Quantum Chemical Study, Russian Journal of Physical Chemistry A 96 (2022) 2909–2920.

[49] E. Lanez, A. Kedadra, T. Lanez, A. Adaika, N. Zegheb, In vitro antioxidant activity, QSAR, in silico toxicity prediction, molecular docking studies, and molecular dynamics of a series of N-ferrocenylmethylanilines as potent antioxidant agents, J. Organomet. Chem. (2024) 123284.

[50] C. Filote, E. Lanez, V.I. Popa, T. Lanez, I. Volf, Characterization and Bioactivity of Polysaccharides Separated through a (Sequential) Biorefinery Process from Fucus spiralis Brown Macroalgae, Polymers (Basel). 14 (2022) 4106. https://doi.org/10.3390/polym14194106.

[51] A. Boutarfaia, L. Bechki, T. Lanez, E. Lanez, M. Kadri, Synthesis, Antioxidant Activity, and Determination of Binding Parameters of Meso-Tetra-4-Actophenyl-Porphyrin and its Palladium (II) Complex with Superoxide Anion Radicals, Curr. Bioact. Compd. 16 (2019) 1063–1071. https://doi.org/10.2174/1573407215666191017105239.

[52] A. Yahiaoui, N. Benyza, A. Messai, T. Lanez, E. Lanez, Voltametric and molecular docking investigations of ferrocenylmethylaniline and its N-acetylated derivative interacting with DNA, Journal of Electrochemical Science and Engineering (2023). https://doi.org/10.5599/jese.2061.

[53] A. Kedadra, T. Lanez, E. Lanez, H. Hemmami, M. Henni, Synthesis and antioxidant activity of six novel N-ferrocenylmethyl-N-(nitrophenyl)and-N-(cyanophenyl)-acetamides: Cyclic voltammetry and molecular docking studies, Journal of Electrochemical Science and Engineering 12 (2022) 293–304. https://doi.org/10.5599/jese.1162.

[54] A. Khennoufa, L. Bechki, T. Lanez, E. Lanez, N. Zegheb, Spectrophotometric, voltammetric and molecular docking studies of binding interaction of N-ferrocenylmethylnitroanilines with bovine serum albumin, J. Mol. Struct. 1224 (2021) 129052. https://doi.org/10.1016/j.molstruc.2020.129052.

[55] M. Meraghni, T. Lanez, E. Lanez, L. Bechki, A. Kennoufa, Experimental and theoretical study on corrosion inhibition of mild steel by meso-tetraphenyl-porphyrin derivatives in acid solution, Journal of Electrochemical Science and Engineering 13 (2023) 217–229. https://doi.org/10.5599/jese.1400.

[56] T. Lanez, M. Feizi-Dehnayebi, E. Lanez, Assessment of the electrostatic binding of ferrocenylmethyl-nitroaniline derivatives to DNA: A combined experimental and theoretical study, J. Mol. Struct. (2024) 138386.

[57] Z. Nadjiba, B. Chérifa, T. Lanez, E. Lanez, In Silico Study on N-ferrocenylmethyl-N-phenylpropionohydrazide and N-ferrocenylmethyl-N-pheylbenzohydrazide as anticancer drugs for breast and prostate cancer, International Journal of Pharmacology, Phytochemistry and Ethnomedicine 11 (2018) 17–25.

[58] L. ZERROUK, L. BECHKI, E. LANEZ, T. LANEZ, Synthesis, characterization, cyclic voltammetry, and molecular docking studies of the antioxidant activities of superoxide anion radicals towards meso-tetramethophenyl-porphyrin and meso-tetrabiphenyl-porphyrin, Not. Sci. Biol. 16 (2024) 11823. https://doi.org/10.55779/nsb16211823.

[59] A. Adaika, A. Adaika, T. Lanez, E. Lanez, in Vitro and in Silico Evaluation of Anticancer Activity of N,N-Dimethylaminomethylferrocene, Journal of Fundamental and Applied Sciences 11 (2019) 748–768. https://jfas.info/index.php/JFAS/article/view/289.

[60] T. Lanez, H. Benaicha, E. Lanez, M. Saidi, Electrochemical, spectroscopic and molecular docking studies of 4-methyl-5-((phenylimino)methyl)-3H- and 5-(4-fluorophenyl)-3H-1,2-dithiole-3-thione interacting with DNA, Journal of Sulfur Chemistry 39 (2018) 76–88. https://doi.org/10.1080/17415993.2017.1391811.

[61] N. ZEGHEB, L. Elhafnaoui, T. Lanez, N-ferrocenylmethyl-derivatives as spike glycoprotein inhibitors of sars-cov-2 using in silico approaches, (2020).

[62] E. Lanez, T. Lanez, N. Zegheb, In silico ADMET, toxicological analysis, molecular docking studies and Molecular dynamics simulation of Afzelin with potential antibacterial effects against Staphylococcus aureus, Turkish Computational and Theoretical Chemistry 7 (2023) 10–16.

[63] H. Mouada, T. Lanez, E. Lanez, Investigations of the binding parametres of the interaction of N'-ferrocenylmethyl-N'-phenylaceto-and propionohydrazide with DNA, Journal of Fundamental and Applied Sciences 11 (2019) 875–882.

[64] E. Lanez, L. Bechki, T. Lanez, Computational molecular docking, voltammetric and spectroscopic DNA interaction studies of 9N-(Ferrocenylmethyl)adenine, Chemistry and Chemical Technology 13 (2019) 11–17. https://doi.org/10.23939/chcht13.01.011.

[65] T. Lanez, E. Lanez, A molecular docking study of N-ferrocenylmethylnitroanilines as potential anticancer drugs, International Journal of Pharmacology, Phytochemistry and Ethnomedicine 2 (2016) 5–12.

[66] L. Guan, H. Yang, Y. Cai, L. Sun, P. Di, W. Li, G. Liu, Y. Tang, ADMET-score-a comprehensive scoring function for evaluation of chemical drug-likeness, Medchemcomm 10 (2019) 148–157. https://doi.org/10.1039/C8MD00472B.

[67] G. Xiong, Z. Wu, J. Yi, L. Fu, Z. Yang, C. Hsieh, M. Yin, X. Zeng, C. Wu, A. Lu, ADMETlab 2.0: an integrated online platform for accurate and comprehensive predictions of ADMET properties, Nucleic Acids Res. 49 (2021) W5–W14.

[68] D. Dascalu, D. Larisa Roman, M. Filip, A. Ciorsac, V. Ostafe, A. Isvoran, Solubility and Admet Profiles of Short Oligomers of Lactic Acid, ADMET DMPK 8 (2020) 425–436. https://doi.org/10.5599/admet.801.

[69] J. Hodgson, ADMET—turning chemicals into drugs, Nat. Biotechnol. 19 (2001) 722–726.